High Temperature Superconducting Partial Core Transformer and Fault Current Limiter

Jit Kumar Sham

A thesis presented for the degree of

Doctor of Philosophy

in

Electrical and Computer Engineering

at the

University of Canterbury,

Christchurch, New Zealand.

2015

ABSTRACT

The thesis begins with an introduction to transformer theory. The partial core transformer is then introduced and compared with a full core design. A brief introduction to superconductors and high temperature superconductors is then presented. High temperature superconducting fault current limiters are then examined and the advantage of a high temperature superconducting partial core transformer and fault current limiter as a single unit is highlighted.

The reverse design model is discussed followed by the model parameters that are used in designing the high temperature superconducting partial core transformer. Partial core transformers with copper windings and high temperature superconductor windings at the University of Canterbury were then tested and the measured results compared with the results calculated from the reverse design model, to validate the model. The high temperature superconducting partial core transformer failed during an endurance run and the investigation of the failure is then presented. The results of the failure investigation prompted an alternative winding insulation design. A model to calculate the time at which the high temperature superconducting winding of the partial core transformer would melt at different currents was then built. The time was calculated to be used in the operation of the quench detection mechanism and it could also be used in choosing a circuit breaker with a known operating time.

The design of the high temperature superconducting partial core transformer and fault current limiter is then presented. Design configurations with different core length and winding length are examined. The idea behind choosing the final design for the high temperature superconducting partial core transformer and fault current limiter is then discussed. The final design of the high temperature superconducting partial core transformer and fault current limiter is then presented.

A new 7.5 kVA, 230-248 V high temperature superconducting partial core transformer and fault current limiter was designed, built and tested. The windings are layer wound with first generation Bi2223 high temperature superconductor. A series of electrical tests were performed on the new device including open circuit, short circuit, resistive load, overload and fault ride through. These tests were performed to determine the operational characteristics of the new high temperature superconducting partial core transformer and fault current limiter. The measured results from the tests were compared with the calculated results. The fault ride through test results were then compared to a 15 kVA high temperature superconducting partial core transformer that was designed and built at the University of Canterbury. Since the resistive component of the silver matrix in Bi2223 high

temperature superconductor plays a very little role in controlling the fault current, the current limited by the leakage reactance is compared between the two devices. The high temperature superconducting partial core transformer and fault current limiter was found to be 99.1% efficient at rated power with 5.7% regulation and fault current limiting ability of 500 % over the 15 kVA high temperature superconductor partial core transformer from University of Canterbury.

CONFERENCE PAPER

SHAM, J., BODGER, P., (2013) **'**HTS Partial Core Transformer-Fault Current Limiter', *In Electricity Engineers' Association (EEA) Conference*, Auckland, New Zealand, pp.1-10.

ACKNOWLEDGEMENTS

I would like to thank my supervisor Prof Pat Bodger for the support, guidance and knowledge that he has given me all these years. I would also like to thank the technical staff, Ken Smart, Dave Healy and Jac Woudberg for all the help and advice they have given me in the machines lab, workshop and high voltage lab.

I would also like to thank Andrew Lapthorn for your guidance and support.

I would like to take this opportunity to thank my parents for their mental and financial support throughout my whole life.

Finally, thank you Lala for your support and listening to my nagging and whining. I couldn't have it without you.

CONTENTS

LIST OF FIGURES

LIST OF TABLES

GLOSSARY

The following glossary contains the abbreviations that were commonly used in this thesis.

HTSPCT	High temperature superconducting partial core transformer
PCT	Partial Core Transformer
dc	Direct Current
ac	Alternating Current
FEA	Finite element analysis
HTS	High temperature superconductor
mmf	Magneto motive force
PIT	Powder in tube
LN_2	Liquid Nitrogen
BSCCO	Bismuth strontium calcium copper oxide
CAM	computer-aided manufacturing
HTSPCTFCL	High temperature superconducting partial core transformer and fault current limiter
UoC	University of Canterbury

Chapter 1
Introduction

1.1 General Overview

In the fast moving world of technology there is a need to modernize and develop new devices that would make our existing systems very efficient. In power systems the primary focus remains on sustainability and the economics behind it.

The process of generation which can be distinguished into renewable and non-renewable generation is itself very intriguing. This can be complimented by the transmission and distribution systems which transfer the electrical energy generated from the generator to the end user.

1.2 Thesis Objectives

This thesis investigates a new device that can be used in the transmission and distribution system .The device involved is a combined transformer and fault current limiter. A transformer is device which transfers electrical energy through the process of mutual induction. A fault current limiter is a device which limits an excessive current flowing through the power system. This protects the various devices from exceeding their specified ratings and thereby making the system more reliable. The combined device uses the construction of the core and windings to which make the transformation and fault current limiting processes feasible.

1.3 Thesis Outline

Chapter 2

The thesis starts with background information on transformers and fault current limiters. An ideal transformer is discussed, followed by the components that add losses in a transformer.

Full core transformers are compared with partial core transformers. A brief about HTS transformers is outlined. Fault current limiters are discussed, followed by some of the different types of superconducting fault current limiters that were studied. The chapter concludes with a

brief description of some of the parameters that limit and/or determine the performance of HTS and the most common manufacturing process of HTS.

Chapter 3

The various design techniques that have been investigated and employed in the course of work has been detailed. Various parameters that form the structure of the design calculations are explained in conjunction with their relationship to each other.

Chapter 4

Partial core transformers with copper windings are tested at room temperature and in liquid nitrogen to investigate the properties of the winding at low temperatures. The measured results are compared with the results obtained using the model discussed in chapter 3. A high temperature superconducting partial core transformer designed at the UoC is presented and also tested. The transformer failed during endurance test and the cause of failure is investigated.

Chapter 5

A model to estimate time at which the high temperature superconductor would melt is then built. The time was calculated to be used in the operation of quench detection mechanism. It could also be used for choosing a circuit breaker based on operating time.

Chapter 6

The proposed design of the high temperature superconducting transformer and fault current limiter is then discussed. Design configurations with different core length and winding length are examined. The chapter concludes with a discussion on the idea behind choosing the final design.

Chapter 7

The process which was adopted in fabricating the prototype of a transformer-fault current limiter is outlined. An alternative design of insulation for the windings is then discussed. The various auxillary units that are used with the new prototype are then highlighted.

Chapter 8

The device was then tested to verify its suitability as a transformer and a fault current limiter. The calculations obtained from the design technique are verified with the ones obtained from experimental results.

Chapter 9

In this chapter the potential application of the new device is outlined.

Chapter 10

The conclusion of this thesis is presented in this chapter.

Chapter 2
Background

2.1 Introduction

An efficient transmission requires power generated to be transmitted with the least possible losses. This can be achieved using transformers which step up or step down the voltages thereby eliminating I^2R losses. The losses occur due to the inherent resistance of the copper conductors used for transmitting electricity. A transmission network uses these transmission lines connected in between through a substation. The components that make this transmission possible are transmission lines, reactors, circuit breakers and other protection equipments that can relay the power generated at the source with the least amount of interruption. While reactors are useful to control the power flow between the various power systems, circuit breakers ensure any overcurrent that occurs due to fault can be isolated without affecting all the feeders in the network. The existing circuit breakers have a current rating which when overcome will cause the circuit breaker to trip. With urbanised growth the power consumption has increased many folds and this requires upgrading the existing system to cope with the new demand. Circuit breakers in the network are expensive to upgrade and therefore a more viable option would be installing fault current limiters to protect the circuit breakers from the overcurrent without altering their ratings.

2.2 Transformers

Transformers tend to take a very large portion of capital investment in a distribution section of a power system. Along with other components that are involved in power distribution, transformers represent an opportunity to make the system cost effective and efficient. Efficiency of a transformer can be gauged by the losses that are present in a transformer. These losses can be categorized as core losses that are the losses that arise due to the type of material used in a core. Losses can also arise due to the dimensions and the structure in which the core is assigned in the transformer. They can be categorized as eddy current and hysteresis losses.

The windings of a transformer can also contribute to losses referred to as winding losses. These winding losses originate due to the types of the material used in the windings. Generally, either copper or aluminium is used, hence due to the resistance of these metals, I^2R losses occur, which

increases the temperature rise of the windings due to the losses being converted into heat. The weight of a transformer also plays a whole in its deployment. As real estate is expensive it becomes necessary to induct a transformer that requires less space and is also light in weight. Combining all the above factors of cost effectiveness, efficiency and weight various transformers results in various types of transformer designs.

2.2.1 Transformer Fundamentals

A transformer consists of a core of magnetic material, primary winding and secondary winding. The primary winding is connected to the power supply which is considered the input side and wound over the core material. The output is taken from the secondary winding and it is also wound over the core material. There is no electrical connection between the input and the output side. Power is transferred by electro-magnetic induction. The electrical circuits of the input and output side are linked by the magnetic field of the core [Hindmarsh, 1977] [Steinmetz, 1895]. Figure 2.1 shows a conventional full core transformer.

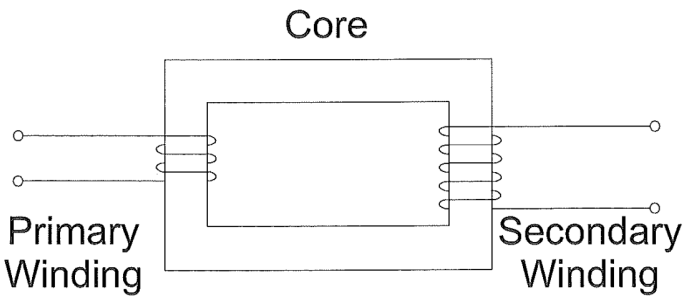

Figure 2.1 A conventional full core transformer

2.2.2 Ideal Transformer

To understand the operation of a transformer, an ideal transformer is considered. In an ideal transformer, the resistance of the windings are negligible, all the magnetic flux links both the primary and secondary windings, the permeability of the core material is extremely high and constant, the hysteresis loss in the core is negligible and there are no eddy current losses in the core or the windings [Connelly, 1950].

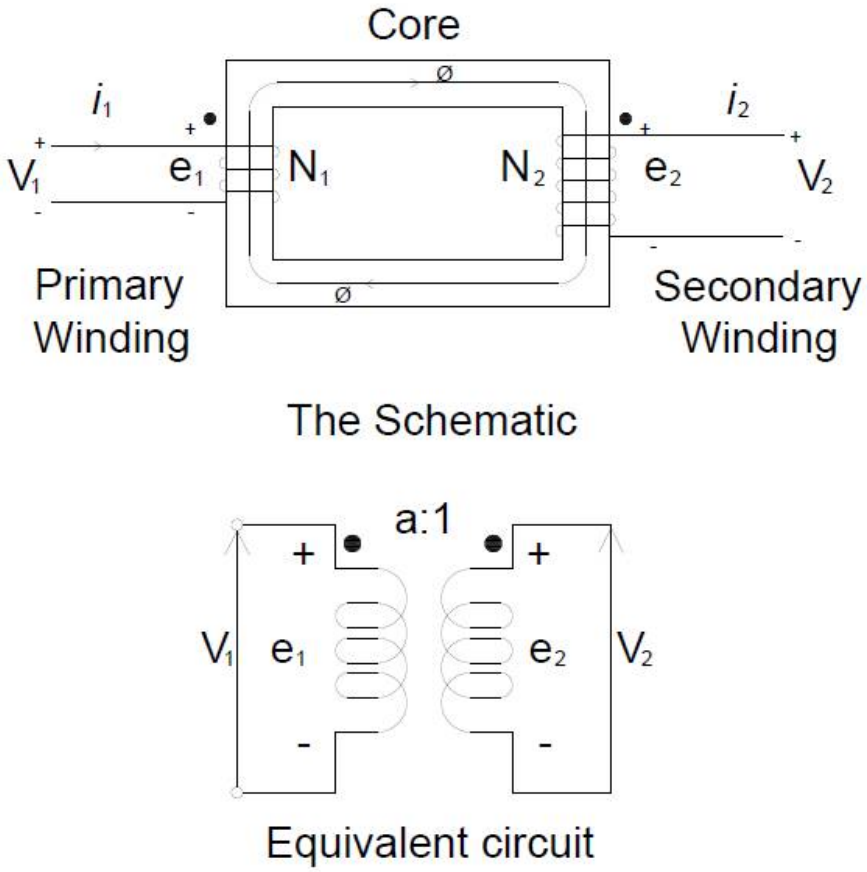

Figure 2.2 An ideal full-core transformer

Figure 2.2, depicts an ideal full core transformer with N_1 turns for the primary winding, N_2 turns for the secondary winding wound on the core. The emf induced in the primary and secondary windings are given by

$$|e_1| = N_1 \left| \frac{d\phi}{dt} \right| \tag{2.1}$$

and $$|e_2| = N_2 \left| \frac{d\phi}{dt} \right| \tag{2.2}$$

For an ideal transformer, $e_1 = v_1$ and $e_2 = v_2$. Therefore, from equation 2.1 and 2.2,

$$\frac{e_1}{e_2} = \frac{V_1}{V_2} = \frac{N_1}{N_2} = a \tag{2.3}$$

where a is the nominal turns ratio.

If the flux varies sinusoidally, then the induced emf linking the N turn winding is given by Faraday's law as

$$E = \frac{\omega N \phi_m}{\sqrt{2}} = 4.44 f N \phi_m \tag{2.4}$$

where $\omega = 2\pi f$ and f is the frequency (Hz). Equation 2.4 is also referred to as emf or Transformer equation [Nasar,1984].

In figure 2.2 , the magnetomotive force (mmf) required to produce the flux is negligibly small. The mmf is due to a combination of the primary current, i_1, and the secondary current, i_2, so that

$$N_1 i_1 = N_2 i_2 \tag{2.5}$$

Therefore,

$$\frac{i_1}{i_2} = \frac{N_1}{N_2} = \frac{1}{a} \tag{2.6}$$

From Equations 2.3 and 2.6, it can be shown that

$$e_1 i_1 = e_2 i_2 \tag{2.7}$$

The apparent powers of the primary winding and secondary winding at any instant are therefore equal. The primary winding absorbs power from the source, while the secondary winding delivers power to the load. In an ideal transformer there is no internal power loss so that these two quantities are equal.

2.2.3 Departure from the ideal

Though it would be ideal to have a transformer, which has the operational characteristics like the ideal transformer, an actual transformer has losses due to their design and physical properties of the materials used [Connelly, 1950].

The most obvious defect is the existence of a current in the primary, even when the secondary is open circuited. This current results from the imperfections of the core which has a finite permeability. Therefore, it requires an appreciable magnetizing force to produce the operating flux. This is represented by a shunt reactance path also known as the magnetizing reactance on the primary side of the transformer. The time varying magnetic flux in the core also causes heating of the core. The heating is due to a combination of hysteresis and eddy current losses. Therefore, some real power is absorbed at no-load. This is represented by the shunt resistance at the primary side, through which core loss current flows.

Both the primary and the secondary winding have finite resistance, which means there are power losses in the windings. In an ideal transformer, all the flux generated by the primary winding links the secondary windings. However in an actual transformer, some of the flux generated travels through the air and doesn't link the secondary winding. This is referred to as the leakage flux. It is modelled as an inductance in series with each winding. The leakage flux causes the voltage to drop and therefore, the turns is no longer equal to the voltage ratio as observed in an ideal transformer.

Figure 2.3 is an equivalent circuit of an actual transformer which comprises of the core resistance, R_{core} magnetizing reactance of the core X_m, the primary resistance, R_1,secondary resistance, R_2 and the leakage reactance of the primary winding, X_1 and the secondary windings, X_2.

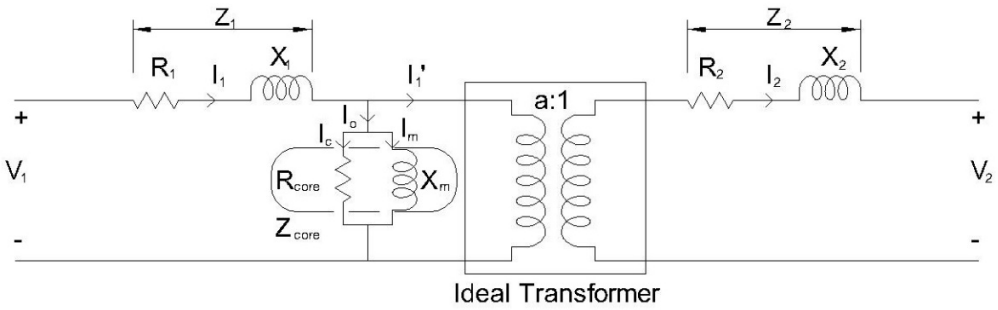

Figure 2.3 Equivalent circuit of an actual transformer

2.2.4 Full core transformers

A full core transformer has a closed core of low reluctance magnetic material to contain the time varying flux. Therefore, the mmf required to drive the flux is minimized and the magnetizing current is negligible when compared to the load current.

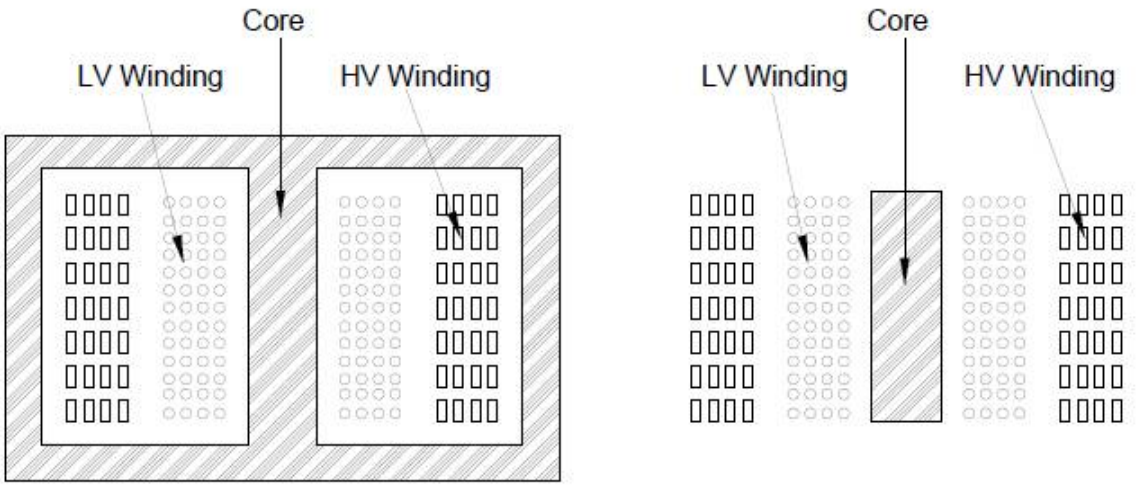

Full core transformer Partial core transformer

Figure 2.4 A full core and a partial core transformer

2.2.5 Partial core transformers

In a partial core design, the core occupies the central space. The windings are wrapped around the core, with the primary winding inside the secondary winding. Layers of insulation separate the primary and secondary winding and also the core and the primary winding. Due to the absence of outer limbs and connecting yokes, the weight is reduced when compared to a full core transformer. The magnetic circuit of a partial core transformer consists of the core and the surrounding air. This results in a high magnetic reluctance when compared with a full core transformer [Liew and Bodger 2001]. The copper losses and efficiency are poor due to the high magnetizing current when compared to a full core transformer. This affects the feasibility of partial core transformer in a power system. However, with high temperature superconductors

(HTS), the conductor losses can be reduced and with the smaller cross sectional area, HTS can be used to design compact partial core transformers.

2.2.6 HTS transformers

A HTS transformer like any transformer consists of a core and windings. The core can be either based on a partial core design or a full core. The core material consists of silicon steel. The windings are made of high temperature superconducting (HTS) material. The use of HTS reduces the winding resistance to approximately zero, which reduces the heat loss caused by the resistance. Therefore, the efficiency of the transformer can be improved substantially.

2.3 Fault current limiters

Large currents flow during a fault, short circuit or any other abnormal conditions in a power system. They can also be due to an ever increasing growth in the load which can translate to a wider network of distribution than the existing one. Upgrading the existing power system is one way to cope with an increasing fault current level. However, the cost involved to upgrade the existing switchgear can be detrimental towards this initiative. A device is required to limit the flow of these large currents in order to protect the existing switchgear from the increasing fault levels. This eliminates the cost involved in upgrading the switchgear and the various components of a power system. Fault current limiters serve the purpose of limiting these large currents. They can be distinguished based on their operating principal. Superconducting fault current limiters (SFCL) and magnetic fault current limiters are certain types that have been investigated in the Engineering community.

2.4 Superconductivity

In 1908, Dutch physicist Kamerlingh Onnes, was the first person to liquefy helium at 4.2 K. Subsequently in 1911, he was able to discover that mercury, when cooled by liquid helium, has no electrical resistance. He named this phenomenon “Superconductivity”. Although superconductors were discovered in 1911, high temperature superconductors were only discovered in 1987. This enabled material to become superconducting at liquid nitrogen

temperatures, rather than at liquid helium temperatures As a result, the operating cost of using superconductors came down. This opened the way to use superconductors in power system applications [NREL, 1998].

Superconductors are classified into two types, type-I and type-II. Type-I superconductors are defined as conventional superconductors that have a transition temperature (T_c) below 30K. Type-I superconductors are described by two major theories. BCS [Bardeen et al. 1957] and Ginzburg-Landau [Ginzburg *et al.* 1950] theorem. BCS theory is a microscopic theory. It explains the second-order phase transition in critical temperature. BCS theory describes superconductivity as a microscopic effect which results from a Bose condensation of Cooper Pair [Bardeen *et al.* 1957] electrons. Ginzburg-Landau theory on the other hand, considers modeling superconductivity using mathematical methods to explain the macroscopic elements of superconductors.

However, for type-II superconductors, there is no widely accepted theory to explain their properties. Type-II superconductors are also known as High Temperature Superconductors (HTS). HTS have a critical transition temperature above 30K. This was thought to be un-achievable by BCS theory. HTS are mostly cuprate based superconductors . Yttrium-Barium-Copper-Oxide and Bismuth-Strontium-Calcium-Copper-Oxide (BSCCO) are the most common HTS. They have critical temperatures at 92 K and 110 K respectively.

The basic premise behind using HTS is that they tend to quench once the magnetic field density, temperature and conductor current are breached beyond their critical limits. Once this limit is breached they tend to change from a superconducting state to a resistive state. It is this behavior of superconductors that has carved the path towards using superconductors as fault current limiters.

2.5 Types of fault current limiters

Superconducting fault current limiters are based on high temperature superconductors (HTS). They rely on the change of electrical properties of the superconducting wire. The wire posses very low resistance during the normal state which is also known as the superconducting state. It offers a very large resistance during the fault state and thereby limits the fault current. [E.Thuries *et al.* 1991] [Meerovich *et al.* 1995, Weijers *et al.* 1995, Xiao *et al.* 1999, Coway *et al.* 2000]

A magnetic current limiter is based on saturable core and windings. During normal operation the inductance offered by the limiter is negligible; while during fault conditions the large value of the fault current forces the core to come out of saturation and go to an unsaturated state. This causes

a change in inductance and this large unsaturated inductance is used to limit the fault current. [Darmann *et al.* 2003]

Several types of superconducting fault current limiters (SFCL) have been designed and tested by the engineering community, they include self-limiting transformer combining the functions of a power transformer with the functions of a current limiter [Vajda *et al.* 2007], inductive fault current limiters with closed and open core [Janowski *et al.* 2003], inductive/electronic fault current limiter that can double as a fast sub-cycle solid state breaker [Leung *et al.* 2000], hybrid high temperature superconducting FCL [Steurer *et al.* 2000] [Tixador 1995], series and shunt based FCL [Kalsi *et al.* 2004], inductive SFCL [Paul *et al.* 1995]. The most widely explored have been based on an inductive or resistive principle.

2.6 Parameters of a HTS tapes

The advantages highlighted the advantages of having a high temperature superconductor as a winding material. HTS tapes have certain operational parameters which can limit their use in our proposed device. Therefore, it is important to investigate these parameters before incorporating a HTS BSSCO tape in our design.

2.6.1 Parameters Defined

Width, thickness, critical strain, critical stress, critical temperature, critical current, quench stability and insulation are some of the parameters that have been investigated for the BSCCO tape.

Critical Current

The critical current of a HTS tape is the maximum current which would allow a voltage drop of 1 μV over a distance of 1 cm. In short, the critical current defines the transition between superconducting and normal state. It's dependent on magnetic field, temperature and strain.

The critical current density is the critical current divided by the total cross-sectional area of the HTS ceramic, in the case of the HTS tape it can be further stated as the critical current divided by the cross-sectional area of the HTS tape. The critical current is denoted as I_C, while critical current density is denoted as J_c [Vase *et al.* 2000].

Critical Temperature

A HTS tape exhibits the property of superconductivity only below a certain temperature. The critical temperature is the minimum temperature where the critical current is zero. Equation 2.1 displays the relationship between the critical current density and the temperature [Vase *et al.* 2000]

The current density is inversely proportional to the temperature.

$$J_c = J_c(0)\left(1-\frac{T}{T_C}\right) \tag{2.8}$$

Where T_c is the critical temperature and $J_c(0)$ is the critical current density at 0 K.

Magnetic field

HTS tapes have a very strong magnetic field dependence that is also strongly anisotropic. Magnetic fields parallel to the tape's wide surface have less impact on the critical current than fields perpendicular to the tape's wide surface. The critical current density has a logarithmic dependence on magnetic fields. It can be described for all fields by the equation,

$$J_c = \frac{J_{c0}}{\log(B_{Self} / B_{irr})}\log(B / B_{irr}) \tag{2.9}$$

Where J_{co} is the J_c with no external field, B is the applied magnetic field, B_{self} is the calculated self-field generated by the critical current in zero external field and B_{irr} is the irreversibility field [Vase *et al.* 2000].

The relationship between the perpendicular and the parallel magnetic field to the critical current can be further described by the formulae [Kim et *al.* 1962],

$$I_{c\perp} = \frac{I_{c0}}{1+\left(\frac{B}{B_\perp}\right)^{P\perp}} \tag{2.10}$$

and $$I_{c\parallel} = \frac{I_{c0}}{1+\left(\frac{B}{B_\parallel}\right)^{P\parallel}} \tag{2.11}$$

where $I_{c\perp}$ is the critical current in the perpendicular field, $I_{c\parallel}$ is the critical current in parallel field, I_{c0} is the critical current in the self-field, and $B_{\perp}$ and $P_{\perp}$ are the fitted parameters [Kim et *al.* 1962].

2.7 BSCCO tape

2.7.1 Chemical composition

The BSCCO ceramic is abbreviated as $Bi_{1.5}Pb_{0.5}Sr_2Ca_2Cu_3Ox$ where 1.5 and 0.5 refer to the total number of Bi and Pb atoms in a molecule. The HTS tapes are formed by embedding the ceramic in a metal alloy lattice like silver and can also be referred as BSCCO/Ag.

2.7.2 Manufacturing technique of a BSCCO Tape

The HTS tape used in our device is a brittle ceramic material in a silver alloy tube. It is manufactured using powder in tube (PIT) manufacturing process. The fraction of ceramic, λ in the tape is also determined during this process. Under this process, the precursor ceramic powder is placed in a silver alloy tube. The precursor consists of Bi-2212+ secondary phases, which are converted to Bi-2223. Though mechanical deformation is another viable process which can be used to produce this ceramic material, the powder in tube method allows for a ceramic with a better texture.

Silver is used as a lattice material because it doesn't react with the precursor and allows oxidation during heat treatment. The powder in tube is then drawn, cut and placed back into another silver tube with similar HTS/Silver wires. This is then flattened to form a tape. The tape allows for more flexibility and reduces the strain when wound into a coil. The flat shape is also required due to the anisotropic nature of HTS ceramics. Fig 2.5 illustrates the ceramic wire. The Bi-2223 ceramic filament is surrounded by the silver lattice.[Vase *et al.* 2000] Fig 2.6 (a) shows the tape after it is flattened and figure 2.6 (b) shows the tape the final tape.

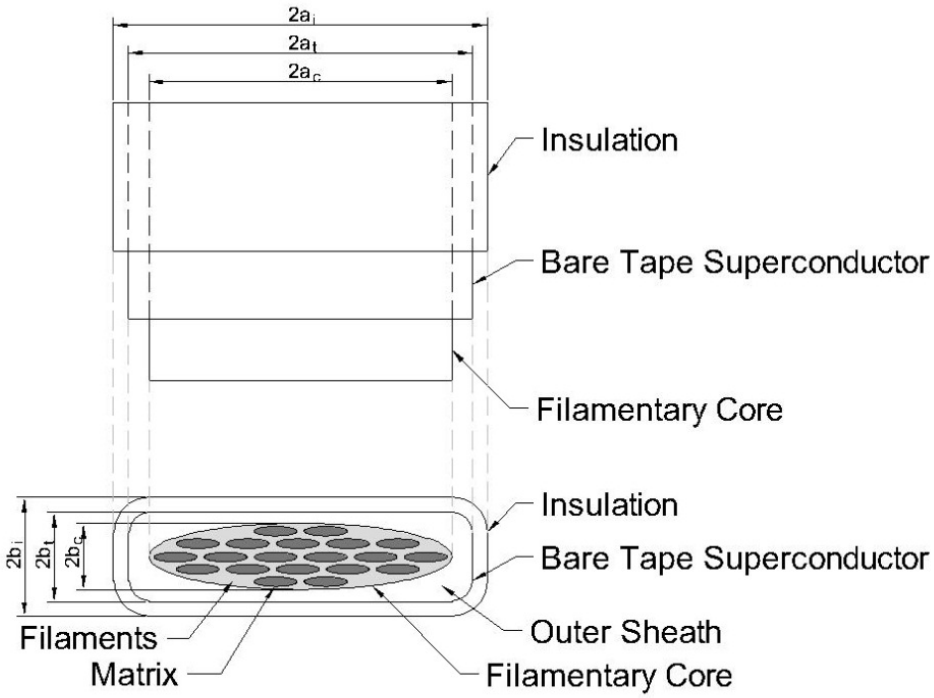

Figure 2.5 Ceramic wire

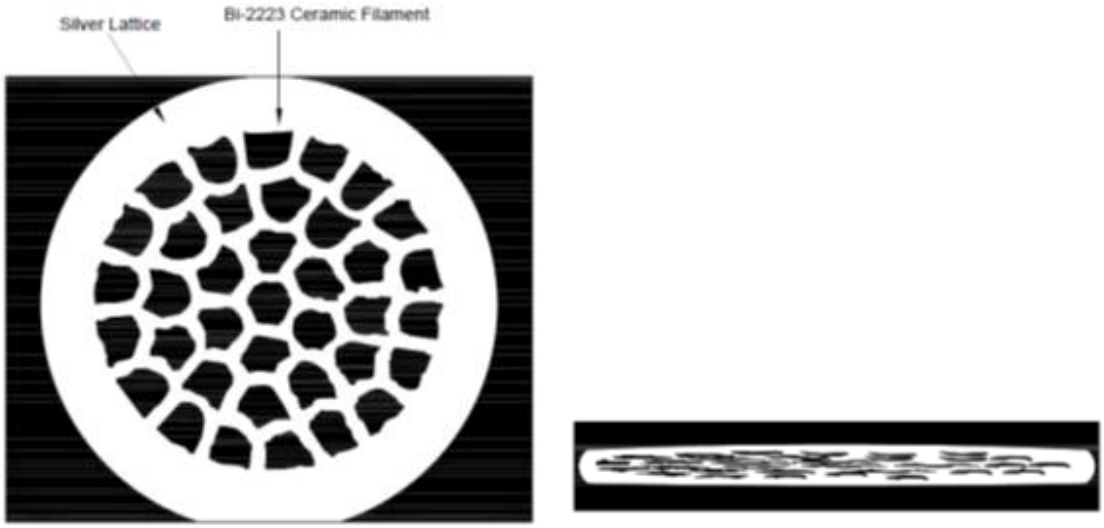

Figure 2.6 (a) Magnified cross-sectional view of the multifilament wire after drawing (b) Magnified cross-sectional view of the final tape

Chapter 3
Design method

3.1 Introduction

In this chapter, the reverse design model that is used to design the partial core unit is detailed.
The model takes into account the physical characteristics, such as material resistivities and permeabilites, and dimensions of the windings and the core as the specifications. By altering these specifications, the performance of the device can be optimized and a suitable design can be obtained. A Steinmetz model is used to depict the equivalent circuit parameters of the device.
An Excel program has been developed for this reverse design model. The model serves as a better gauge to test the proposed design before actually fabricating it.

3.2 Reverse design

In a conventional transformer design approach the terminal voltages, VA rating and frequency determine the material to be used and their dimensions. It is not always feasible to obtain materials with the exact characteristics and dimensions that the conventional design approach requires. Vendors provide their catalogues with fixed sizes for core and winding materials. This can be partially due to economic considerations and partially due to limitations in the manufacturing capabilities of the vendors. Therefore, in the absence of materials which do not match the required specifications, a customized design might be required. The conventional approach leads to fixed sized transformers which are often over-rated and therefore lead to uneconomic products [Bodger et *al.* 2000].
The reverse design method takes into account the physical characteristics and the dimensions of the core and windings. By manipulating the type and amount of material required, the performance of the transformer can be determined. This allows for a cost effective solution especially when there are limitations in the availability of materials to build a transformer.

3.3 Reverse design method

The physical dimensions of the core, primary winding and the secondary winding are taken as the input parameters. As shown in Fig 3.1, the resistivity of the winding $\rho_1 and \rho_2$, the core material resistivity ρ_{core} are also the input specifications which can be set for different materials chosen in the design process. The stacking factor is calculated from the ratio of the iron to total volume. In conjunction with the above parameters, the insulation thickness can also be specified.

The primary voltage and the frequency are the only rating requirements in the design process. The secondary voltage and the transformer VA rating are a result of the construction of the transformer.

Once the dimensions and the material characteristics of the transformer are known the equivalent circuit components are calculated.

Fig 3.1 represents the axial view of a transformer designed using reverse design method. The number of layers are modified to suit the transformer rating requirements and the insulation thickness is adjusted for high voltage applications.

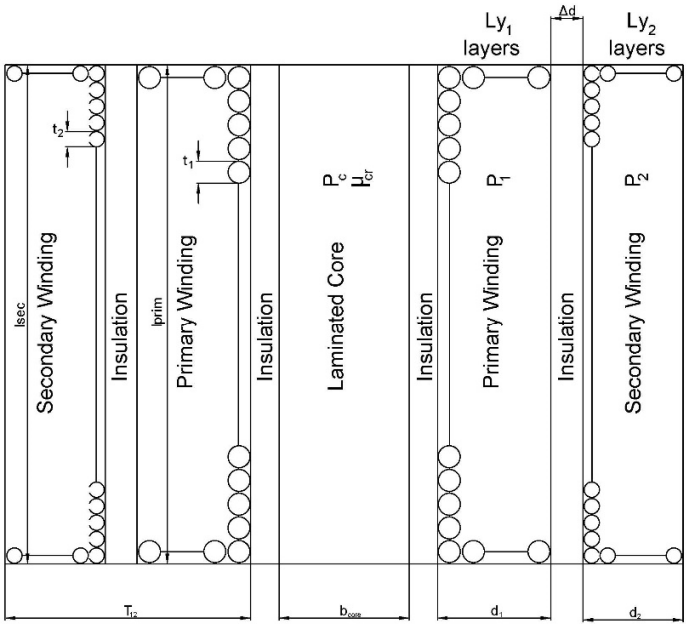

Figure 3.1 Axial representation of the proposed HTSPCTFCL

3.4 Excel model

Tables 3.1 to 3.3 tabulate the input specifications of the core and the windings that are used in the Excel design sheet.

Table 3.1 Core input parameters

Abbreviations	Specifications	units
d_{core}	External diameter of the circular core	m
l_{core}	Length of the core	m
SF_c	Stacking factor	
th_{former}	Former thickness	m
μ_{rc}	Relative permeability	
ρ_{core}	Resistivity of the core material	Ωm
$\Delta\rho_{core}$	Thermal resistivity coefficient	/C
T_{core}	Operating temperature	C
γ_{core}	Material Density	kg/m^3
c_{lam}	Lamination thickness	m

Table 3.2 Primary winding input parameters

Abbreviations	Specifications	units
l_{prim}	Length	m
Ly_1	Layers	
PC_1	Parallel conductors	
w_1	Width of HTS tape	m
th_1	Thickness of the HTS tape	m
w_{i1}	Tape insulation thickness	m
I_{th1}	Insulation layer thickness	m
ρ_{1_20C}	Resistivity at 20 ^{0}C	Ωm
$\Delta\rho_1$	Thermal resistivity coefficient	/C
I_{c1}	Critical current	A
T_1	Operating temperature	C
γ_1	Material density	kg/m^3
C_1	Material cost	$/kg
$\rho_{1optemp}$	Resistivity at operating temperature	Ωm
$I_{th\_form\_1}$	Insulation between former and primary winding	m

Table 3.3 Secondary winding input parameters

Abbreviations	Specifications	units
$l_{\sec}$	Length	m
Ly_2	Layers	
PC_2	Parallel conductors	
w_2	Width of HTS tape	m
th_2	Thickness of the HTS tape	m
w_{i2}	Tape insulation thickness	m
I_{th2}	Insulation layer thickness	m
ρ_{2_20C}	Resistivity at 20^0C	Ωm
$\Delta\rho_2$	Thermal resistivity coefficient	/C
I_{c2}	Critical current	A
T_2	Operating temperature	C
γ_2	Material density	kg/m^3
C_2	Material cost	$/kg
$\rho_{2optemp}$	Resistivity at operating temperature	Ωm
$I_{th\_1\_2}$	Insulation between primary and secondary	m

3.5 Calculations of individual components of the core and windings

In this part of the design process the individual components of the windings and the core are calculated.

3.5.1 Number of turns of the primary winding

The number of turns of the primary winding is given by:

$$N_1 = Ly_1 \frac{l_{prim}}{w_1 + 2w_{i1}} \tag{3.1}$$

where l_{prim} is length of the primary winding

Ly_1 is number of layers of the primary winding

w_1 is width of the HTS tape

w_{i1} is tape insulation thickness

3.5.2 Number of turns of the secondary winding

The number of turns of the secondary winding is given by:

$$N_2 = Ly_2 \frac{l_{\text{sec}}}{w_2 + 2w_{i2}} \tag{3.2}$$

where l_{sec} is length of the secondary winding
Ly_2 is number of layers of the secondary winding
w_2 is width of the HTS tape
w_{i2} is tape insulation thickness

3.5.3 Turns ratio

The turns ratio can be calculated by dividing the number of turns of the primary winding by the number of turns of the secondary winding:

$$a = \frac{N_1}{N_2} \tag{3.3}$$

3.5.4 Core flux characteristics

In order to calculate the core flux characteristics of a partial core transformer, the core cross sectional area, A_{core}, length of the core, l_{core} and the diameter of the core, d_{core} are used as input parameters. An axial view of the transformer as shown in figure 3.2 is used to highlight these parameters.

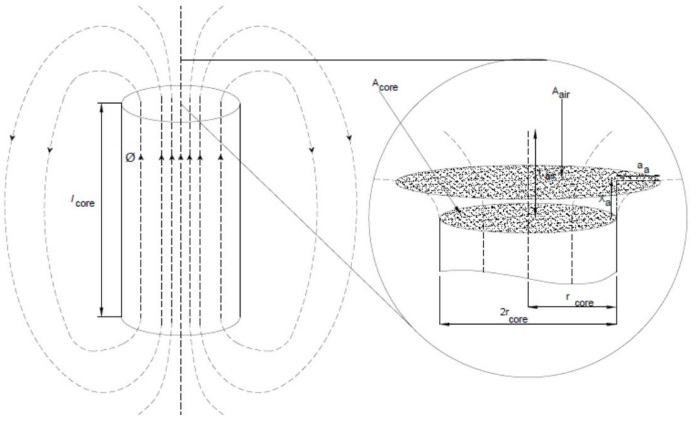

Figure 3.2 Axial view of the transformer

3.5.4.1 Core cross sectional area

The cross sectional area of the core is calculated as:

$$A_{core} = \pi \frac{d_{core}^{\ 2}}{4} SF_c \tag{3.4}$$

where A_{core} is core cross sectional area
d_{core} is diameter of the core
SF_c is stacking factor of the core

3.5.4.2 Maximum flux density

The maximum flux density is calculated as:

$$B_{core} = \frac{V_1}{4.44 f N_1 A_{core}} \tag{3.5}$$

where V_1 is the supply voltage
f is fundamental frequency of the system
N_1 is number of turns of the primary winding
A_{core} is core cross sectional area

3.5.4.3 Air reluctance

In a partial core transformer the flux density in the air is only significant near both ends of the core. Therefore, only the air reluctance at the ends are considered. By applying integration over the entire air path, the air reluctance can be calculated in simplified form as [Liew, 2001]:

$$R_{air} = \frac{169356}{A_{core}^{\ 0.345} l_{core}^{\ 0.31}} \tag{3.6}$$

where A_{core} is core cross sectional area
l_{core} is length of the core

3.5.4.4 Core reluctance

In a partial core transformer the flux lines are considered to be uniform within the core. The core reluctance is [Liew, 2001]:

$$R_{core} = \frac{l_{core}}{\mu_0 \mu_{rc} A_{core}} \tag{3.7}$$

where l_{core} is length of the core
μ_0 is permeability of free space
μ_{rc} is relative permeability of the core
A_{core} is cross sectional are of the core

Since in a partial core transformer the flux path is through air and the core, the total core reluctance is the sum of core reluctance and twice the air reluctance. Fig 3.3 depicts the equivalent magnetic circuit of the transformer.

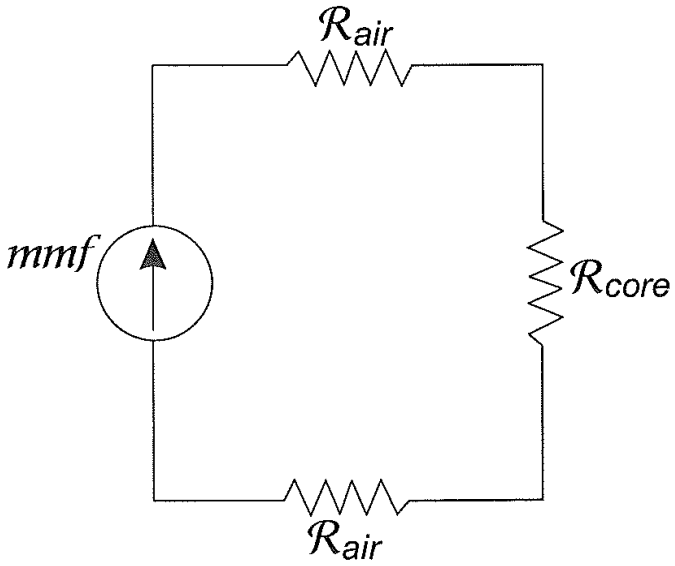

levice

Figure 3.3 Magnetic circuit of the transformer

Therefore the total core reluctance is:

$$R_{total} = R_{core} + 2R_{air} \tag{3.8}$$

3.5.5 Core characteristics

3.5.5.1 Equivalent permeability

The equivalent permeability of the core can be calculated as:

$$\mu_{rc} = \frac{l_{core}}{\mu_0 R_{total} A_{core}} \tag{3.9}$$

where μ_0 is permeability of free space
R_{total} is the total core reluctance
A_{core} is core cross sectional area

3.5.5.2 Volume of the core

The volume of a partial core is used to calculate the weight of the core and also the hysteresis losses of the core. Since the partial core has a geometry, the volume is calculated as follows:

Volume of the partial core, $v = \pi r^2 h$ (3.10)

3.5.5.3 Power losses in a transformer

Transformer losses are divided into losses in the windings and those in the magnetic circuit. In a HTS transformer the winding losses are minimal and most of the losses associated with it are the magnetic losses, which are also known as iron losses. These iron losses can be further divided into hysteresis and eddy current losses.

3.5.5.3.1 Hysteresis losses

When the magnetic field of a transformer is reversed, a small amount of power is lost due to hysteresis within the core. The loss is proportional to the frequency, and is a function of the peak flux density to which it is subjected [Liew, 2001].

$$P_h = 0.11 \times v \times \gamma_{core} \times f \times B_{core}^{1.85} \tag{3.11}$$

where v is the volume of the core
γ_{core} is the density of the core
f is the frequency at which voltage is supplied
B_{core} is the flux density of the core

3.5.5.3.2 Eddy current losses

In a partial core transformer eddy currents circulate within the core in a plane normal to the flux. They add to the resistive heating of the core material. The eddy current losses in a partial core transformer are calculated as [Liew, 2001]:

$$P_{ec} = \frac{c^2{}_{lam}}{12\rho_{core}} \frac{l_{core}}{N_1{}^2 A_{core}} e^2{}_1 \tag{3.12}$$

3.5.6 Winding parameters

3.5.6.1 Length of the winding

To calculate the length of the tape, the circular geometry of the device is taken into consideration. First the radius of the circular core is factored, followed by the thickness of each winding and the thickness of insulation between the various windings of the primary and the secondary. Once these parameters are calculated, the circular thickness for each winding is multiplied with the number of turns of each winding.

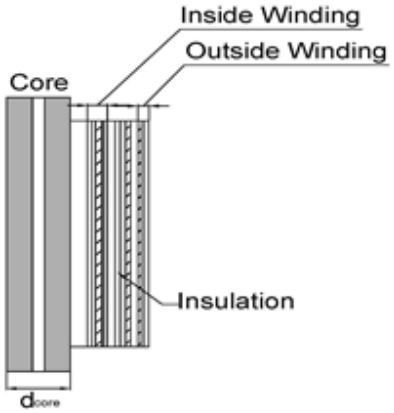

Figure 3.4 Axial view of a partial core transformer

Figure 3.1 and 3.4 are used to formulate the length of the wire conductor as:

Wire length per conductor for primary= $\pi\times((d_{core}+2\times th_{former}+2\times((Ly_1\times(th_1+2\times w_{i1})+(Ly_1-1)\times I_{th1}))\times N_1$ (3.13 a)

Similarly, Wire length per conductor for secondary = $\pi\times((d_{core}+2\times th_{former}+2\times((Ly_1\times(th_1+2\times w_{i1})+(Ly_1-1)\times I_{th1})+2\times I_{th\_1\_2}+2\times(Ly_2\times(th_2+2\times w_{i2})+(Ly_2-1)))\times N_2$ (3.13 b)

for multiple windings the above formula can be expanded to include the individual winding thicknesses and the respective insulation.

3.5.7 Equivalent circuit parameters

The equivalent circuit parameters of a transformer can be combined into the Steinmetz model [Steinmetz. 1895] as shown in Figure 3.6. The parameters such as winding resistance, core resistance, magnetizing reactance and leakage reactance of the partial core transformer are calculated as follows.

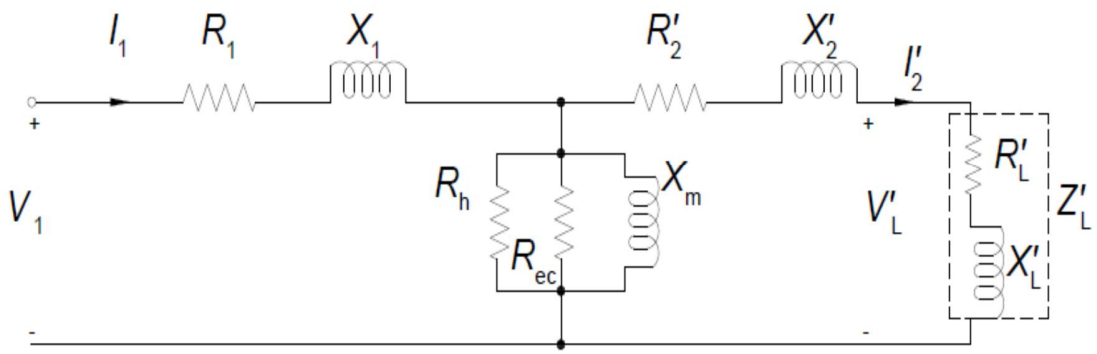

Figure 3.5 Equivalent circuit of a transformer

3.5.7.1 Winding resistance

In a traditional transformer, the windings are usually made from cooper wire. The resistance of the winding depends on the conductor resistivity and its dimensions.

The resistance is given by:

$$R_w = \rho \times \frac{l}{A_{winding}} \tag{3.14}$$

where ρ is the resistivity of the conductor
l is the length of the conductor
$A_{winding}$ is the cross sectional area of the conductor

However, for the superconducting transformer, part of the winding losses are due to ac losses of the HTS material. The rest are due to the resistance of the connecting lead-outs and bushings.

3.5.7.2 AC losses in a superconducting tape.

There are many different types of AC losses associated with a superconducting tape. There are many engineering formulas that have been developed to describe these losses. The one thing that many theories have in common is the dependence of these losses on the direction and amplitude of an alternating magnetic field combined with an alternating current. Empirical methods such as the pickup coil method [Carr. 1979] [Kawabata et al. 2003], which can determine the total loss density of the tape, but not much work has been done in exploring the deducing the individual loss components. The ac loss for the superconducting tape is comprised of two components, losses due to the transport current and power loss due to the magnetic interaction of HTS.
The transport losses are further comprised of resistive losses, self-field losses, and dynamic resistance losses. However, the resistive losses only make up a small fraction of the transport current losses. The majority of the transport current losses consist of the dynamic resistance and self-field losses. The two losses were considered in the model for calculating the resistance of the superconductor under superconducting state.

3.5.7.2.1 Self Field Loss

The self-field loss is associated with the magnetic field that is generated by the tape itself when an alternating current is passed through the tape. It is independent of external magnetic fields and is due to the penetration of the magnetic field into the tape [Rabbers *et al.* 2001]. The self-field loss is described by [Oomen *et al.* 2003] and simplified as:

$$P_{sf} = \frac{\mu_0 f}{4\pi} \frac{I_{sc}^{3.5}}{I_{c,avg}^{1.5}} l_{sc} \tag{3.15}$$

where, I_{sc} is the current amplitude through the superconducting filaments (A)
$I_{c,avg}$ is the average critical current of the superconductor (A)
l_{sc} is the total length of the superconductor (m)

3.5.7.2.2 Dynamic Resistance

The dynamic resistance is defined as the resistance due to the interaction between the transport current and the external alternating magnetic field [Oomen *et al.* 2003].

The dynamic power loss is given by:

$$P_{dyn} = (C_5 \cos(\Theta) + C_6 \sin\Theta) B_a I_a{}^2 V \quad \text{(W)} \tag{3.16}$$

where C_5, C_6 are constants obtained from measurement
V is the total volume of the superconductor tape

Equation 3.16 is further simplified as

$$P_{dyn} = P_{dyn,\,perpendicular} + P_{dyn,\,parallel} \tag{3.17}$$

$$P_{dyn,\,perpendicular} = \eta_{\,perpendicular} \frac{fw}{I_{c,avg}} B_a I_{a,sc}{}^2$$

And $$P_{dyn,\,parallel} = \eta_{\,parallel} \frac{fd}{I_{c,avg}} B_a I_{a,sc}{}^2 \tag{3.18}$$

where $\eta_{\,perpendicular}$ and $\eta_{\,parallel}$ are the percentage of superconductor in the parallel and perpendicular direction respectively.

3.5.7.3 Resistance of the Ag matrix

When the critical current is breached, the superconducting transitions from superconducting state to conducting state. The resistance during its conducting state is calculated as [Oomen *et al.* 2003],

$$R_{Ag} = \rho_{Ag} \frac{l_w}{A(1-\lambda)} \tag{3.19}$$

where λ is the fraction of the superconducting filaments in the cross sectional area of the tape
ρ_{Ag} is the resistivity of silver at 77 K
l_w is the length of the superconducting tape
and A is the cross sectional area of the tape

3.5.7.3 Core resistance

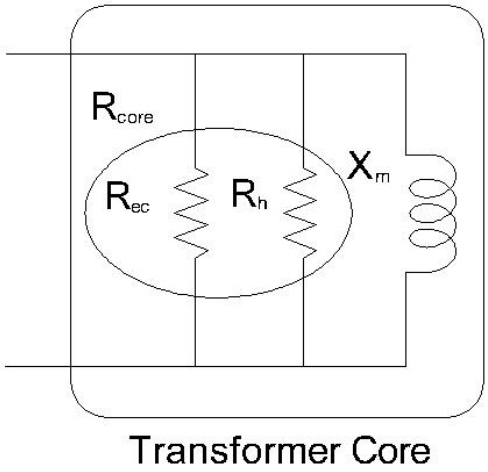

Figure 3.6 Transformer core equivalent circuit

Referring to the equivalent circuit in figure 3.6 core resistance can be calculated as:

$$R_c = \frac{R_{ec} R_h}{R_{ec+} R_h} \tag{3.20}$$

where R_c is the core resistance

R_{ec} is the eddy current resistance

R_h is the hysteresis resistance

3.5.7.4 Eddy current resistance

The eddy current resistance of the core is [Liew, 2001]

$$R_{ec} = \frac{N_1^{\,2} \times A_{core} \times 12 \times \rho_{core}}{l_{core} \times c_{lam}^{\,2}} \tag{3.21}$$

where N_1 is the number of turns of the primary winding

A_{core} is the core cross sectional area

ρ_{core} is the resistivity at 20^0 which is the assumed room temperature

l_{core} is the length of the core

c_{lam} is the thickness of each lamination of the core

3.5.7.5 Hysteresis resistance

The hysteresis resistance of the core is [Liew, 2001]

$$R_h = \frac{V^2}{P_h} \tag{3.22}$$

where V is the voltage of the inside winding voltage
P_h is the hysteresis loss of the core

3.5.7.6 Magnetizing reactance of the core

From Faraday's law, the induced voltage in the primary winding of the transformer is given by [Liew, 2001]

$$e_1 = N_1 \frac{\delta\phi}{\delta t} \tag{3.23}$$

The correlation between the maximum flux density, B_{core} in the transformer and the magnetic field strength, H_{core} is further taken into account to derive the following

$$\phi = B_{core} A_{core} \tag{3.24}$$
$$B_{core} = \mu_0 \mu_{rc} H_{core} \tag{3.25}$$
$$H_{core} l_{core} = N_1 i_1 \tag{3.26}$$

Substituting equations 3.22, 3.23 and 3.24 in equation 3.21

$$e_1 = \frac{N_1{}^2 A_{core} \mu_0 \mu_{rc}}{l_{core}} \frac{\delta i_1}{\delta t} \tag{3.27}$$

The induced voltage can also be defined as

$$e_1 = L_m \frac{\delta i_1}{\delta t} \tag{3.28}$$

Therefore, from equations 3.25 and 3.26, the magnetizing inductance can be defined as

$$L_m = N_1{}^2 \frac{\mu_0 \mu_{rc} A_{core}}{l_{core}} \tag{3.29}$$

Since $X_m = \omega L_m$ (3.30)

The core magnetizing reactance is deduced from 3.27 and 3.28 as follows

$$X_m = \frac{\omega N_1^{\,2} \mu_0 \mu_{rc} A_{core}}{l_{core}} \tag{3.31}$$

However, in a partial core transformer, the magnetic flux generated by the energized primary winding flows through the core and returns via air, back to the core. Hence the reluctance of the magnetic flux path is significantly greater that if it was constrained in a full core. Therefore, the overall relative permeability of the transformer should be much lower than that of core material. And a new overall relative permeability, which takes into account the magnetic flux path in the air, was deduced [Liew, 2001].

$$\mu_{rT} = \frac{l_{core}}{\mu_0 R_T A_{core}} \tag{3.32}$$

where R_T is the total reluctance of the partial core

Therefore the magnetizing reactance of a partial core transformer can be deduced as

$$X_m = \frac{\omega N_1^{\,2} \mu_0 \mu_{rT} A_{core}}{l_{core}} \tag{3.33}$$

3.5.7.7 Leakage reactance of the transformer

To calculate the leakage reactance of a partial core transformer, the axial view of a partial core shown in figure 3.8 is used as reference.

The leakage reactance of the transformer is calculated as [Liew, 2001]

$$X_{12} = \omega \mu_0 \frac{N_1^{\,2}}{l_c} \left(l_p \frac{d_1}{3} + l_s \frac{d_2}{3} + l_{ps} \Delta d \right) \tag{3.34}$$

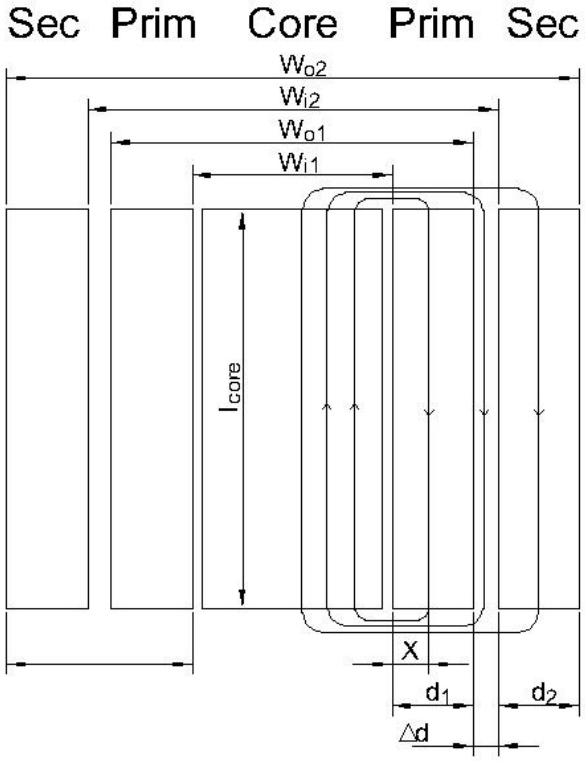

Figure 3.7 Axial view of a partial core to deduce leakage reactance

where $l_p = \pi \frac{wi_1 + wo_1}{2}$ (3.35)

$$l_s = \pi \frac{wi_2 + wo_2}{2} \quad (3.36)$$

$$l_{ps} = \pi \frac{wo_1 + wi_2}{2} \quad (3.37)$$

And $wi_1 = d_{core} + th_{form}$

$wo_1 = d_{core} + th_{form} + 2 \times d_1$

$wi_2 = d_{core} + th_{form} + 2 \times d_1 + 2 \times I_{th\_1\_2}$

$wo_2 = d_{core} + th_{form} + 2 \times d_1 + 2 \times I_{th\_1\_2} + 2 \times d_2$

Where in d_1 and d_2 are the thickness of the primary and the secondary windings respectively.
The winding thickness are calculated as follows

$$d_1 = d_2 = (th_1 + 2 \times w_{i1} + I_{th1}) \times (Ly_1 - 1) + (th_1 + 2 \times w_{i1})$$

3.5.8 Performance Measures

3.5.8.1 Open circuit performance

A transformer is said to be in an open circuit condition when there is no load connected across the secondary terminals. Since the secondary winding is open circuit, there is no current flowing through it. Fig 3.8 displays the circuit diagram of the transformer under open circuit. A phasor diagram relating the variables of the circuit digram is displayed in fig 3.9

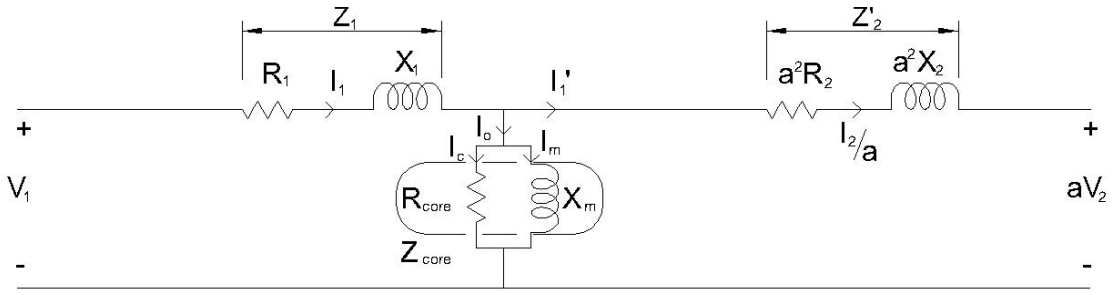

Figure 3.8 Circuit diagram of a transformer for no-load test [Steinmetz. 1895]

The voltage applied across the terminals of the primary is the sum of voltage drop across the primary winding parameters and the core emf. The real power input to the transformer is the sum of the losses across the winding resistance R_1 and the core loss. Also, since the impedance of the core is larger than the impedance of the windings, the voltage drop across the core is much larger than the voltage drop across the winding. Therefore the loss in the winding resistance can be neglected and the real power drawn from the source is dissipated as heat in the core. If I_o and Pin are the current and power into the transformer at the rated voltage, then:

$$\text{Cos } \theta = \frac{Pin}{V_1 I_0} \qquad (3.38)$$

$$I_c = I_0 \cos \theta \qquad (3.39)$$

$$I_m = I_0 \sin \theta \qquad (3.40)$$

$$R_m = \frac{V_0}{I_c} \text{ and } X_m = \frac{V_0}{I_m} \qquad (3.41)$$

The phasor diagram in fig 3.9 gives a representation of the circuit under no-load conditions.

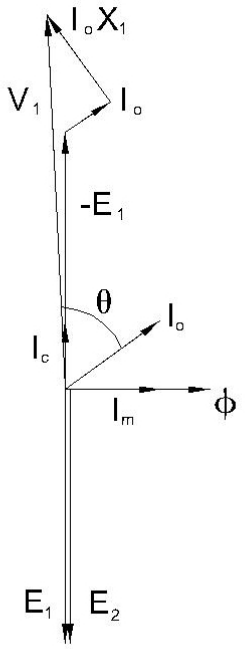

Figure 3.9 Phasor diagram under no-load condition

3.5.8.2 Short circuit test

The circuit in figure 3.10 represents the transformer under short circuit. The input voltage is reduced to a small fraction of the rated value and the secondary terminals are short circuited. Since a small fraction of the rated voltage is applied to the primary side of the transformer, the flux in the core is very small. The test also enables the equivalent circuit series parameters to be determined.

When performing this test, the primary voltage is gradually applied till the rated current flows in the windings. As most of the current flows through the secondary winding the current flowing through the core is negligible. This translates to a very low core loss. Thus effectively, all the real power losses are in the windings.

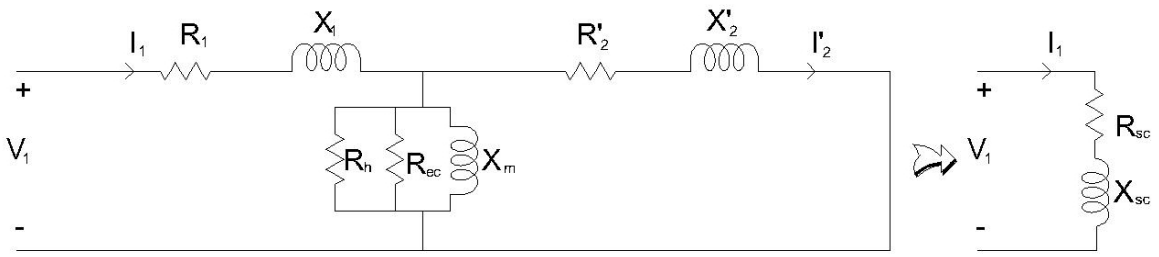

Figure 3.10 Short circuit test diagram

If $V_1 = V_{sc}$ in the circuit then the equivalent parameters can be calculated as:

$$V_{SC} = \frac{Z_{SC}}{I_{SC}} \quad (3.42)$$

$$Z_{SC} = V_{SC} \times I_{SC} \quad (3.43)$$

$$P_{in} = V_{SC} \times I_{SC} \times \cos\theta \quad (3.44)$$

where *cos*θ is the power factor of the transformer under this test.

The equivalent components of resistance and leakage reactance of the transformer can be calculated by:

$$R_{SC} = Z_{SC} \times \cos\theta \text{ and } X_{SC} = Z_{SC} \times \sin\theta \quad (3.45)$$

$$R_{sc} = R_1 + R_2' \quad \text{and} \quad X_{sc} = X_1 + X_2' \quad (3.46)$$

In these equations the magnetizing reactance and the core resistance have been ignored as in a short circuit condition the voltage drop across the core is negligible and therefore the current across it is approximately zero.

3.5.8.3 Load test

The total loss that takes place in a transformer can be determined by applying a rated load across the secondary terminals. In this test, a rated voltage is applied across the primary terminals in conjunction

with the rated current. The rated current is determined by dividing the transformer VA rating by the rated voltage. Similarly, the rated load is calculated from the rated voltage and the rated current of the transformer. The transformer is said to be fully loaded when the rated load is across the secondary terminals.

Once the total transformer losses are determined, the power output across the load can enable yhe determination of the efficiency of the transformer. Further, the voltage drop across the secondary terminals enables the transformer's regulation to be determined.

The efficiency and regulation of a transformer can be summarized using.

$$\text{Efficiency, } = \frac{output\_realpower}{input\_realpower} = \frac{P_{out}}{P_{in}} \quad (3.47)$$

The input real power can also be designated in terms of the losses as:

$$\text{Efficiency, } \eta = \frac{output\_realpower}{output\_realpower + winding\_losses + core\_losses} \quad (3.48)$$

Also the regulation is defined as:

$$\%\ \text{Regulation} = \frac{Vno\_load - Vfull\_load}{Vno\_load} * 100 \quad (3.49)$$

3.6 Conclusion

The reverse design approach matches the available materials with their given physical characteristics and dimensions and predicts the ratings and performance of the partial core device. Based on the approach, various iterations are performed to obtain the device which best matches the desired characteristics of a partial core transformer/fault current limiter.

Chapter 4
Testing Partial Core Transformers

4.1 Introduction

Two partial core transformers with a rating of 15 kVA were made available in the Department of Electrical and Computer Engineering at the University of Canterbury (UoC). For simplicity they were designed as 1:1 transformers. However, partial core step-up or step-down transformers can also be designed.

A copper wound 15 kVA partial core transformer was tested under ambient and liquid nitrogen conditions. The results from these tests elaborate the performance and operational characteristics of this transformer. The variac used in this test has a maximum output current of 65 A. This limited the tests to within this current rating.

Secondly, a 15kVA HTS (BSCCO) superconducting partial core transformer (HTSPCT) was tested under cryogenic conditions to confirm the mathematical models derived using the reverse design method. Open circuit, short circuit and load tests were performed. This was ensued by a full load endurance run.

The tests also enabled understanding of the basic working principle of the test partial core transformers and confirmed the mathematical models that form the basic premise of the transformer design. During the testing process, the HTSPCT passed the open circuit, short circuit and load test. However, a failure in the primary winding during the full load endurance run caused the transformer to fail. An investigation was made into the cause of the failure [Lapthorn *et al.* 2011] and the resulting modifications made to ensure this failure did not occur again. These modifications were implemented in the proposed high temperature superconducting partial core transformer and fault current limiter (HTSPCTFCL) design model.

4.2 Transformer Description

The copper and the superconducting transformer both share the same rating and physical characteristics. The only difference lies in the dimensions of the winding. The specifications of the copper transformer are tabulated in table 4.1 and table 4.2.

Core Specifications

Table 4.1 Core Specifications

Lamination Thickness	0.23 mm
Stacking Factor	0.96
Operating Temperature	20 ^{0}C
Core length	484 mm
Core Diameter	80 mm

Winding Specifications

Table 4.2 Winding Specifications

Diameter of winding	4 mm
Length of winding	384 mm
Insulation thickness	0.2 mm
Number of layers on Primary	4
Number of layers on Secondary	4
Number of parallel conductors on Primary	1
Number of parallel conductors on Secondary	2

4.3 Test procedure

The circuit was connected as shown in figure 4.1 (a). The variac used in this test is provided with a fuse of 70 amps which would enable a current greater than the transformer rating. The power analysers used in these tests were Fluke 41 B. Currents were measured using current clamps connected to the power meters. The resistances of the windings were measured using a micro-ohmmeter.

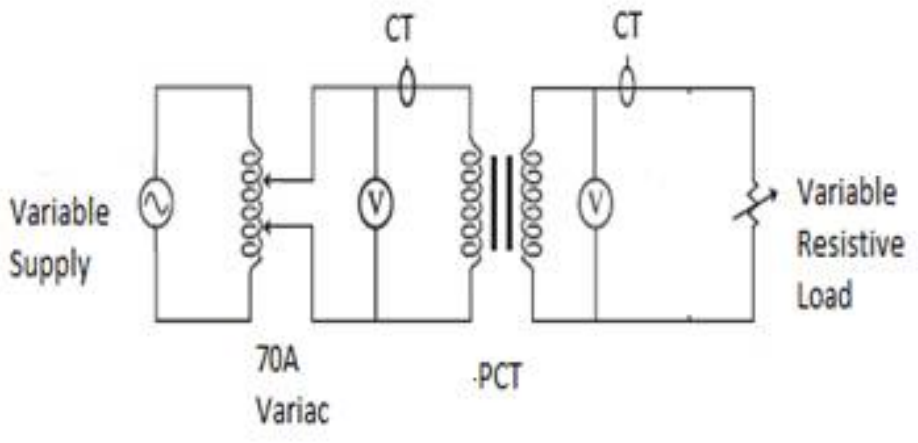

(a) Test circuit for the PCT testing

Figure 4.1 (b) Picture of Experimental setup for the test

4.4 Test Results

4.4.1 Open circuit test

The secondary terminals of the transformer were open circuited and the transformer earthed. A 50 Hz variable voltage power supply was applied to the primary terminals of the transformer. The transformer was energized in increments of 40 V up to the rated voltage and the current in the primary and the power drawn from the source were recorded. The results are tabulated in table 4.3. A plot of the inside winding voltage and inside winding current was plotted in figure 4.2

Table 4.3 Test results for open circuit test

Inside winding voltage (V)	Inside winding current (A)	Real power (W)	Outside winding voltage (V)	Power factor	Core resistance (ohm)	Core magnetising reactance (ohm)
40.30	3.47	9.00	40.00	0.065	177.77	11.55
80.50	7.00	30.00	79.80	0.054	212.26	11.43
120.80	10.53	70.00	119.90	0.055	205.37	11.40
160.00	13.98	120.00	159.00	0.054	210.67	11.40
200.00	17.40	190.00	199.00	0.055	208.42	11.46
230.00	20.00	200.00	228.00	0.044	259.92	11.41

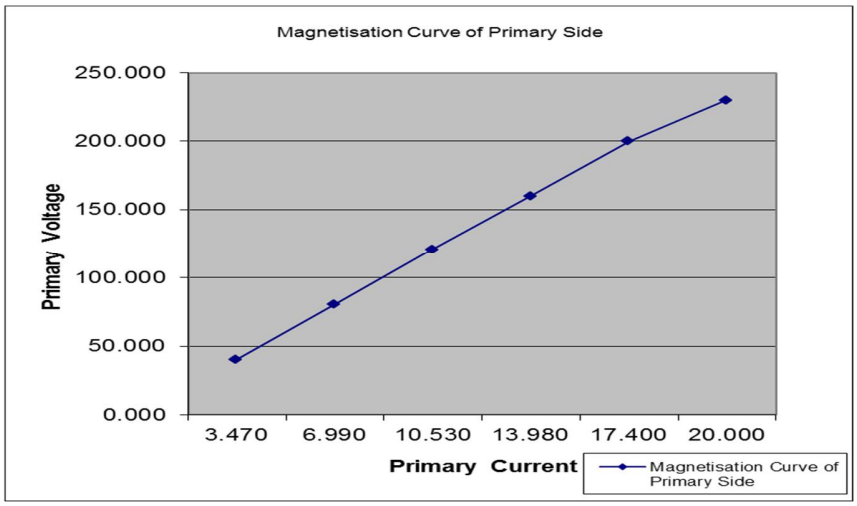

Figure 4.2 Magnetization curve of primary side

4.4.2 Short circuit test

The secondary terminals of the transformer were short circuited. The transformer was energised and the voltage increased until the rated current of 62.5 amps flowed through the secondary windings. The applied voltage, current and input power were recorded. The results are tabulated in table 4.4. The winding temperature rise was plotted against the outside winding (secondary) current in figure 4.3.

Table 4.4 Short Circuit test results

Inside winding voltage (V)	Inside winding current (A)	Outside winding current (A)	Inside winding real power (W)	Winding Temperature (˚C)
6.90	12.70	12	70.00	17.00
13.30	24.30	24.10	260.00	19.00
19.60	35.50	34.70	560.00	22.00
27.40	48.30	47.50	1070.00	34.00
34.80	60.70	59.70	1730.00	51.00
42.70	71.50	70.90	2500.00	59.00

The inside and outside winding resistance were measured for different temperatures and tabulated in table 4.5. They were compared with the calculated values tabulated in table 4.6.

Table 4.5 Measured values of the primary and secondary resistance at different temperatures

RA1RA2(ohm)	Ra1a2(ohm)
0.247	0.203
0.250	0.206
0.256	0.210
0.276	0.227
0.305	0.251
0.319	0.262

Table 4.6 Calculated values for resistance at different winding temperatures

Zs (ohm)	Rs(ohm)	Xs(ohm)	R1=R2'(ohm)	X1=X2'(ohm)
0.543	0.434	0.327	0.217	0.163
0.547	0.440	0.325	0.220	0.163
0.552	0.444	0.328	0.222	0.164
0.567	0.459	0.334	0.229	0.167
0.573	0.470	0.329	0.235	0.164
0.597	0.489	0.343	0.245	0.171

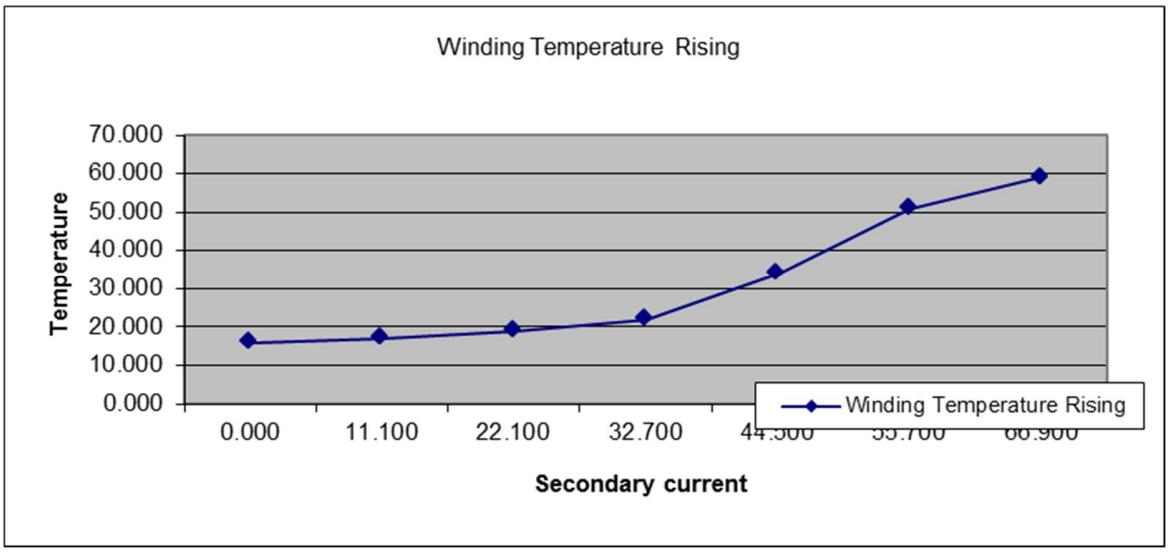

Figure 4.3 Winding temperature rise in partial core transformer

4.4.3 Load test

A resistive load ranging from 22 ohms to 3.52 ohms was connected to the secondary terminals of the transformer. A temperature probe was connected to the secondary winding to measure the temperature rise. The probe was connected to a temperature recording system, an Escort VA 271.

The transformer was energised with a voltage of 50V. The voltage was then increased in steps of 50V till it reaches the rated voltage. The input voltage, input current, input power and output voltage, output current and output power during each measurement were recorded. The

results are tabulated in table 4.7. In conjunction to the above, the winding temperature rise for each reading was also noted. The voltage regulation and efficiency for an increasing load current are plotted in figure 4.4 and figure 4.5 respectively.

Table 4.7 Load test of the partial core transformer

Vin (V)	Iin (A)	Pin (kW)	Vout (V)	Iout (A)	Pout (kW)	Winding Temperature (˚C)	Efficiency (%)	Load (ohm)	Regulation (%)
237	23.0	2.8	231	10.5	2.4	15	86	22	2.5
236	29.6	5.2	225	20.4	4.6	16	88	11	4.6
235	37.8	7.6	219	30.1	6.6	16	86	7.27	6.8
234	46.2	9.7	213	39.0	8.3	19	85	5.46	8.9
233	54.8	11.8	208	48.0	9.9	21	83	4.33	10.7
235	62.6	13.8	205	55.7	11.4	25	82	3.68	12.76

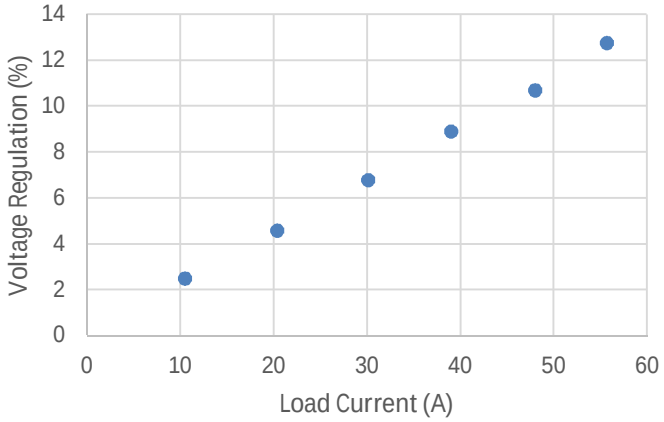

Figure 4.4 Measured voltage regulation for varying resistive load

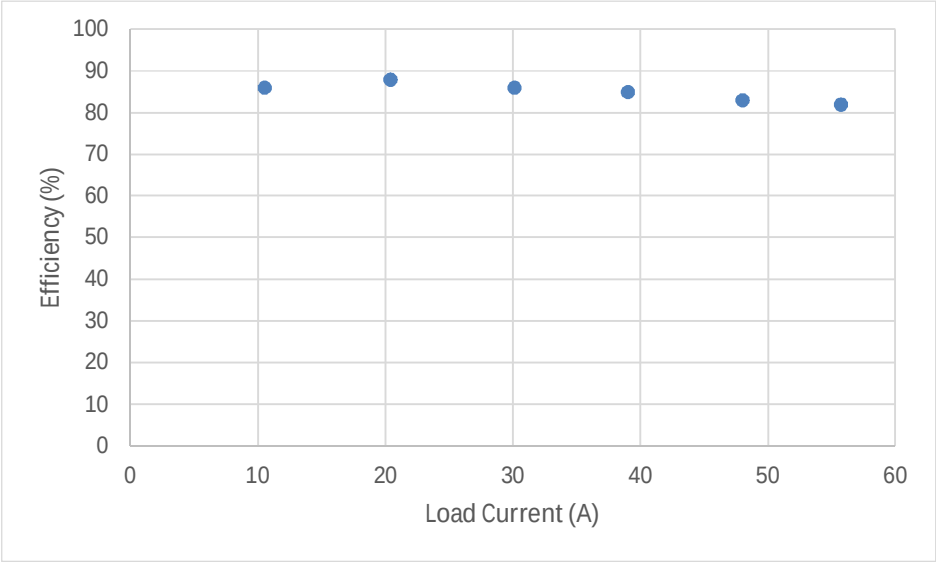

Figure 4.5 Measure efficiency for varying resistive load

4.4.4 Discussion

The magnetizing curve plotted in figure 4.2 shows a linear increase in excitation current with applied voltage. The result also indicates that magnetic saturation of the core was not occurring in the partial core transformer. The results show that there is much larger excitation current, approximately 30% of the full load current, than would be measured in a full core transformer. This is due the lower magnetizing reactance in a partial core transformer which results in a high magnetizing current.

The higher excitation current causes a voltage drop across the series impedance of the primary winding. This results in a reduced secondary winding voltage. Therefore, the open circuit voltage ratio is not equal to the turns ratio of the transformer.

For the short circuit test, the ratio of the inside winding current and outside winding current are not equal. This is once again due to the lower magnetizing reactance of the partial core transformer which results in some current flowing through the core.

The short circuit test results also show that the outside winding temperature increases dramatically once it gets close to the rated current. The increase in temperature is attributable to an increase in losses in the copper windings.

The lower than expected value at rated current is due to the reduced time taken to take recordings as the experiment proceeded. Thus there was less energy dissipated and less heat to increase the temperature as would have occurred with evenly timed readings.

Thus as the time varies with each reading, an accurate depiction of the temperature rise has not been observed.

The measured values for the resistances and the calculated values at different winding temperatures have a good agreement.

The load test verifies that the mock-up transformer exhibits an efficiency of 88 % under ambient conditions which can further be enhanced by immersing the windings in liquid nitrogen. The voltage regulation plotted in figure 4.4 has an increasing trend with an increasing load current. This is due to an increase in voltage drop across the windings of the transformer as the load current increases.

4.5 Mock-up transformer in Liquid nitrogen

The mock-up transformer was immersed in a double skinned insulated Dewar to study the effects of low temperature on the transformer. The Dewar was made out of two buckets where one bucket was smaller than the other bucket and fits inside the other bucket. The walls between the two buckets was filled with thermal insulation. The top of the Dewar was covered with a thick piece of polystyrene. The Dewar is not ideal for long term application, as the thermal insulation is not very efficient at keeping the heat from the ambient air from heating the liquid nitrogen.

The photograph of the transformer being immersed in a Dewar is shown in figure 4.6 (a). The core was insulated by filling the chamber between the former and core with vacuum. Vacuum was maintained through a turbo molecular vacuum pump connected to the vacuum chamber through copper pipes shown in figure 4.6 (b). Sufficient time was given to cool the transformer windings before the tests were commenced. Due to the poor insulation of the Dewar, it was refilled with liquid nitrogen before the tests were commenced to ensure the windings were sufficiently cooled during the tests as shown in figure 4.6 (c).

Resistance tests were performed on the transformer windings, prior to immersing the transformer in liquid nitrogen and also after immersing the transformer in liquid nitrogen. The tests determine whether the submersion in liquid nitrogen caused any damage to the windings and the joints to the terminals.

The test circuit was similar to the tests performed on the transformer under ambient condition.

(a) Copper wound transformer being Immersed in Dewar

(b) Core chamber filled with vacuum to insulate the core

(c) Dewar being re-filled with LN_2

(d) Transformer removed after testing

Figure 4.6 Copper wound transformer tested in Liquid Nitrogen

4.5.1 Open circuit test

The open circuit test was performed by applying 230 V on the inside winding. The measurements were recorded using two Fluke 41 meters. The meters were calibrated prior to testing.

The inside winding voltage and current and the outside winding voltage were measured. The results are given in Table 4.8.

Table 4.8 Open circuit test in the transformer under liquid nitrogen

Inside winding voltage (V)	Inside winding current (A)	Outside winding voltage (V)	Inside winding real power (W)
230	19.6	229	180

4.5.2 Short circuit test

The short circuit test was performed by shorting the outside terminals and applying a voltage on the inside winding with the 70 A variac until 62 A was flowing through the inside winding. The results are given in Table 4.9.

Table 4.9 Short circuit test in a transformer under liquid nitrogen

Inside winding voltage (V)	Inside winding current (A)	Outside winding current (A)	Inside winding real power (W)
24	62	61.9	210

4.5.3 Load test

The load test was performed at 230 V with a 15 kW resistive load bank. The results are tabulated in Table 4.10.

Table 4.10 Load test in a transformer under liquid nitrogen

Inside winding voltage (V)	230
Inside winding current (A)	37.6
Inside winding real power (kW)	7.2
Outside winding voltage (V)	220
Outside winding current (A)	31.9
Outside winding real power (kW)	7
Real Power loss (kW)	0.2
Efficiency (%)	97.2
Regulation (%)	4.34

In the open circuit test, the drop in output voltage is lower for the transformer under liquid nitrogen than the same transformer when tested in ambient condition. This is due to the decreased resistance of the windings which are temperature dependent (O' Neill. 2001). As a result, the voltage ratio is improved for the transformer under liquid nitrogen as compared to the same transformer when tested under ambient condition.

The measured power loss in the open circuit test under liquid nitrogen was only 10 % lower than the one measured under ambient condition. This was due to the core resistance being the dominant component in the measurement. Since the core was insulated using vacuum, the resistivity of the core didn't change under liquid nitrogen.

In short circuit test, the measured power loss under liquid nitrogen are compared with the measured losses under ambient condition. The power loss at rated current under liquid nitrogen is approximately 8 % of the power loss measured for the transformer tested under ambient condition.

Similarly, with respect to the load tests, due to the reduction in the power losses in the two windings, the power available at the load is much higher when the transformer is operating in liquid nitrogen. The efficiency of the transformer is 97.2 % as compared to 88 % when the

transformer is operating under ambient conditions. The voltage regulation also improves as the voltage drop across the windings is less.

The above tests validate the effect of low temperature on the transformer windings. With reduced resistivity at lower temperatures the transformer is more efficient and has lower voltage regulation.

4.6 Reverse design method calculation

Constructing a transformer is a costly task. If the transformer is constructed and the desired results are not there, it is impossible to go back and refabricate the entire transformer. Therefore, before the transformer is constructed it is important to validate the transformer design method. To achieve this the results obtained from the mock-up copper transformer are compared to the results obtained from the reverse design method highlighted in chapter 3.

4.6.1 Open circuit test

The open circuit test results for the reverse design method are tabulated in table 4.11 and table 4.12

Table 4.11 Open circuit test under room temperature from Reverse design method

Inside winding voltage (V)	230
Inside winding current (A)	17
Outside winding voltage (V)	226
Real power (W)	190

Table 4.12 Open circuit test in liquid nitrogen from Reverse design method

Inside winding voltage (V)	230
Inside winding current (A)	19.6
Outside winding voltage (V)	229
Real power (W)	170

Comparing the results for measured and calculated value, there seems to be good correlation. The difference in the calculated values may be due to the lack of exact knowledge of the composition of the core material or differences in the calibration of the measuring device.

4.6.2 Short circuit test

The short circuit test results are tabulated for the revere design method in table 4.13 and table 4.14.

Table 4.13 Short circuit test under room temperature from Reverse design method

Inside winding voltage (V)	32
Inside winding current (A)	62
Outside winding current (A)	60
Inside winding real power (W)	1800

Table 4.14 Short circuit test in liquid nitrogen from Reverse design method

Inside winding voltage (V)	27
Inside winding current (A)	62
Outside winding current (A)	61
Inside winding real power (W)	230

The measured and calculated results are compared. They seem to exhibit good correlation with very little difference in the calculation of the winding current.

4.6.3 Load test

The load test was performed for ambient conditions and under liquid nitrogen using Reverse design method. The results from the calculation are tabulated in table 4.15 and table 4.16.

Table 4.15 Load test under room temperature from Reverse design method

Inside winding voltage (V)	230
Inside winding current (A)	34.8
Inside winding real power (kW)	7.2
Outside winding voltage (V)	220
Outside winding current (A)	29.3
Outside winding real power (kW)	6.2
Real Power loss (kW)	1
Efficiency (%)	86
Regulation (%)	4.3

Table 4.16 Load test in liquid nitrogen from Reverse design method

Inside winding voltage (V)	230
Inside winding current (A)	35
Inside winding real power (kW)	7.5
Outside winding voltage (V)	224
Outside winding current (A)	29
Outside winding real power (kW)	7.2
Real Power loss (kW)	0.3
Efficiency (%)	97
Regulation (%)	2.6

The results obtained from the reverse design calculation are in close correlation with the measured results under ambient condition and in liquid nitrogen. This validates the reverse design method from chapter 3 and it can used in the design process.

4.7 The 15 KVA HTSPCT prototype

A 15 KVA HTSPCT prototype was first designed and tested in 2005 by Professor Pat Bodger and Dr. Wade Enright at UoC [Bodger et *al*.2005]. However, due to a failure that occurred in the prototype's LN_2 Dewar further tests such as a load test and endurance test were not performed. Due to various projects involving HTS transformers in 2008 and 2009, repairs were

made to the Dewar and tests were performed on the prototype. The open circuit, short circuit and load tests were executed as expected, however the full load endurance run couldn't be completed due the failure in the prototype's primary windings. In figure 4.7(a), the winding insulation sheets are being wrapped around the windings. Figure 4.7 (b) shows the G10 composite Dewar.

(a) Fabrication of windings

(b) G10 Dewar

Figure 4.7 HTSPCT fabricated in 2005

4.7.1 Transformer Design

4.7.1.1 Core design

The core of the prototype was made of 420 Laminations of grain oriented silicon steel. Each lamination was 0.23mm in thickness and exhibited a high permeability. (ABB product code 23JGSD085). The length of the core was 484 mm. The laminations were stacked together and bound with Vidatape S which is a woven high shrink polyester tape. It was then hot dipped twice in an electrical baking varnish. The core had been provided with a hole in the centre along its axis to accommodate a 1240mm long G-10 fibre glass 5/8" UNC threaded rod. The fibre glass threaded rod is used to insert the core in the core vessel. A square G-10 fibre bolt at both ends of the core holds the core and the G-10 fibred thread together. This prevents the core from slipping while it is being inserted in the core vessel.

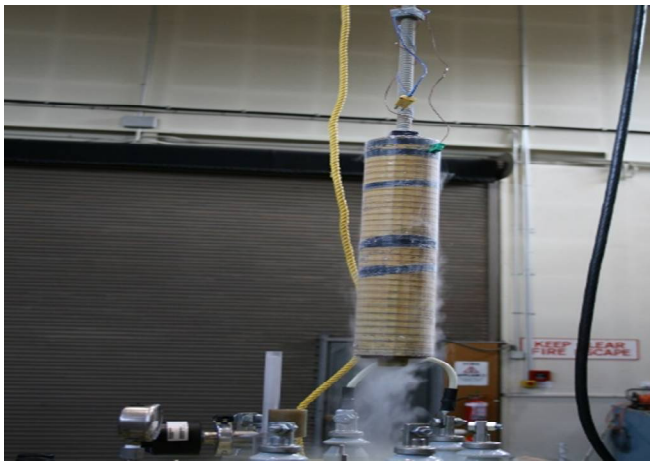

Figure 4.8 Core of the transformer made from silicon steel

4.7.1.2 Winding design

The HTSPCT has a winding configuration of one primary winding at 230V and two secondary windings at 115V each. The windings were wound with 1G-BSCCO HTS tape procured from American Superconductors. The tape had a critical dc current of 124.2 A under a self-field at 77k. However, this value cannot be used while performing the tests under ac as the critical current tends to change due to the presence of an external magnetic field. (Zhu et al.). As a result, 50% of the dc current value was considered in the transformer tests under ac.

Nomex (T-410 with dimensions 0.13 × 10mm) was used to insulate the HTS tape. The insulation was applied parallel to the wire length on the wide surface of the conductor. Any excess insulation was folded over the conductor's thin edge to the opposite side surface (Lapthorn. 2012). A second layer of insulation was applied and folded on the opposite side to the first so that the conductor was completely covered. The overlap of the insulation on the wide surface of the conductor was between 3 and 4 mm throughout.

The windings were layer wound with 80 turns per layer. The high voltage winding was located on the inside of the transformer and consisted of four layers for a total of 320 turns. The first low voltage windings, a1-a2, consisted of two layers of 80 turns each. The second low voltage winding, a3-a4, was wound over the first low voltage winding, a1-a2, and also had 80 turns for

each of 2 layers. This configuration was designed to allow for different winding configurations and its application in a variety of future projects.

4.7.1.3 Insulation

The insulation for the transformer consisted of a combination of Nomex 411 and Nomex 410 insulation paper [Lapthorn *et al.* 2011]. Six layers of Nomex 411 were used directly on the former to allow for a firm wound of the tape on the former. Four layers of Nomex 410 were used on either side of the HTS layers to allow room for copper lead-outs. In conjunction with the above arrangement of insulation, four layers of Nomex 410 were used for inter-winding insulation.

4.7.1.4 Liquid nitrogen vacuum Dewar

The vaccum Dewar consisted of an inner vessel for containment of liquid nitrogen (LN_2) and an outer vessel exposed to room temperature with a vacuum between them. The vacuum was present to limit thermal convection losses to the LN_2 from the outside. In order to limit the external heat from heating the LN_2, several layers of aluminized non-stretch polyester was wrapped around the inner vessel.

A pressure relief port was present on the outside of the Dewar which would prevent venting of nitrogen gas into the vacuum chamber on event of failure of the inner vessel.

4.7.2 Experimental Results

Tests were performed on the transformer to determine the operational characteristics of the HTS transformer. The tests included an open circuit test, short circuit test and load test. An endurance test was performed to validate its viability for operation for a long duration.

Figure 4.9 shows the filling process of liquid nitrogen in the Dewar. In figure 4.10, the venting of the HTS transformer is observed.

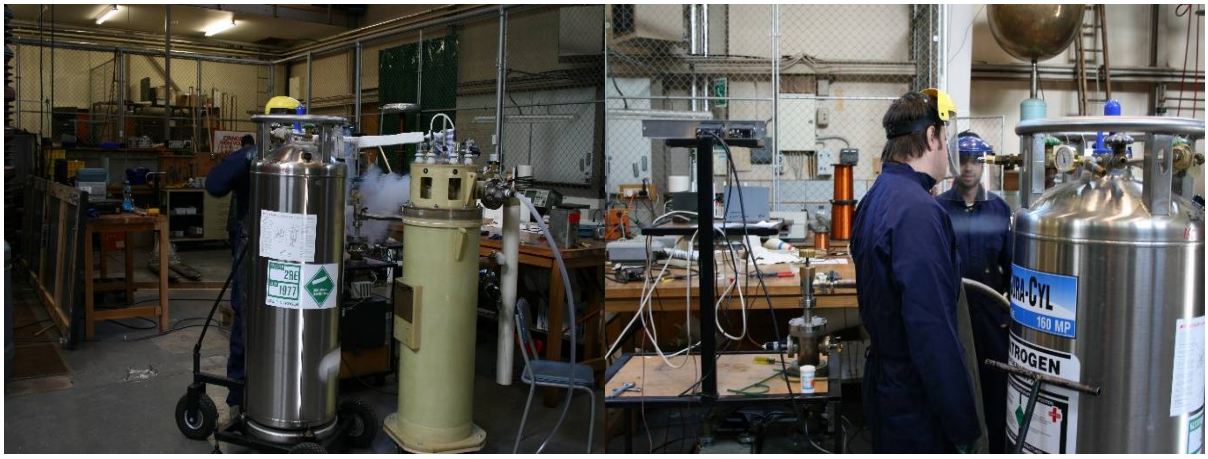

Figure 4.9 Filling the dewar with liquid nitrogen and ensuring pressure is maintained

Figure 4.10 Testing the HTSPCT transformer

4.7.2.1 Open Circuit Test

With the open circuit test, the secondary windings a1-a2 and a3-a4 were left open circuit. Since the core used in the HTS transformer was the same core as used in testing the copper wound transformer under liquid nitrogen conditions, the open circuit results were expected to the same for both the transformers. The open circuit results are tabulated in table 4.17.

Table 4.17 Open circuit test

Inside winding voltage (V)	230
Inside winding current (A)	19
Outside winding voltage (V)	113 and 111
Inside winding real power (W)	200

4.7.2.2 Short Circuit Test

The secondary windings a1-a2 and a3-a4 were shorted and approximately 50% of the dc critical current was supplied through the transformer windings. This current was also close to the HTSPCT's rated current. The results from the test are given in table 4.18.

Table 4.18 Short circuit test

Inside winding voltage (V)	25
Inside winding current (A)	65
Outside winding current (A)	65
Inside winding real power (W)	80

The copper wound transformer and the HTSPCT had similar ratings and core dimensions. The results from the copper wound transformer, the power loss was much higher at 210 W as compared to the power loss of the HTSPCT of 80 W. The higher power loss for the copper wound transformer are due to the higher resistivity of the copper windings.

4.7.2.3 Load Test

Figure 4.11 Load banks for performing the load test on the HTSPCT

For the load test, the secondary windings a1-a2 and a3-a4 were connected in series to a resistive rated load of 3.5 Ω. Figure 4.11, shows the load bank used in the resistive load test. The HTSPCT was supplied with 230 V at 65 A. The results obtained from these tests are given in table 4.19.

Table 4.19 Load test

Inside winding voltage (V)	230.9
Inside winding current (A)	65
Inside winding real power (kW)	13.8
Outside winding voltage (V)	223.6
Outside winding current (A)	61
Outside winding real power (kW)	13.6
Real power loss (kW)	0.2
Efficiency (%)	98.6
Voltage regulation (%)	3.2

The HTSPCT and the copper wound transformer under liquid nitrogen both displayed a high efficiency. The high efficiency and regulation can be attributed to the low temperature operation of the HTSPCT and the copper wound transformer from section 4.8. In the presence of liquid nitrogen, the resistivity decreases for the copper windings which provides for a high efficiency while the absence of any resistance in the HTSPCT windings provides for a higher efficiency.

4.7.2.4 Load endurance test

A full load endurance test was performed on the HTSPCT. At approximately 1 minute 30 seconds into the test, the secondary voltage collapsed and a surge in nitrogen gas venting from the Dewar was observed. The power was disconnected. Resistance tests were performed on the inside and outside windings. The inside winding, A1-A2 was found to be open circuited. The outside windings a1-a2 and a3-a4 were found to be normal. The liquid nitrogen in the Dewar was at a normal operating level. The surge in nitrogen gas was created by the heating of the conductors. The emergency venting rupture disc was successful in preventing excessive build-up of nitrogen gas in the liquid nitrogen chamber.

The windings on the HTSPCT were unwound to visually inspect the damage (Lapthorn et al. 2009). The outer windings were found to have black contaminants on the surface of the insulation as seen in photographs in figure 4.12 (a), (b), (c). A close inspection of the insulation suggested that the contaminants were attracted only on the surface of the windings. The lower half of the windings as shown in figure 4.12 (c), appeared to have vertical white traces on the black contamination. This could have occurred due to nitrogen bubbling. A small area of burnt insulation above the A1-A2 winding was found with an area of burnt fibre glass immediately above it. The burnt fibre glass is shown in figure 4.13 (e).

The outside winding a3-a4 was found to be normal but on further unwinding, the middle winding a1-a2 was found to have damaged Nomex. The insulation of the a1-a2 winding was burnt in an area in the upper region of the winding. The HTS wire of this winding didn't appear to be visibly damaged. However, once the inside winding A1-A2 was unwound, substantial thermal damage was found.

Radial buckling was found on the inner winding layers as shown in figure 4.13 (d). The buckling was most likely caused by the thermal expansion of the HTS wire. As mentioned in [Weiss *et al.* 2007], the thermal expansion of the HTS wire over the temperature range experienced could have been 2-3 mm/m.

As the windings were tightly wound and wrapped in Nomex insulation, thermal expansion of the inner layers could have resulted in radial buckling.

Since there was little provision of cooling due to the tightly wound HTS wire, it is assumed that the losses dissipated during heating of the HTS wire (with the HTS wire being possibly

quenched) would have cascaded the effect of temperature rise and thereby cause the insulation to fail with open circuited turns in the windings. The excessive build-up in temperature would have resulted in the former above the windings being damaged as shown in figure 4.12 (e). Therefore emphasis was laid in mitigating any build-up in temperature due to insufficient cooling of the HTS windings for future transformer design with HTS windings. The windings also need to be operated within a reasonable margin from the dc critical current prescribed for them by the manufacturer.

(a) Close up of the insulation of the outer windings

(b) Black contaminants observed while the windings are removed from the Dewar

(c)Black contaminants on the upper and lower portion of the insulation of the outer windings

Figure 4.12 Photograph of HTSPCT windings being removed from the Dewar

(a) Windings of the HTSPCT being unwound after failure

(b) Unwinding the outer winding

(c) unwinding the middle layer

(d) Radial buckling on the inside windings

(e) Damage to former due to excessive heating

Figure 4.13 Photograph of unwinding the HTSPCT and studying the damage caused during failure

4.8 Conclusion

Transformers with different winding materials were tested in ambient and liquid nitrogen conditions. At ambient temperature, the copper wound transformer exhibited operational characteristics that should be found in partial core transformers. Operating the same transformer in liquid nitrogen resulted in less losses in the windings and therefore a much more

efficient transformer. This was due to the change in resistivity of the copper windings at low temperature.

A HTSPCT with a similar rating to the copper wound transformer was tested. The tests performed to estimate the operational characteristics yielded satisfactory results. However, on performing a full load endurance test, the HTSPCT failed catastrophically. The HTSPCT was unwound to study the damage and investigate the cause of the failure. The HTSPCT was found with open turns on the primary and significant damage to the former. The damage could have been caused due to excessive heating of the windings. This was only possible if the windings of the HTSPCT quenched. Therefore, for future work and improvements in a HTS wound transformer, cooling of the windings and the dc critical current of the HTS are of considerable importance. Experiments on the current characteristics of HTS tapes suggest that with sufficient cooling, the HTS tapes can be operated at current levels higher than the critical current for short periods of time. [Kim *et al.* 2008].

Chapter 5
Relationship between temperature and time for a HTS tape

5.1 Introduction

HTS is temperature dependent and the HTS tapes are only superconducting below a certain temperature. This temperature is called the critical temperature. The critical temperature of a HTS is the minimum temperature where the critical current is zero. Taking into account this critical temperature of the HTS BSCCO tapes, a model is deduced to calculate the time it takes to melt the tape. The model takes into account radiation, convection and conduction losses. Once these losses are estimated, the time it takes to melt the HTS tape is calculated. This model is confirmed with empirical values obtained from an experiment using a 10 cm length of HTS BSCCO tape. The HTS tape was subjected to different currents at room temperature.

The time to melt the HTS tape was used as a reference to model the response time of a circuit breaker operation in quench detection system for the proposed HTSPCTFCL.

5.2 Time calculation

Resistive heating is the process by which the passage of an electric current through a conductor releases heat. Consider a metallic conductor of resistivity ρ (Ωm), uniform cross section area A (m^2) and length (m).

The resistance is

$$R = \rho \frac{l}{A} ohms \qquad (5.1)$$

If electrodes are fixed to the ends of the conductor and *V* volts applied to the electrodes, the current *I* is given by

$$I = \frac{V}{R} amps \qquad (5.2)$$

The power dissipated in the conductor is

$P = I^2 R$ *Watts*

and the amount of heat generated is

$W = I^2 Rt$ *Joules* (5.3)

where *t* is how long the current is flowing through the conductor.

The amount of heat absorbed by the conductor is

$W = \Delta TVC\gamma$ (5.4)

where ΔT = mean temperature rise of the conductor K

V = volume of the conductor m^3

C = volume specific heat J/m^3K

γ = density of the conductor kg/m^3

Equating equation 5.3 and 5.4,

$I^2Rt = \Delta TVC\gamma$ Joules (5.5)

Therefore the time it takes to heat the conductor is

$$t = \frac{\Delta TVC\gamma}{I^2R} \quad \text{secs} \qquad (5.6)$$

5.3 Heat Transfer

There are 3 modes of heat transfer from a body that is at a temperature higher than its surroundings. They are conduction, convection and radiation.

5.3.1 Conduction

Heat flows from a high temperature region of a solid to a lower temperature region of a solid when they are in contact [Lienhard, 1981] .

The quantity of heat transferred per unit time is

$$Q = kA\frac{dT}{dl} \quad \text{Watts} \qquad (5.7)$$

Where k = thermal conductivity of material W/mK

A = heat flow path cross sectional area m^2

dT/dl = temperature gradient along the heat flow path K/m

5.3.2 Convection

Convection is heat transfer by mass motion of a fluid such as air or water when the heated fluid is caused to move away from the source of heat in a solid, carrying energy with it. Convection above a hot solid surface occurs because hot fluid expands, becomes less dense, and rises. [Lienhard, 1981]. In an electrical conductor the convection losses will be negligible as the conductor is contained in an insulating material enclosure for safety reasons and inter-turn isolation

The quantity of heat transferred due to convection is given by:

$$Q = hA(T_s - T_\infty) \quad \text{W} \quad (5.8)$$

where h = heat transfer coefficient W/mK

A = flow path cross-sectional area m^2

T_s = absolute temperature of surface K

T_∞ = absolute temperature of free steam K

5.3.3 Radiation

Thermal radiation is the transfer of energy from a surface in the form of electromagnetic waves. It carries the energy away from the emitted object [Lienhard, 1981]. The power radiated by a conductor per unit area is

$$\frac{P_R}{A} = 5.73 \times 10^{-8} \in (T_s^{\,4} - T_a^{\,4}) \quad \text{W/m}^2 \quad (5.9)$$

Where $\in$ = emissivity coefficient of the surface (0-1)

T_s = absolute temperature of radiating surface K

T_a = absolute ambient or the receiving surface temperature K

5.4 Estimation of total time to melt for a HTS BSCCO tape

Figure 5.1 displays the relationship between the resistivity and the temperature of the conductor. 77k is the boiling point of liquid nitrogen which is an essential cryogen for HTS like BSCCO. Therefore, the range of temperature spans from 77k to the melting point of silver. However, as the BSCCO tape has its resistive component only after quenching, the start temperature of this calculation is 110K.

The total time for a HTS BSCCO tape to melt is calculated by equating the energy dissipated in the conductor with the energy absorbed by the conductor as given by equation 5.6. The surface area of the HTS conductor is the upper and the lower surface of the conductor. Therefore, equation 5.8 and 5.9 are multiplied by 2 to consider the rectangular geometry of the HTS conductor.

The net heat in the conductor is calculated by subtracting the losses due to conduction, convection and radiation from the power dissipated in the conductor.

Therefore, subtracting 5.7, 5.8 and 5.9 from the power dissipated component of equation 5.3 gives

$$P_{net} = I^2R - \frac{kAdT}{dl} - 2hA(T_s - T_\infty) - 5.73\times10^{-8} \in 2A({T_s}^4 - {T_a}^4) \qquad (5.10)$$

Therefore, equation 5.6 can be modified as

$$t = \frac{\Delta T \gamma C V}{I^2R - \frac{kAdT}{dl} - 2hA(T_s - T_\infty) - 5.73\times10^{-8} \in 2A({T_s}^4 - {T_a}^4)} \qquad (5.11)$$

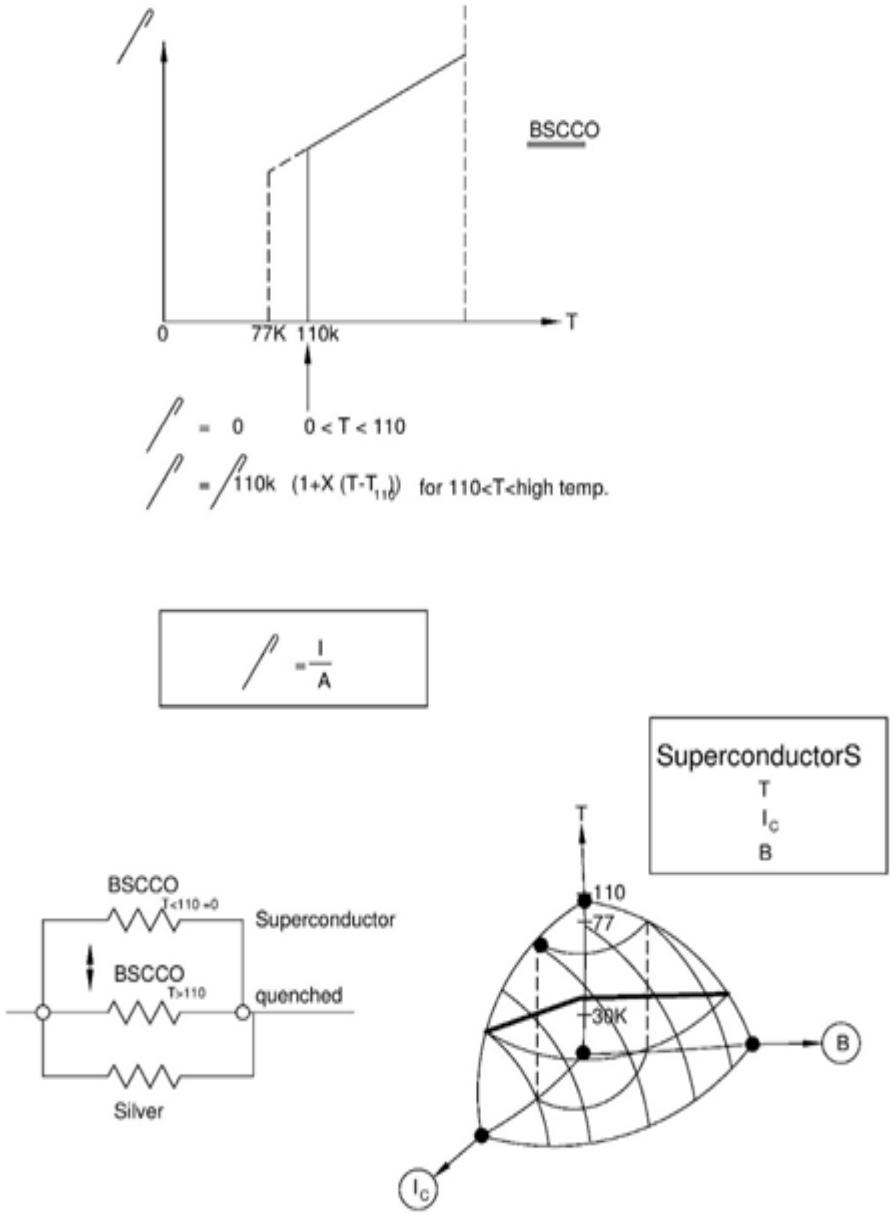

Figure 5.1 Temperature calculation

The quenching temperature of BSCCO is 110K. Using this as the start temperature, each increment in the rise in temperature of the conductor is used to calculate the respective time to achieve that temperature rise. The calculations are done till the conductor reaches the melting point. In this case, the silver's melting point is used as the end temperature. The time for each segment of temperature rise is added to form the cumulative time or total time. This is the time at which the conductor will melt.

While designing the transformer fault current limiter, the total length of the conductor is used to calculate the resistivity. As the length of the conductor is directly proportional to the resistance of the conductor, the energy in the conductor is also directly proportional to the length of the conductor.

Once the program is run for the entire iteration, I^2R losses, Q_{convec}, Q_{cond} P_{Rad} and the rise in temperature are obtained and plotted against time, as shown in Figures 5.2 and 5.3 for 2 different current values. The parameters used in the program are tabulated in table 5.1.

Table 5.1 Parameters used in calculation model

Volume Specific heat, C	**233**	**J/m^{3}K**
Thermal Conductivity, k	**406**	**W/mK**
Surface area, A	**0.0004551**	**m^2**
Temperature Increment, Δ T	**1**	**K**
Emissivity, ϵ	**0.11**	
Heat transfer coefficient, h	**1**	**W/mK**
Start temperature, T_S	**293**	**K**
Length of the tape,l	**0.11**	**m**
Width of the tape, w	**0.0041**	**m**
Thickness of the tape, th	**0.0003**	**m**
Flow path cross sectional area, *A*	**0.00000123**	**m^2**
Resistivity of silver at 293 K	**1.59E-08**	**Ωm**
Thermal resistivity coefficient, α	**0.00001392**	**/K**
Mass, m	**0.0014322**	**kg**
Volume, V	**1.3653E-07**	**m^3**
Density of silver, ϒ	**10490**	**kg/m^3**

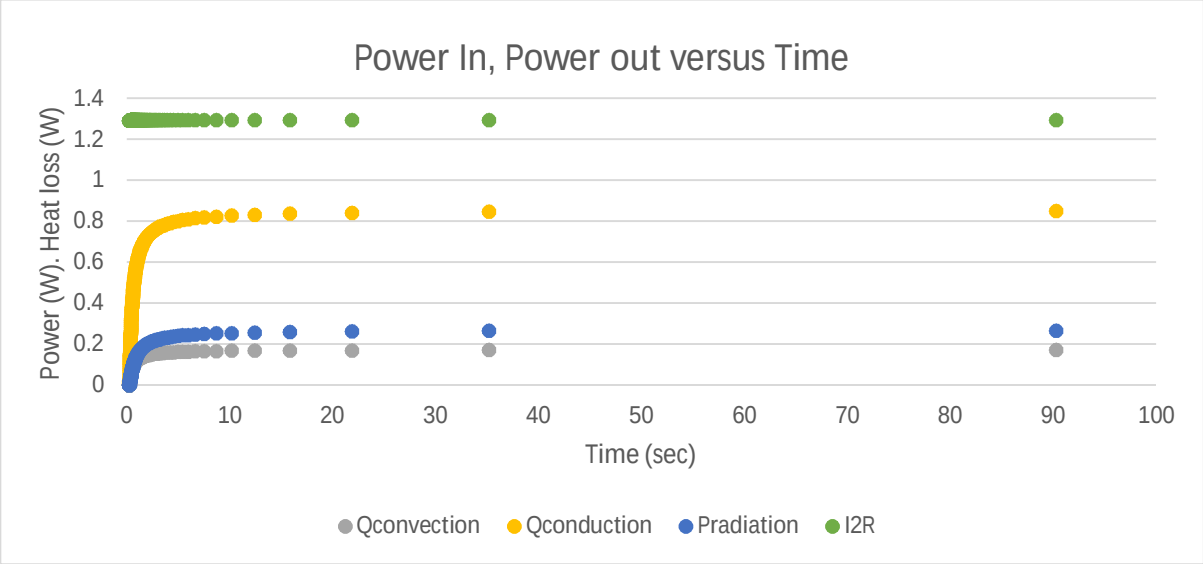

Figure 5.2 Power in and Power dissipated from the conductor versus time for 30 A current

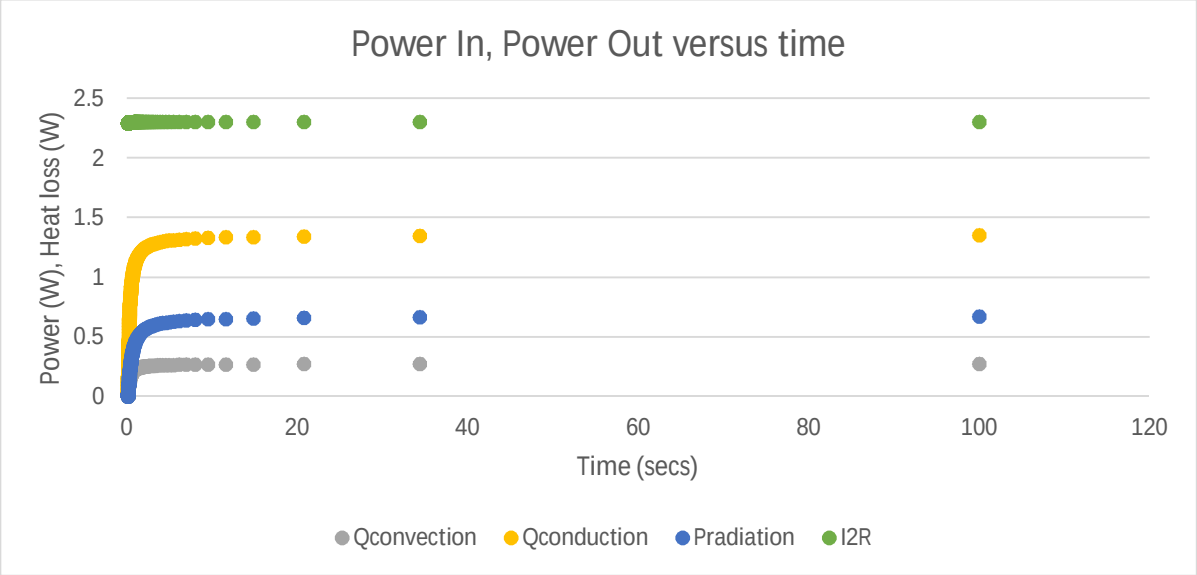

Figure 5.3 Power in and Power dissipated from the conductor versus time for 40 A current

From figure 5.2 and figure 5.3, it can be seen that the conduction losses are much higher than the radiation and convection losses. This is due to the short length of the conductor used in the experiment and the relatively large masses of the terminal blocks the HTS tape is suspended between. For a conductor length envisioned to be used in the HTS transformer fault current limiter, the conduction losses are only present at the ends of the conductor

and are therefore negligibly small. The dominant heat losses would be due to the radiation and convection losses that take place in the conductor during heat transfer.

In figure 5.2, for a current of 30 A passing through the HTS conductor the temperature rises for 90 secs and thereafter there is no rise in temperature. Similarly in figure 5.3, for a current of 40 A passing through the HTS conductor the temperature rises till 100 secs and thereafter there is no rise in temperature.

A relationship between the rise in temperature and time is plotted in figure 5.4 for the HTS conductor with 30 A current. The temperature in the conductor increases substantially for about 10 secs. The increment in temperature is not substantial as it reaches steady state at about 90 secs.

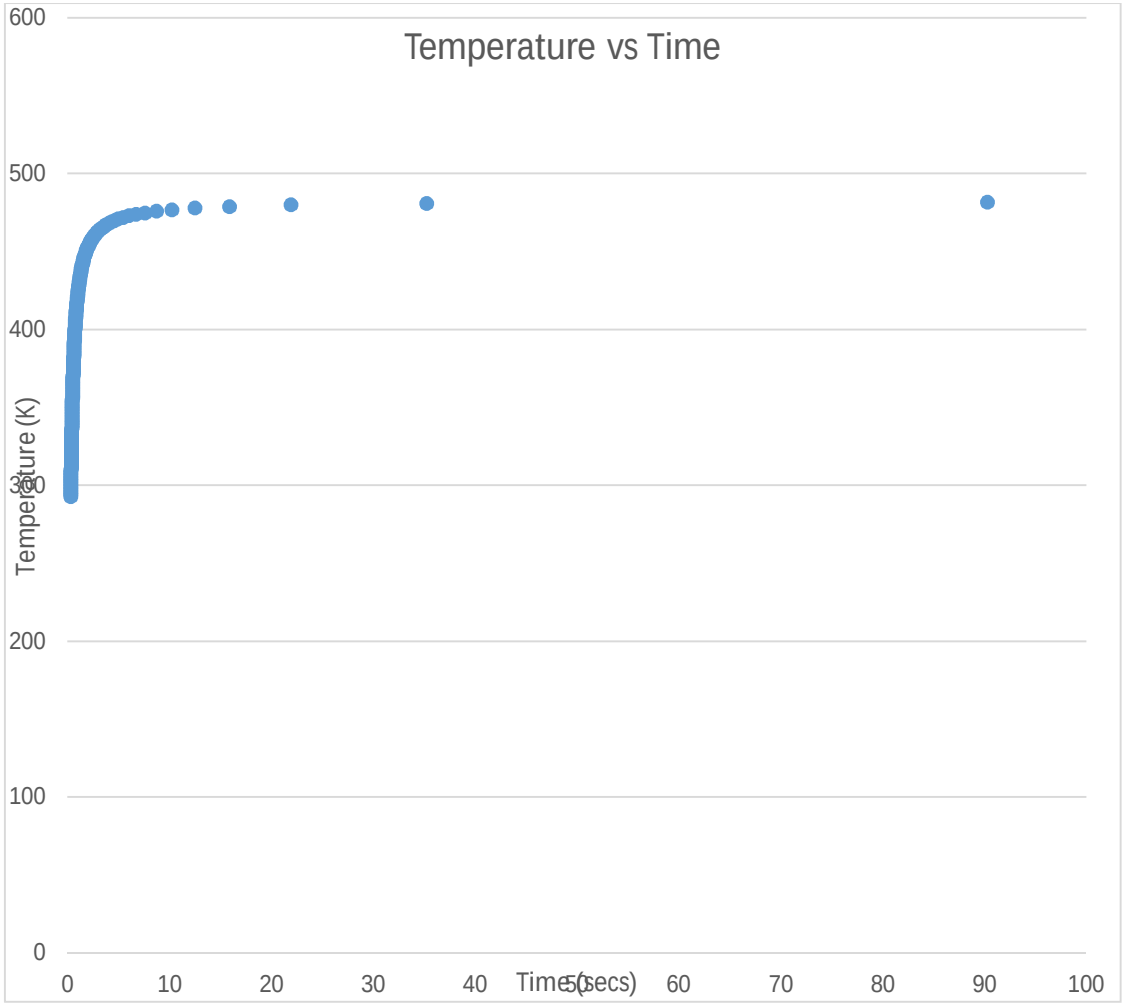

Figure 5.4 Increase in temperature versus time for a 30A current flowing through the HTS conductor

5.5 HTS Temperature determination experiment

The empirical values gives an estimation of the time the HTS tape can withstand a particular current before it melts. The experimental setup is illustrated in figure 5.5.

In the figure 5.5 (b), the HTS BSCCO superconductor is clamped between two metal contacts. It is covered with a fibre casing for safety reasons. The contacts of the HTS conductor are cleaned with ethyl alcohol to remove any residue of the insulation. This is done to prevent losses due to conduction at the joints of the HTS conductor and the metal contacts. A thermal gun is used to verify the absence of any loss at the conductor and metal joint.

A variac as shown in figure 5.5 (a) is used to apply voltage to the HTS conductor. The variac had a current rating of 70 A. In figure 5.5 (b), the 1:1 voltage probes are connected across the conductor joints. A current transformer measures the current for each increment in voltage. Current was varied from 10A to upwards of 30A to obtain a relationship between temperature and time.

The BSCCO tape has a dc critical current of 110A, however when used as a winding in a HTS transformer, the presence of external magnetic fields reduces the dc critical current. The resultant ac critical current tends to be much lower than the dc critical current [Oomel *et al.* 2002]

The tape is initially subject a room temperature of 20^0C. Room temperature was chosen for the experiment to obtain a conservative value for the time to melt for the HTS tape. At this temperature the HTS BSCCO tape is assumed to be a resistive conductor with the silver being the conducting element inside the HTS tape. A thermocouple was used to measure the rise in temperature while current flows through it.

The thermocouple consists of two wires made of separate alloys, welded together at their tips, to create a bimetallic junction. It measures the difference in voltage and registers it in the digital multimeter. It is attached to the centre of the HTS tape as shown in figure 5.5 (d) A Fluke 80 TK thermocouple adapter formed the interface between the thermocouple and a digital multimeter HP 34401A. The measured voltage is directly proportional to the temperature. The temperature is measured by connecting the digital multimeter to the computer with a USB GPIB controller. The computer runs LabVIEW to log these results. The temperature measurements are noted against time for which the current is applied as

shown in figure 5.6. Measurements are taken till the rise in temperature reaches steady state.

a) Variac used to apply voltage to the HTS conductor

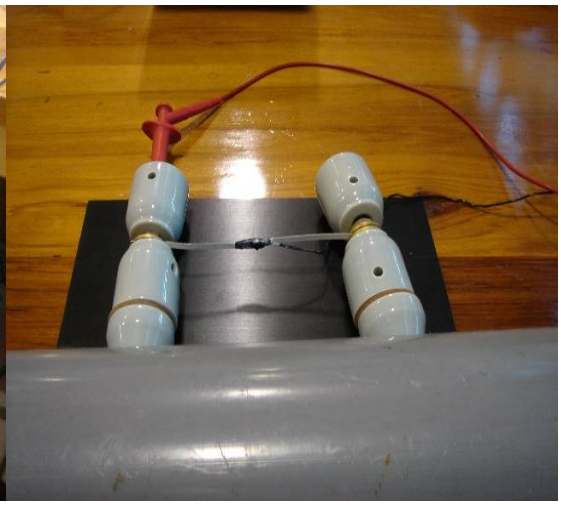

b) Voltage probes across the metal joints

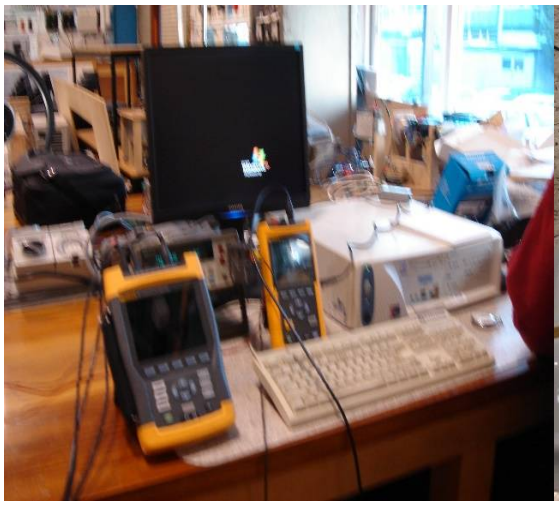

c) Labview set-up to record the Temperature

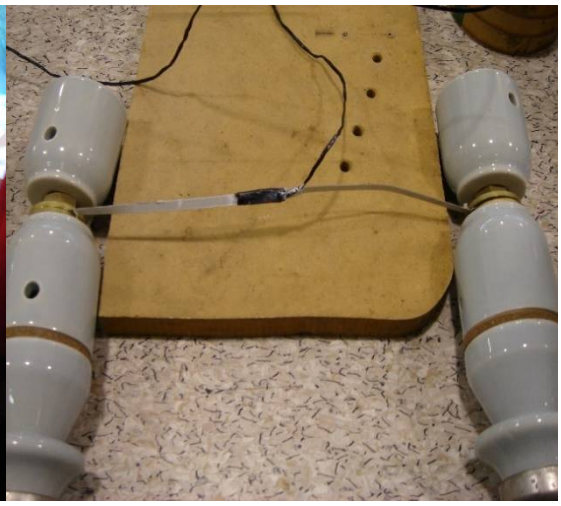

d) Thermocouple attached to the middle of the HTS conductor

Figure 5.5 Experimental setup for time calculation

In the plot of temperature versus time in figure 5.6, noise is observed in the temperature recordings. This was due to the thermocouple attached to the HTS tape. A heat sensitive glue was used to attach the thermocouple in addition to a heat sensitive tape wrapped

around the thermocouple and the HTS tape. This was done to ensure a good connection between the thermocouple and the HTS tape. However, a stable connection was not achieved and therefore noise was observed in the recordings of temperature.

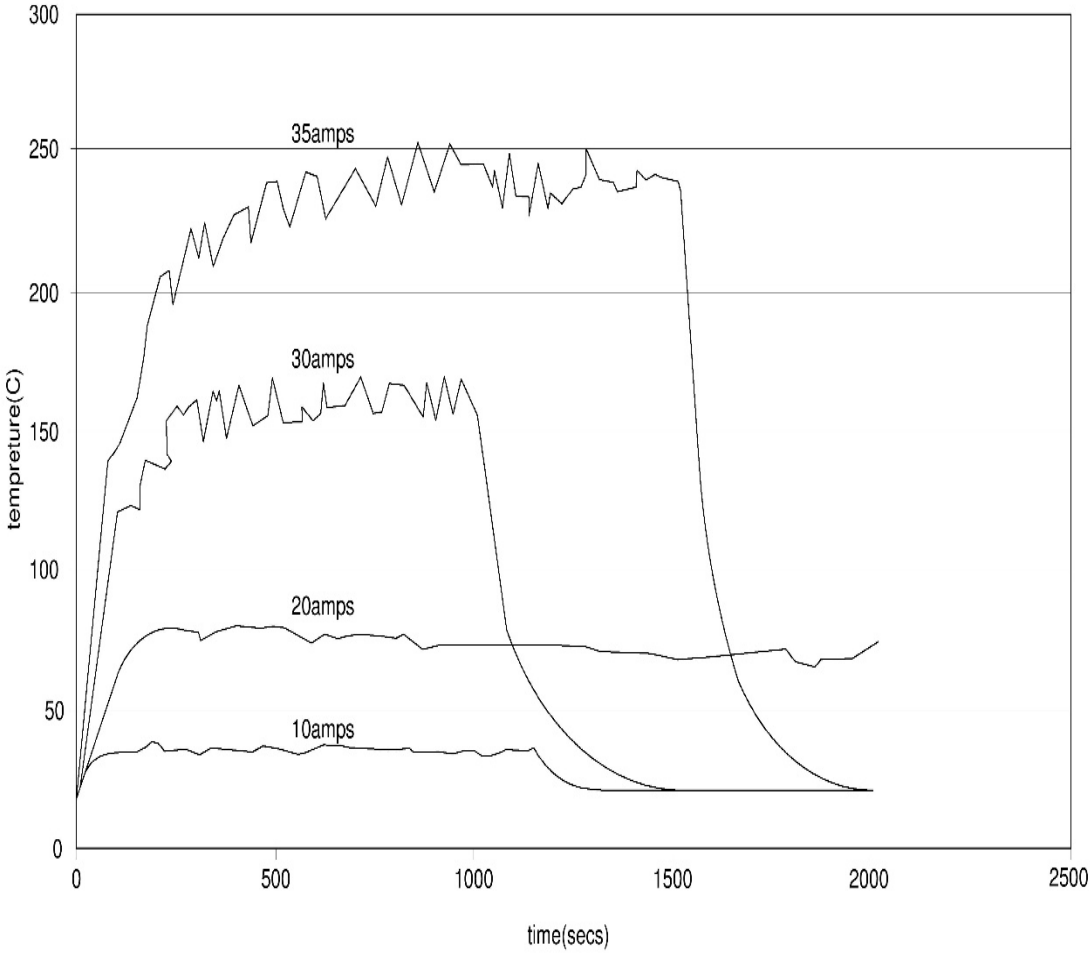

Figure 5.6 Temperature vs time for the conductor at 20^0C for different currents.

5.6 Comparison between Calculated and Measured results

The results obtained from measurements and calculations are plotted against time in figure 5.7 for a current of 30 A.

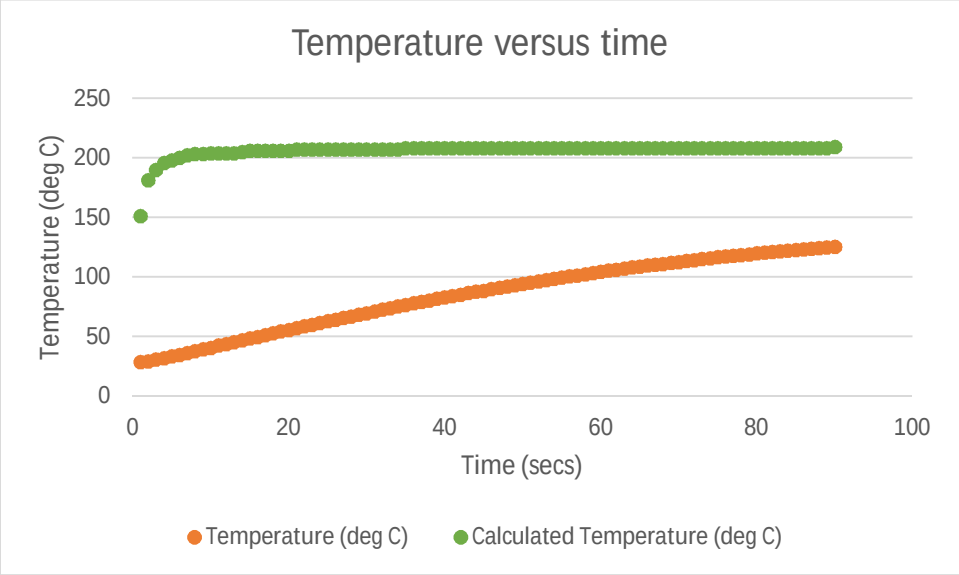

Figure 5.7 Temperature versus time

In figure 5.7, there is a significant difference in the calculated and measured value. The measured temperature takes around 60 seconds before it starts reaching steady state. While the calculated temperature reaches steady state at around 5 seconds. This difference can be attributed to the delay between the measurement taken by the thermocouple and the measurement recording devices used in the experiment. It could also occur due to the heat sensitive glue used to glue the temperature probe to the conductor. An insulation can occur due to the glue thereby causing a delay in the measurement of temperature. Also, the calculated model was a conservative model which factored all the losses from the start temperature. From equation 5.11, a lower melting time for the HTS BSCCO tape could be obtained if the losses were factored in the equation at the start temperature. This time was used in modelling the quench detection system described in chapter 7 of this thesis and could be also used in choosing a circuit breaker based on operating time.

5.7 Conclusion

A model to estimate the time it would take the HTS tape to melt was deduced. This was especially useful after the catastrophic failure of the HTSPCT in chapter 4. As noted in chapter 4, the quenching process caused excessive heating of the HTS windings and due to a flaw in the insulation design, the excessive heating caused the HTS windings to melt. Therefore, by factoring the time it would take for the windings to melt, a circuit breaker can be chosen based on its operating time. This would cut the power supply from the transformer if the HTS tape in the windings was to quench and therefore protect the transformer from being damaged.

Chapter 6
HTS partial core transformer fault current limiter concept and design

6.1 Introduction

A HTS partial core transformer has the benefits of being light weight due to the reduced weight of the core and at the same time the negligible resistance of the HTS windings when superconducting. A HTS transformer should exhibit high efficiency and low regulation. HTS are superconducting at liquid nitrogen temperature and quench once the critical parameters of a HTS are breached. The superconducting ability of HTS at values lower than the critical values of a HTS makes them a good winding material in a transformer.

It is also the property of superconductors to quench when the critical parameters are breached, that can produce good fault current limiting ability. Therefore, the application of a HTS partial core transformer as a fault current limiter is investigated followed by the design of a device which combines the performance characteristics of a partial core transformer and a fault current limiter.

6.2 Concept of HTS partial core transformer and fault current limiter

The basic requirement of the HTS partial core transformer and fault current limiter (HTSPCTFCL) is that it should perform as a transformer under normal operating conditions. However, in the event of a fault, the HTS windings will quench introducing resistance in the windings [Okubo *et al.* 2007]. For HTS windings made from 1G BSCCO/Ag tapes, silver introduces this resistance on quenching. Since the transition from non-quenching to quenching is not instantaneous (Oomen *et al*. 2002) the resistance of the silver matrix is only introduced once quenching takes place.

Figure 6.1 presents equivalent circuits which explain how a HTSPCTFCL would behave as a combined device. Figure 6.1 (a) is for the HTSPCTFCL in superconducting state and working as a transformer. Fig 6.1 (b), depicts the HTSPCTFCL during the occurrence of fault but before quenching, while figure 6.1 (c) depicts the HTSPCTFCL after quenching. The prospective current is the maximum current that flows through the secondary windings of the transformer just after a fault has occurred [Okubo *et al.* 2007]. The impedance in the

HTSPCTFCL is due to the resistance in the HTS due to ac losses and the reactive component at this juncture. However once quenching occurs, the resistance of the silver matrix is introduced into the HTSPCTFCL which further limits the current.

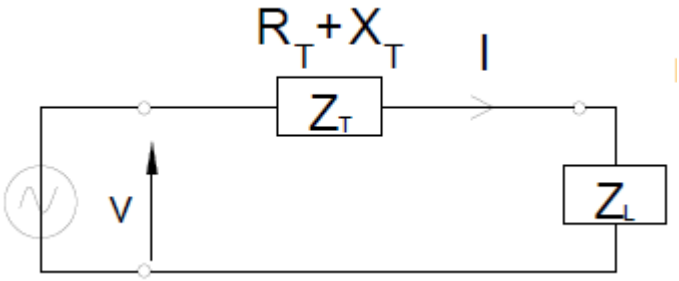

a.) Normal operation as a transformer

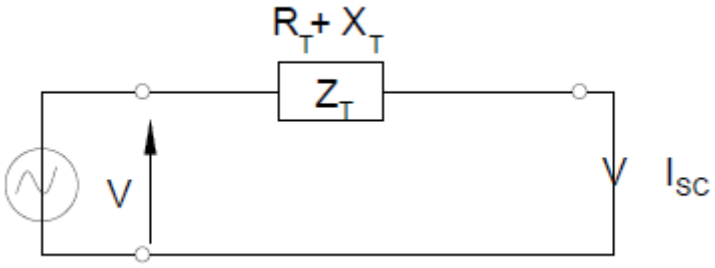

b.) Before Quenching just after a fault

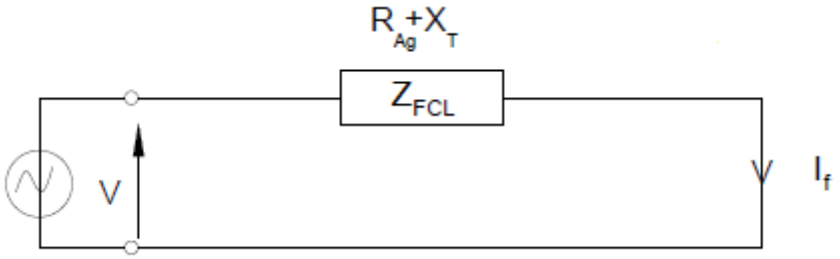

c.) After Quenching occurs during a fault

Figure 6.1 HTSPCTFCL operation

The current in the circuit in figure 6.1 (a) is due to the impedance of the transformer and the load impedance. This is given by

$$I_L = \frac{V}{Z_T + Z_L} \qquad (6.1)$$

where Z_T is the total impedance of the transformer

and Z_L is the impedance of the load

When a fault occurs, the secondary windings of the transformer are shorted as depicted in figure 6.1 (b), the short circuit current immediately after the fault occurrence is referred as prospective current, I_{prosp} .

$$I_{SC} = I_{prosp} = \frac{V}{Z_T} \qquad (6.2)$$

Once quenching occurs, the resistance of the silver matrix is introduced in the transformer impedance, therefore the fault current is given by

$$I_f = \frac{V}{Z_{FCL}} \qquad (6.3)$$

where $\vec{Z}_{FCL} = \vec{R}_{Ag} + \vec{X}_T$ (6.4)

and R_{Ag} is the resistance of the silver matrix in the transformer

X_T is the leakage reactance of the transformer

The performance measure for a resistive HTSPCTFCL is estimated by the ratio of the fault current and the prospective current, I_f / I_{prosp}. BSCCO/Ag tapes have very low resistance in its normal conducting state. Therefore to design a HTS partial core transformer as a fault current limiter, very long BSCCO/Ag tapes would be required to properly limit fault currents [Fushiki *et al*. 2007].

The long BSCCO/Ag tapes for the windings in the HTSPCTFCL would affect the operational characteristics of the HTSPCTFCL as a transformer due to excessive leakage. Therefore, a design consideration which included the resistive property of the BSCCO/Ag tape and the leakage reactance of a partial core transformer for limiting fault current was considered.

6.3 Design Model

The reverse design model discussed in chapter 3 is used to model the HTS transformer fault current limiter. A flow chart depicting the format of the model is shown in figure 6.11. The model consists of an input module which contains the input specifications, main module where all the calculations take place and output module. The input module specifies the supply conditions and physical characteristics and dimensions of the core, former and windings.

The results obtained from the output are checked to see if the HTSPCTFCL exhibits the characteristics of a good transformer. If so, then the fault current limiting ability is checked. If the prospective current is lower than the previous iteration and satisfies the requirement of the design then the iteration is stopped. If not, then the parameters such as the number of layers or number of turns of the winding are altered. The alteration is done while monitoring the flux density of the core in conjunction to the transformer parameters. The saturation flux density of grain oriented silicon steel is 2.03 T. The design should optimise the core while operating within its saturation limits.

Once the design with the most optimum characteristics has been obtained, the output is checked for desired results and the iteration is stopped.

6.4 Proposed design

In this section the proposed design of HTSPCTFCL with different winding configurations and core dimensions is highlighted. The feasibility of inter-leaving windings is reviewed. Modifications made to the inter winding and inter layer insulation for better cooling after the catastrophic failure of the HTSPCT discussed in chapter 4 is been detailed. This is followed by cryogenic testing of the insulation material used in the HTSPCTFCL.

6.4. 1 Preliminary design considerations

The windings of the HTSPCTFCL could be pancake shaped, cylindrical or a combination of both. For a pancake shaped design, the flux linkage with the secondary windings would not be good as the radial leakage from the core decreases as the radial distance increases [Grzesik et al, 2007]. This would not make a good transformer. Its only application can be assumed to be of a fault current limiter. The cylindrical design is a better concept as it would

allow the characteristics of a transformer as proved in chapter 4 for the two partial core transformers. At the same time, the leakage reactance of the transformer can provide fault current limiting capability.

The design for the HTSPCTFCL was proposed on the geometry of a HTSPCT. The HTSPCT tested in chapter 4, formed a platform for this design. There were parameters in the open circuit, short circuit and load test which validated its feasibility as transformer. Therefore, the HTSPCTFCL was based on this platform and some of the materials from the original HTSPCT were reused for economic reasons. The idea of reusing the vacuum Dewar produced a number of constraints on the design of the HTSCTFCL. The geometry of the former in the old HTSPCT meant that the windings had to be wound around this former. The length of the original HTSPCT former and core vessel created a constraint on the axial length of the windings. This in conjunction with the existing diameter of the Dewar also placed a limitation on the radial width of the windings. The size of the core used in the HTSPCTFCL was also limited as the core vessel was attached to the vacuum Dewar. A proposed concept of the design is shown in figure 6.2.

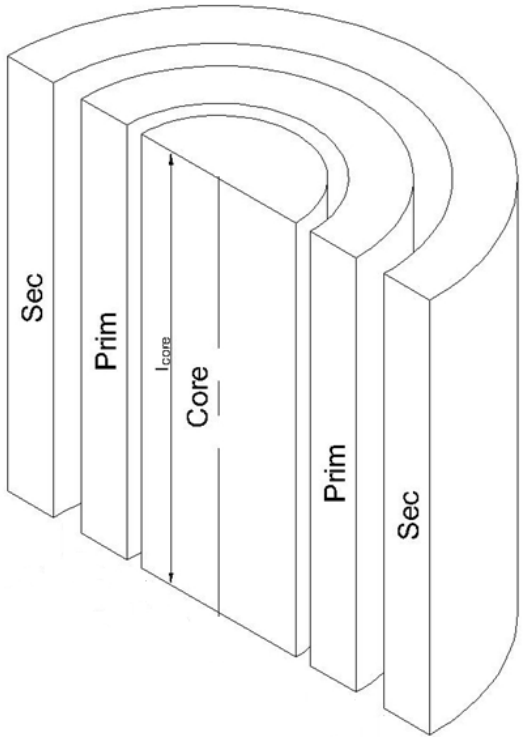

Figure 6.2 Proposed Cylindrical layout of the HTSPCTFCL

6.4.2 Components of the concept HTSPCTFCL

A cryogenic equipment for maintaining the HTSPCTFCL under cryogenic conditions, core of the transformer and the windings form the components of the concept HTSPCTFCL.

6.4.2.1 Cryogenic equipment for cooling

To maintain the HTSPCTFCL under cryogenic conditions, a vacuum Dewar was filled with liquid nitrogen. The Dewar consists of an inner vessel for storing the LN2 and an outer vessel exposed to room temperature with a vacuum between them. The vacuum is present to limit convection losses to the LN2 from the outside. To limit radiation coming into the vessel from the outside, several layers of aluminized non-stretch polyester were wrapped around the inner vessel. Care was taken not to create shorted turns by insulating the aluminized non-stretch polyester with vacuum rated tissue paper. The bottom of the inner vessel was dome shaped so that the joint between the dome and the tube of the inner vessel, when exposed to LN2, expanded and contracted evenly. A pressure relief port is present on the outside of the Dewar in case a failure of the inner vessel results in nitrogen gas venting into the vacuum chamber [Bodger *et al.* 2005].

The core vessel is similar to the vacuum Dewar in that a vacuum is formed between the core and the LN2. A similar arrangement of aluminized polyester and tissue was used in the core vessel.

6.4.2.2 Core

The core used in the design of HTSPCTFCL was the same core from the copper wound transformer and HTSPCT tested in chapter 4. The core was constructed from high permeability, grain oriented silicon steel. It was designed as a circular core with stacked laminations arranged in parallel. There were 348 laminations of 0.23mm each. The core was bound with Vidatape S, a woven high shrink polyester tape and was hot dipped twice in an electrical baking varnish. An axial hole in the core was provided to house a 1240mm G-10 fibreglass 5/8 UNC threaded rod. The rod allowed for correct positioning of the core inside the core vessel relative to the windings. This was necessary for uniform flux distribution. The core had a length of 484 mm. It was cut with a water jet into 8 sections as it was used in another project at the UoC. This also provided an opportunity to consider different core lengths within the limitation of the allowed length of the core vessel. The lengths of the core sections are given in table 6.1. Figure 6.4 shows the laminated circular core that was utilised in the design.

Table 6.1 Section lengths of the silicon steel core

Core section 1	42 mm
Core section 2	42 mm
Core section 3	50 mm
Core section 4	50 mm
Core section 5	60 mm
Core section 6	60 mm
Core section 7	90 mm
Core section 8	90 mm

The properties of grain oriented silicon steel are given in table 6.2

Table 6.2 Properties of Grain oriented silicon steel

Relative Permeability	5000
Resistivity at 20^0C	$472 \times 10^{-9}\Omega$m
Thermal Resistivity Coefficient	0.006 Ωm/K
Material Density	8954 kg/m

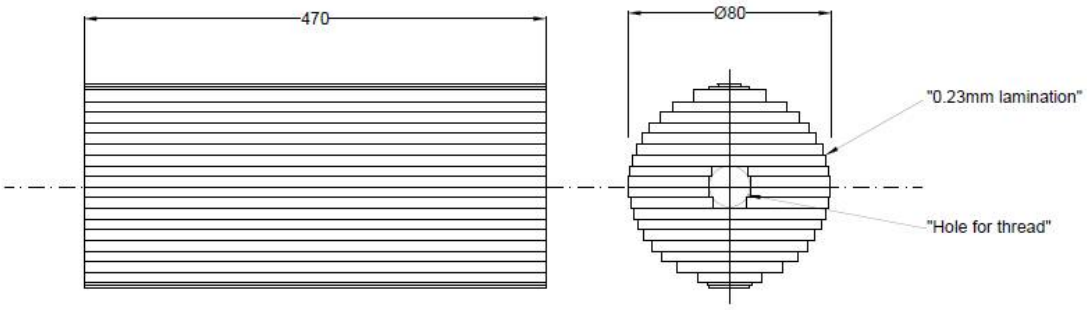

Figure 6.3 Stacked laminations of the core

6.4.2.3 Winding configuration

Three sets of winding configurations were considered for the design for the geometry of the HTSPCTFCL, Inter leaving windings and parallel conductor windings. Inter-leaving windings for HTS can be complex as the windings need to be immersed in LN2. However in a partial core design this can be achieved as the windings are wrapped around a central core. Inter-leaving reduces the leakage reactance due to better coupling between the primary and secondary windings of the HTSPCT. However, the transition of windings around the core can be difficult to manufacture and for the purpose of a HTSPCTFCL, a high leakage reactance can be useful. The second option with parallel conductors can be useful but would require extra lead-outs. The extra lead-outs can result in large conduction losses and therefore this configuration is eliminated from design considerations.

The third option, involves one primary and one secondary winding. This configuration is much simpler to manufacture than the above two and also factors the low losses desired in a transformer and high reactance required in a fault current limiter.

Figure 6.4 shows the three winding configurations considered before making the final decision on the design of the HTSPCTFCL winding configuration. Figure 6.4 (a), (b) are for interleaving winding.

The HTS used in the windings is a BSCCO/Ag 2223 tape. The inventory of HTS tape that was available at UoC for the project is given in table 6.3. The characteristics of the tape selected for the design are given in table 6.4.

From table 6.2, HTS 004 and HTS 005 were chosen as there was sufficient length for the primary and secondary windings of the HTSPCTFCL. The tapes were tested for dc critical current, I_c , their n-value and imperfections in the tapes at IRL, Wellington. Figure 6.5 and figure 6.6 shows tape scope results obtained from the tests for HTS 005 and HTS 004.

HTS 005 had an imperfection between 65m and 77m of the tape. Therefore, the useful length was 200 m for this tape. Thus the length of the tape used in the windings had to be within this dimension. This included the connection to the copper lead outs. Therefore, the length of HTS tape for the windings was taken as 197m. HTS 004 was found to have some imperfections between 100m and 123m. And therefore, only 277 m could be used in the design excluding the allowance for copper leads.

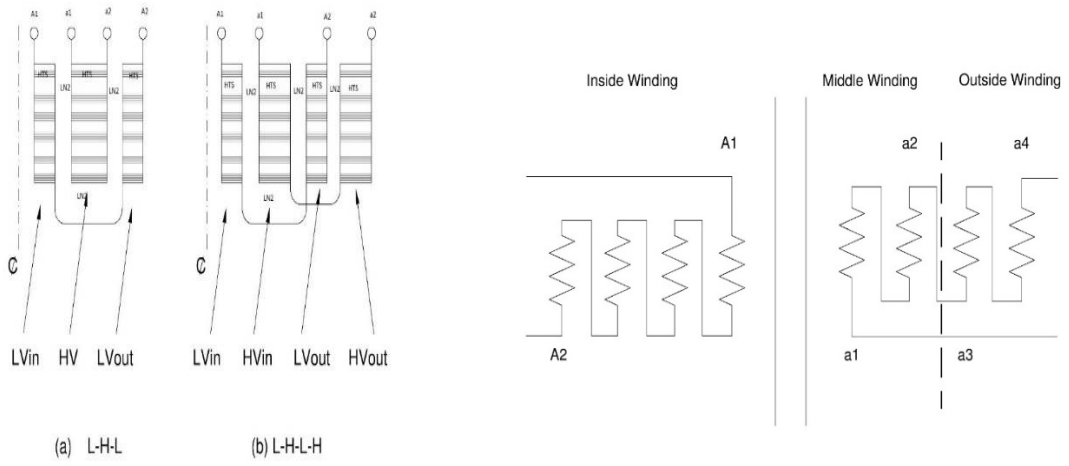

Figure 6.4 Options for Winding configuration of the proposed design

Table 6.3 Inventory of HTS tape stock at UoC

Designation	Description	Length (m)	Ic (A)	n value
HTS001	BSCCO tape with Nomex insulation	30	84.8	15.4
HTS002	Uninsulated BSCCO from HTS-110	100	88.3	16.6
HTS003	BSCCO tape with Nomex insulation from original transformer	35	123.8	16.5
HTS004	Uninsulated BSCCO from HTS-110	371	88	15.3
HTS005	Uninsulated BSCCO from HTS-110	277	91.1	15.6
HTS006	Supplied from Australian Superconductor	130	31.4	15.2
HTS007	BSCCO tape with Nomex insulation from original HTS transformer	22	141.3	16.5
HTS008	BSCCO tape with Nomex insulation	120	91.1	15.6

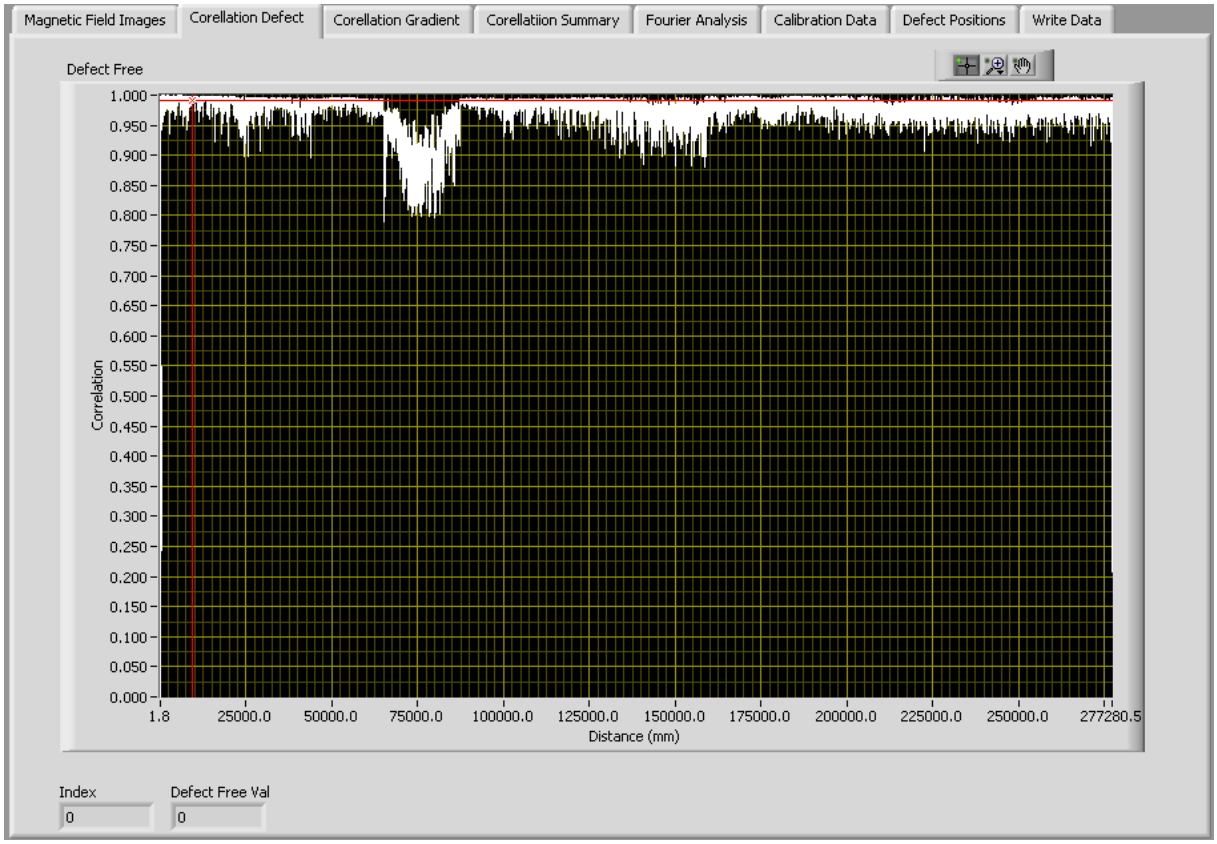

Figure 6.5 Tape scope of HTS 005 tested in lab

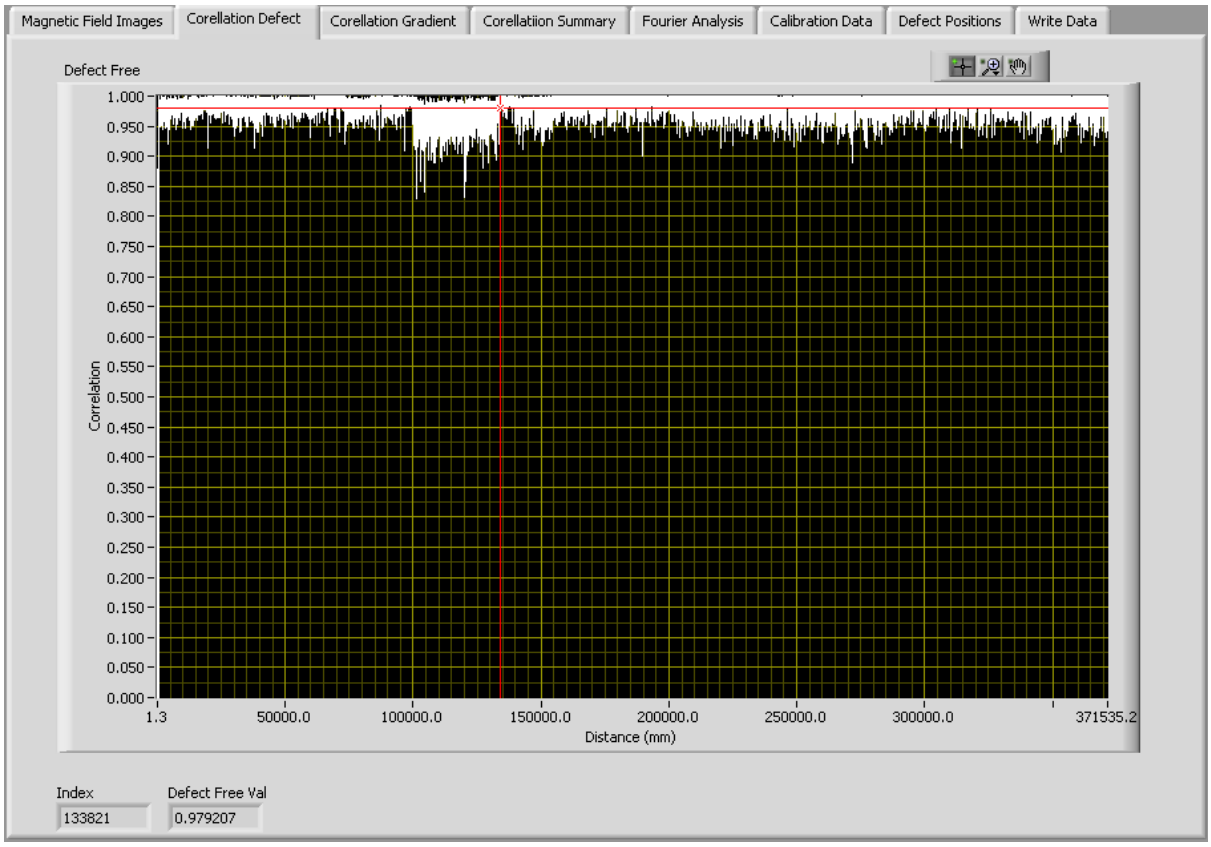

Figure 6.6 Tape scope of HTS 004 tested in lab

Table 6.4 Properties of the two BSCCO tape used as HTS windings

Volume Specific Heat	2.44 J/cm^{3}K
Resistivity @273K	14.67 × 10^{-9} Ωm
Thermal Resistivity Coefficient	60 × 10^{-12} Ωm/K
Material Density	10500 Kg/m^3
n-value	15.3
Critical current	91.1 and 88
Fraction of HTS in tape	0.85

6.4.3 Insulation

6.4.3.1 Modifications made to insulation layers

The HTSPCT tested in chapter 4 had Nomex tape as insulation between layers of the windings. Nomex was tested along with Kraft paper [O'Neill, 2001] and found to have good insulating properties. However, after the failure of the HTSPCT highlighted in chapter 5, an alternative insulation was investigated. Work done by Irvine Chew [Chew, 2011] established that with sufficient cooling an HTS transformer can function well beyond its critical current value.

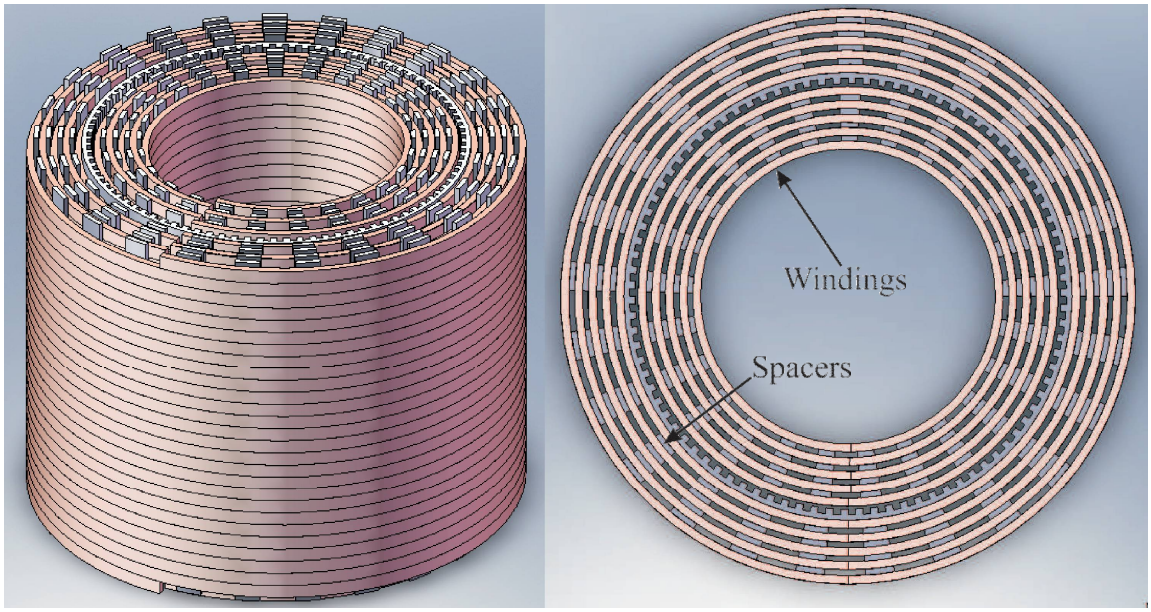

Figure 6.7 Rectangular spacers used in Irvin Chew transformer

Figure 6.7 shows the spacers that make rectangular channels in a full core transformer designed by Irvine Chew. Spacers and insulation mesh were two alternatives considered for the design. The spacers were made from fibre composite. The spacers make channels and the channels are open paths for LN_2 to flow through. The bulkiness of the channels and also the complexity in holding them together in a vertical configuration as in the proposed design made it unfeasible for use. This, in conjunction with the limitation in space between the core vessel over which the former would slide and the inner walls of the vacuum Dewar, eliminated the use of rectangular channels from the proposed design.

The mesh described in the chapter 7 of this thesis was used as the insulation between the different layers of the windings. G10 and PTFE were two materials considered for the insulation mesh. Both materials had good tensile strength and low temperature characteristics. PTFE was sufficiently flexible to be wound on the cylindrical former while G10 was only flexible enough once it had been channelled.

6.4.3.2 Cryogenic testing of insulation material used in HTSPCTFCL

The PTFE was immersed in liquid nitrogen for 4 hours to see if there were any visible changes to the material. As no changes were observed during the prolonged exposure to liquid nitrogen, it was suitable to be used as the material of insulation mesh.

6.4.3.3 Insulation for the HTS tapes.

Nitto™ tapes were wrapped around the HTS tapes for insulating them. The tapes had a high temperature withstand ability, which was a consideration for withstanding the rise in temperature under fault conditions.

6.5 Proposed design iterations

The steps highlighted in the flow chart in figure 6.11 were executed in the reverse design process for the proposed model. The core length, winding layers, flux density of the core were modified to obtain a HTSPCTFCL with good transformer operational characteristics and also work as a fault current limiter. Two designs among the several investigated are given in tables 6.5 and 6.6. The tables highlight the compromise made in the voltage regulation, the prospective current and the maximum flux density of the HTSPCTFCL.

Table 6.5 Design iteration with 484 mm core and 6/6.5 layers winding

Flux Density	0.4 T
Primary Layer	6
Secondary Layer	6.5
Length of windings	484 mm
Diameter of core	80 mm
Length of core	484 mm
Regulation	5.5
Efficiency	98.56 %
Peak Prospective Current	134 A
Fault Current	130.9 A
Wire length per conductor for Primary	240.7 m
Wire length per conductor for Secondary	303 m
Weight	22.7 kg

Table 6.6 Design iteration with 484mm core and 4/4 layers winding

Flux Density	0.6 T
Primary Layer	4
Secondary Layer	4
Length of Windings	484 mm
Diameter of core	80 mm
Length of core	484 mm
Regulation	2.1
Efficiency	99.20 %
Peak Propective Current	524.6 A
Fault Current	415.6 A
Wire length per conductor for Primary windings	152.6 m
Wire length per conductor for Secondary windings	167 m
Weight	21.5 kg

In tables 6.5 and 6.6 the two designs have the same core dimensions. The only difference is the number of layers. Table 6.5 has 6 layers in the primary windings and 6.5 layers in the secondary windings. Table 6.6 has 4 layers in the primary windings and 4 layers in the secondary windings. The first design produces a HTSPCTFCL with high regulation and high

fault current limiting capability, while the design with 4 layers produces a HTSPCTFCL with low regulation and low fault current capability. As the requirement is to have a design which incorporates the features of both a transformer and fault current limiter, the design with 6 layers in the primary windings and 6.5 layers in the secondary windings is more desirable.

Table 6.7 Design iteration with 264mm core and 6/6 layers winding

Flux density	0.8 T
Primary Layer	6
Secondary Layer	6
Axial Length of windings	264 mm
Diameter of core	80 mm
Length of core	264 mm
Regulation	7.2
Efficiency	99.30%
Peak Prospective Current	271.2 A
Fault Current	254.6 A
Wire length per conductor for Primary windings	129.4 m
Wire length per conductor for Secondary windings	147 m
Weight	13.9 kg

The designs presented in tables 6.7 and 6.8 have the same dimensions of the core with only the number of layers in the primary windings and secondary windings being different. Table 6.7 has 6 layers in the primary and secondary windings. While table 6.8 has 4 layers in the primary and secondary windings. Table 6.7 produces a design with 7.2% regulation while table 6.7 produces a design with 4.3% regulation. The design in table 6.8 has a low regulation but at the same time a low current limiting ability. Therefore, for the propose HTSPCTFCL, the design in table 6.7 is more desirable.

The designs in tables 6.5 and 6.7 are suitable designs for further consideration in the HTSPCTFCL model. The design in, table 6.5 meets the criteria for a better HTSPCTFCL since it has better regulation and higher current limiting ability. However, the conductor length of the primary windings is 240m which is not within the scope of the available materials. Therefore, further iteration of the design model was required to produce a HTSPCTFCL with the available materials in disposal. After considering all the iterations and possible combinations for a HTSPCTFCL, the design given in table 6.9 had acceptable regulation and fault current limiting capability and at the same time matched the conductor length at disposal. Therefore, it was selected as the final design of the HTSPCTFCL.

Table 6.8 Design iteration with 264 mm core and 4/4 layers winding

Flux density	1.2 T
Primary Layer	4
Secondary Layer	4
Axial Length of windings	264 mm
Diameter of core	80 mm
Length of core	264 mm
Regulation	4.3
Efficiency	99.58%
Peak Prospective Current	1001.2 A
Fault Current	637.7 A
Wire length per conductor for Primary windings	82 m
Wire length per conductor for Secondary windings	89.9 m
Weight	13.3 kg

Table 6.9 Design iteration with 384 mm core and 6/6.5 layers winding

Flux Density	0.5 T
Primary Layer	6
Secondary Layer	6.5
Length of windings	384 mm
Diameter of core	80 mm
Length of core	384 mm
Regulation	5.8
Efficiency	98.73 %
Peak Prospective current	165.2 A
Fault current	160.8 A
Wire length per conductor for Primary windings	189 m
Wire length per conductor For Secondary windings	238 m
Weight	18.7 kg

The designs presented in tables 6.5,6.6,6.7,6.8 and 6.9 also highlight the difference between the prospective current and the fault current. The difference is not significant as the resistance introduced by the silver matrix is negligible compared to the reactive component of the HTSPCTFCL.

The equivalent circuit parameters obtained by simulating the design from table 6.9 are given in table 6.10.

Parameter	Value (Ω)
R_1	0.023
R_2	0.03
R_{ec}	1.58×10^5
R_h	2.97×10^2
R_c	2.97×10^2
X_1	0.74
X_2	0.74
X_m	14.3

Table 6.10 Equivalent circuit parameters

Sketches of the final design of the HTSPCTFCL are given in figures 6.8 and 6.9.

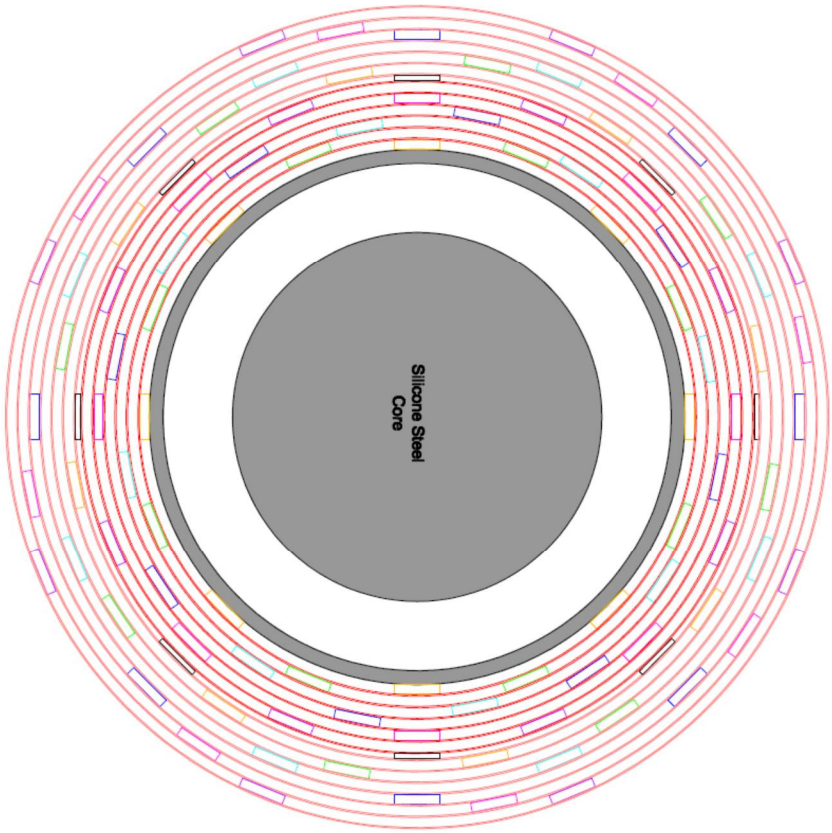

Figure 6.8 Top view of the proposed design

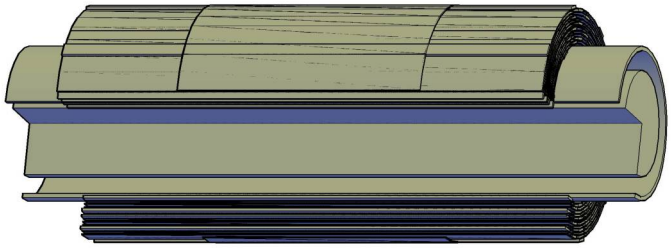

Figure 6.9 3D model of the proposed design with the windings wound on former

6.6 Comparison of leakage in flux plots of the proposed design iteration

Flux plots for the proposed design iterations were plotted in FEA to estimate the leakage flux when the HTSPCTFCL is connected with a resistive load. Figures 6.10 (a), (b), (c) and (d) show the flux plot for the some of the iterations performed in the design model and presented in this chapter. Figure 6.10 (e) shows the flux plot with the smallest core length used in the iteration process.

The effect of changing the core length and the number of layers on the leakage flux between the windings was noted. For the core length of 484 mm and 6 layers of windings on the primary and 6.5 layers of windings on the secondary, the leakage flux was low. This design would be suitable for a transformer operation but since a high leakage reactance is required for limiting the fault current, the design iteration was not one of the best choices for the HTSPCTFCL.

With core length of 264 mm and 6 layers of windings in the primary and secondary, the leakage flux was high. From equation 3.34 in chapter 3,

$$X_{12} = \omega\mu_0 \frac{N_1^{\,2}}{l_c}\left(l_p \frac{d_1}{3} + l_s \frac{d_2}{3} + l_{ps}\Delta d\right) \qquad (6.1)$$

where lc is the length of the core and d1 and d2 are the width of the primary and secondary windings. With more number of layers, the width of the windings increases and so does the leakage. With a smaller core length, the leakage reactance is even higher. However, a very high leakage

reactance will affect the transformer property of the HTSPCTFCL as the voltage regulation would be high.

Therefore, by adjusting the core length and the number of layers in the primary and secondary windings, a design for the HTSPCTFCL was obtained which performed well as a transformer and fault current limiter.

Length of core	484	mm
Length of winding	484	mm
Number of layers in primary	6	
Number of layers in secondary	6.5	

In this plot, the core length is higher than the other design iterations. Therefore, the leakage flux observed is low.

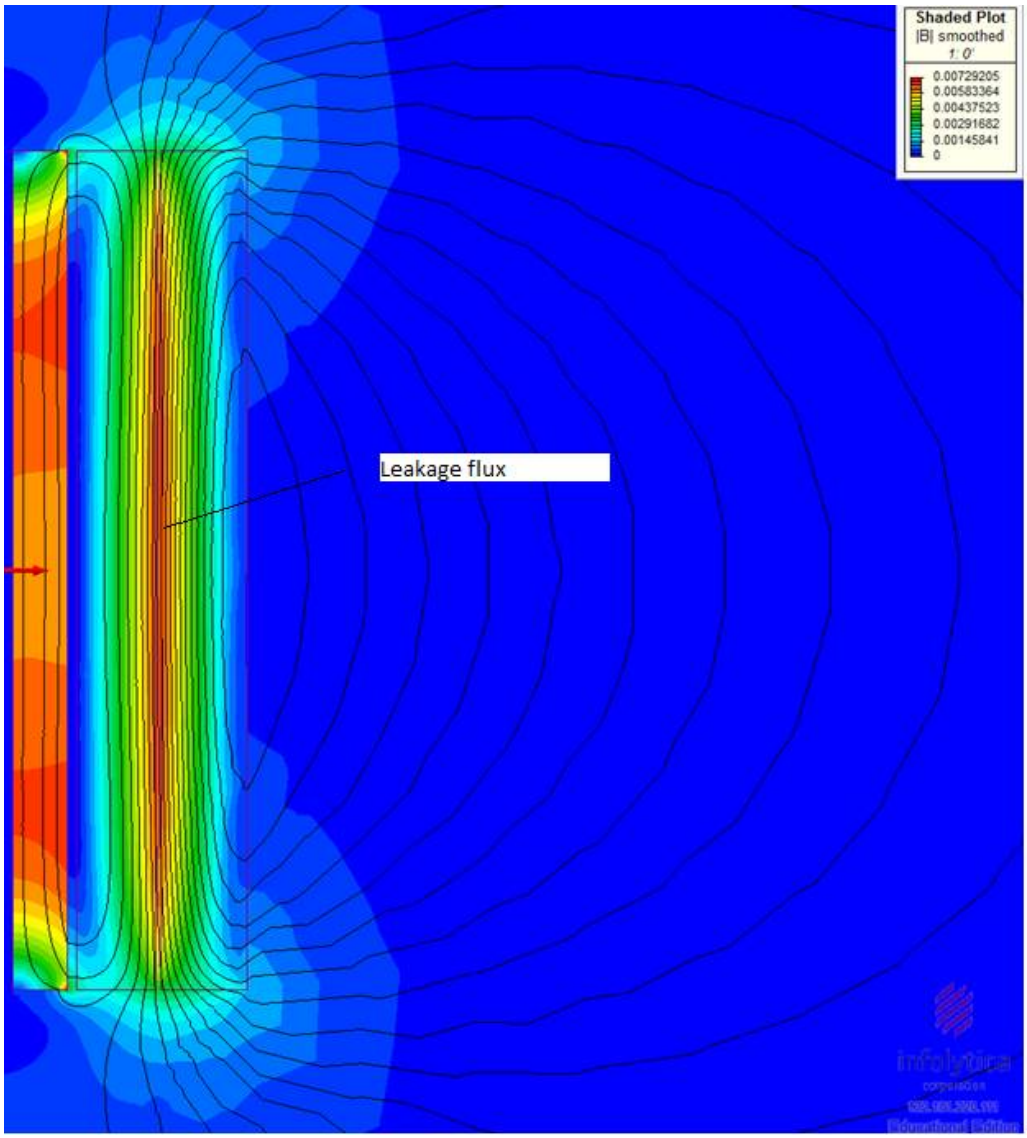

Figure 6.10 (a) Flux plot for 1st Design iteration

Length of core	264	mm
Length of winding	264	mm
Number of layers in primary	6	
Number of layers in secondary	6	

In this plot, a very high leakage is observed. It could work well as a fault current limiter, but the transformer characteristics will be affected.

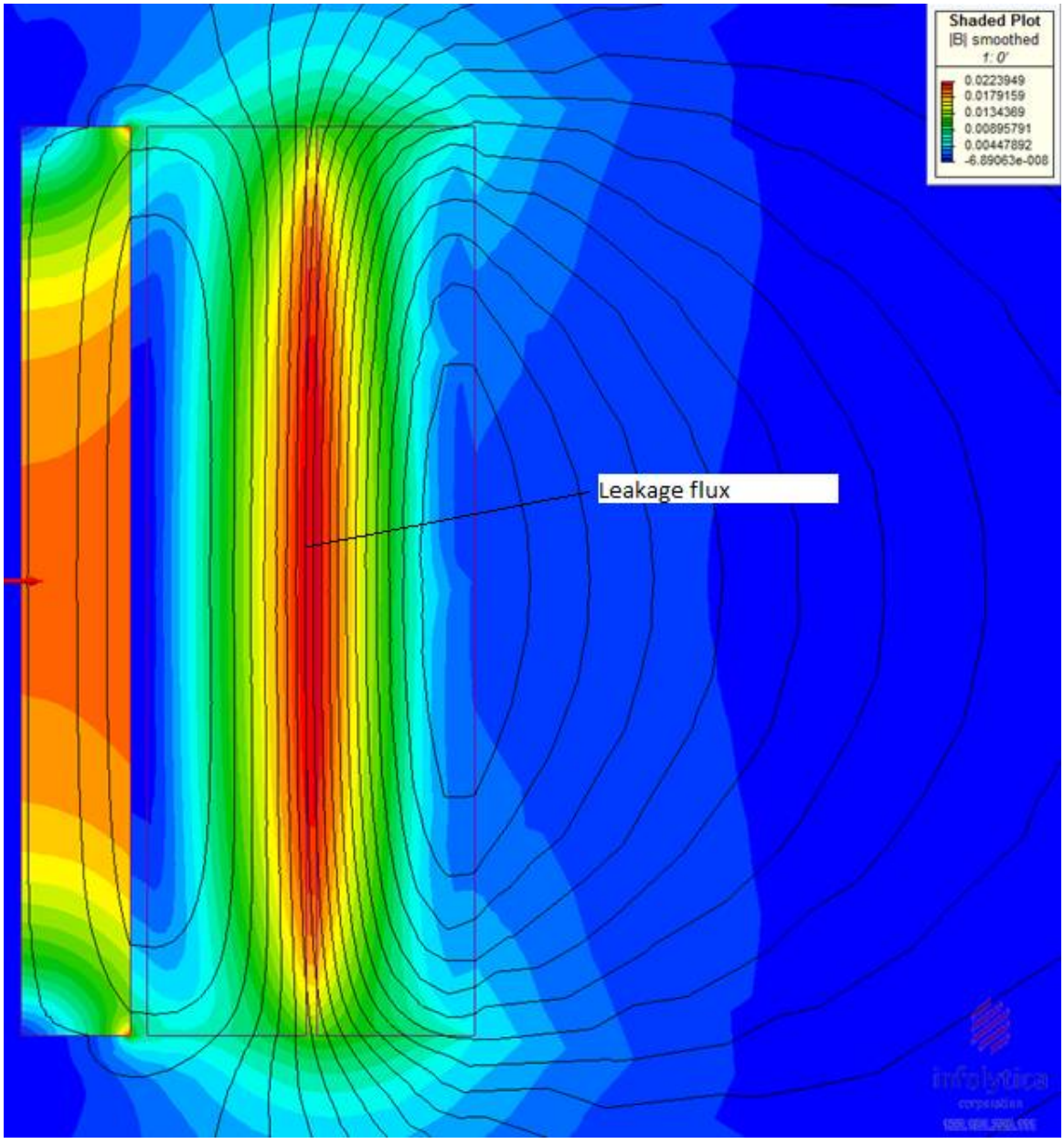

Figure 6.10 (b) Flux plot for 3rd Design iteration

Length of core	264	mm
Length of winding	264	mm
Number of layers in primary	4	
Number of layers in secondary	4	

In this plot, the core length is same as the design in figure 6.10 (b), but with less number of layers in the primary and the secondary. Therefore, a lower leakage flux is observed.

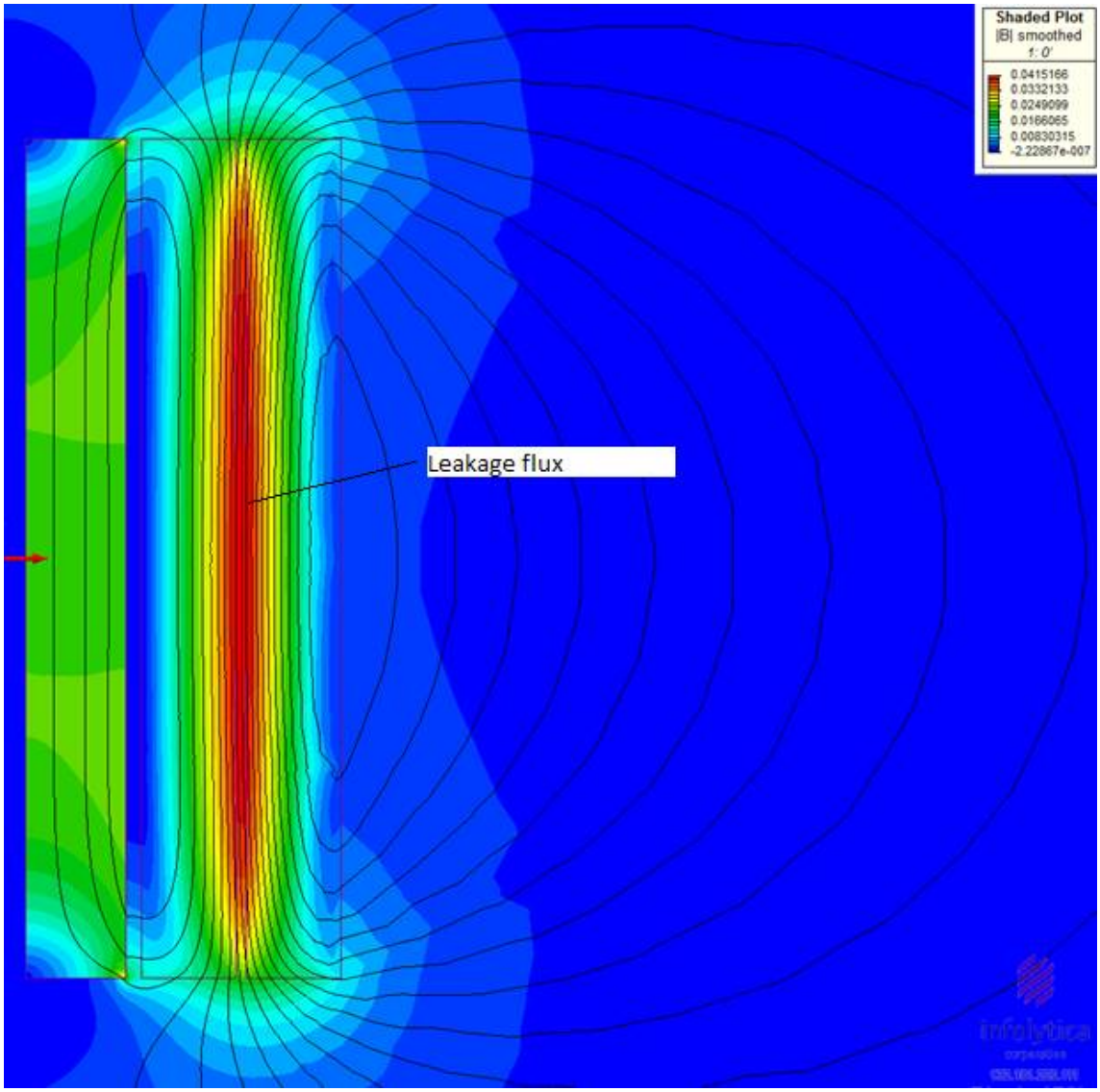

Figure 6.10 (c) Flux plot for 4th Design iteration

Length of core	384	mm
Length of windings	384	mm
Number of layers in primary	6	
Number of layers in secondary	6.5	

In this plot, the leakage flux is within acceptable limits of a transformer and it can be also used as a current limiter.

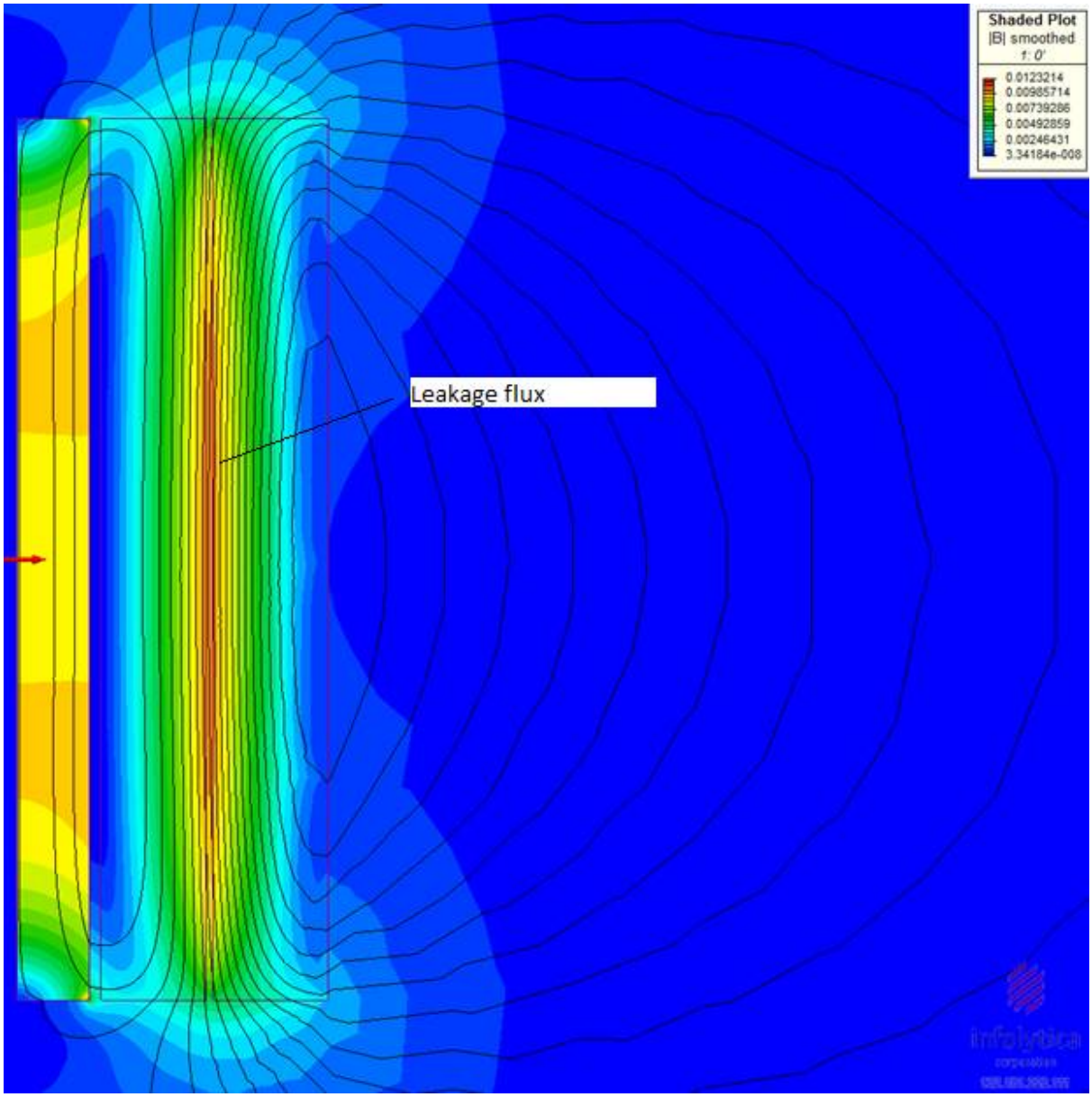

Figure 6.10 (d) Flux plot for Final design iteration

Length of core	170	mm
Length of windings	170	mm
Number of layers of primary	6	
Number of layers of secondary	6	

The flux plot for one of the smallest core length considered in the design process has been plotted in figure 6.10 (e). With a smaller core length, the leakage flux is higher when compared to the other flux plots in this chapter.

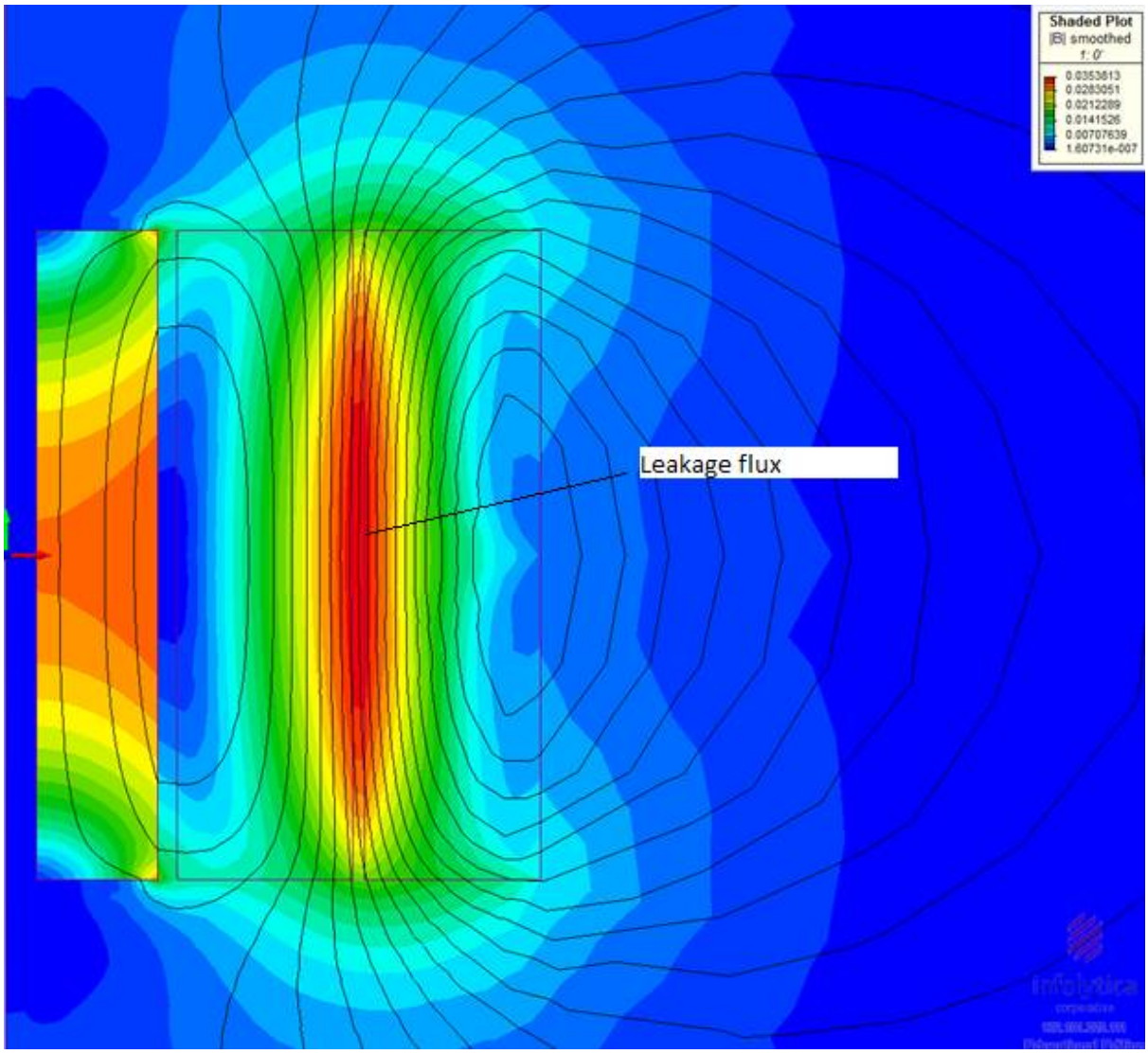

Figure 6.10 (e) Flux plot for the smallest core length used in the iteration

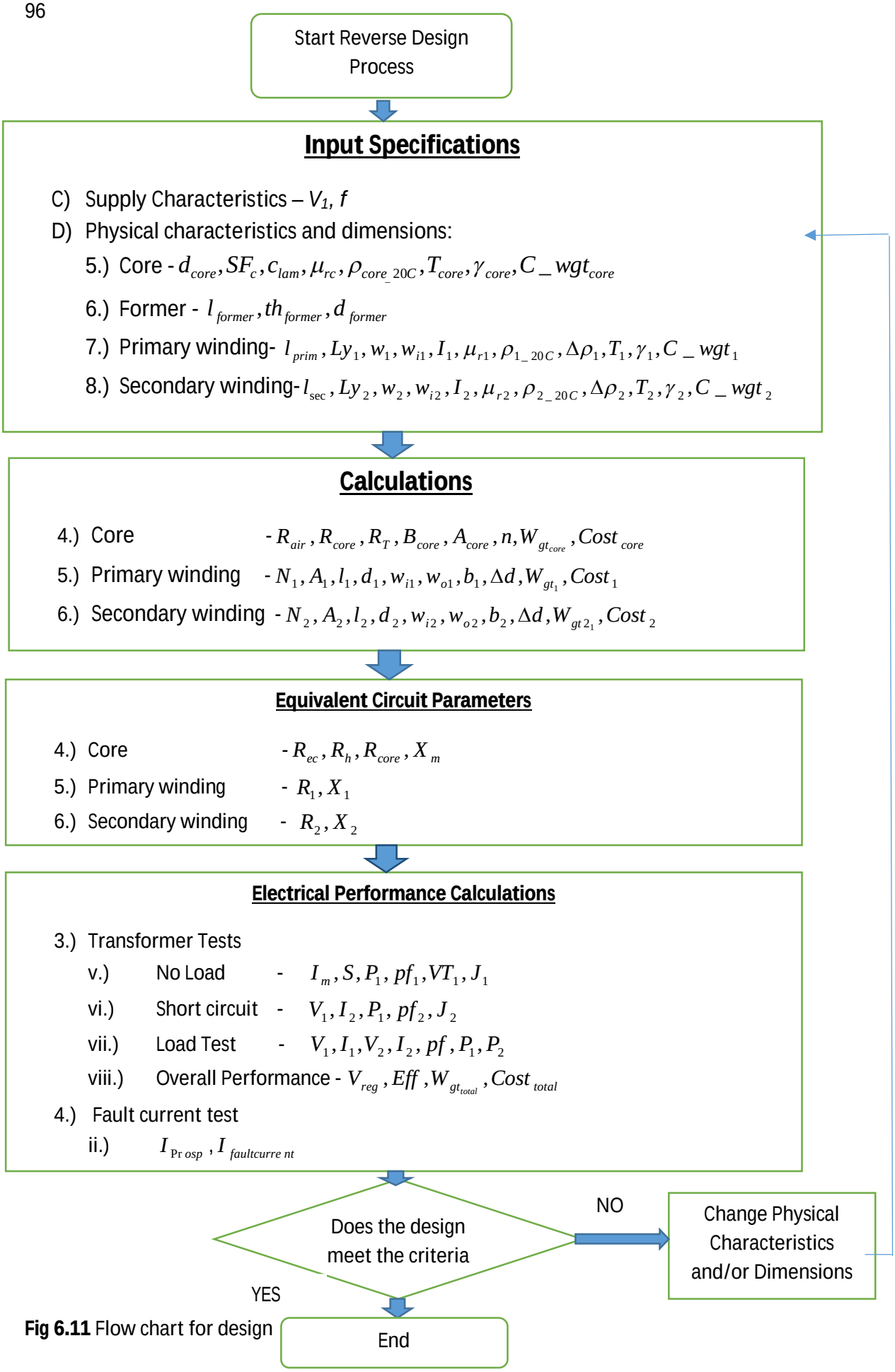

Fig 6.11 Flow chart for design

6.7 Conclusion

A concept HTSPCTFCL was designed with available materials at the UoC. The reverse design process was used to design this model. A flow chart highlighting the design process was displayed with the critical parameters that govern the final design. Materials for insulation and the cryogenic equipment were also highlighted.

Modifications were made to the insulation that was part of the HTSPCT tested in chapter 4. G10 and PTFE were considered as materials for inter-winding and inter-layer insulation. Using the materials for insulation, a new design was proposed which allowed for sufficient cooling of the windings. The materials were tested in liquid nitrogen to confirm the suitability of the materials chosen for the design. Iterations were performed on the model to optimise the design and obtain the final design which exhibited the characteristics of a transformer and fault current limiter. The difference in the prospective current and fault current was highlighted. This difference in the two currents was due to the resistance of the silver matrix in the BSCCO/Ag tape. Flux plots for the various design configurations were compared to observe the change in leakage reactance for different core length and width of the windings.

Chapter 7
Fabrication of the HTSPCTFCL

7.1 Introduction

In this chapter the details of the fabrication of the HTSPCTFCL are presented. This includes fabrication of the former and the inter-layer insulation, insulation of the HTS tapes, the winding construction and the transformer assembly.

The section concludes with details of the cooling system utilised to test the HTSPCTFCL prototype.

7.2 Fabrication

The HTSPCTFCL was fabricated with some materials that were readily available at the UoC and materials sourced from a third party. The Dewar and the core were reused from the HTSPCT tested in chapter 4, while the windings were constructed from the HTS tapes available from the UoC inventory. The former was fabricated with the help of a third party.

7.2.1 Insulating the HTS tapes

The HTS tapes were initially uninsulated. They were insulated to prevent shorted turns. A device was built to insulate the tapes. Figure 7.1 shows the insulating device. It folded two separate lengths of Nitto^{TM} tape onto the HTS tapes while it was extruded through the machine. The HTS tape was fed through rollers and two reels of Nitto^{TM} tape were folded over the bare HTS. The folding action is done by a copper fold that folds half of the tape onto each side of the HTS tape. The Nitto^{TM} tape has a width that is twice the width of the HTS tape. There are two copper folds in the insulating machine, so that both sides of the HTS tape are insulated by the Nitto^{TM} tape. Figure 7.2 and Figure 7.3 shows the two halves of Nitto^{TM} being applied on the HTS tape. In figure 7.2, the first half of the HTS tape is being insulated through the copper fold. Tension is applied using the tension mount that holds the HTS tape while the Nitto tape is being applied. This ensures uniform application of the insulation of both the halves of the Nitto^{TM} tape on the HTS tape. Similarly in figure 7.3, the other half of the HTS tape is insulated with the

second copper fold. The insulated HTS tape is collected at the other end on an empty reel as shown in figure 7.1.

Figure 7.1 Insulation device

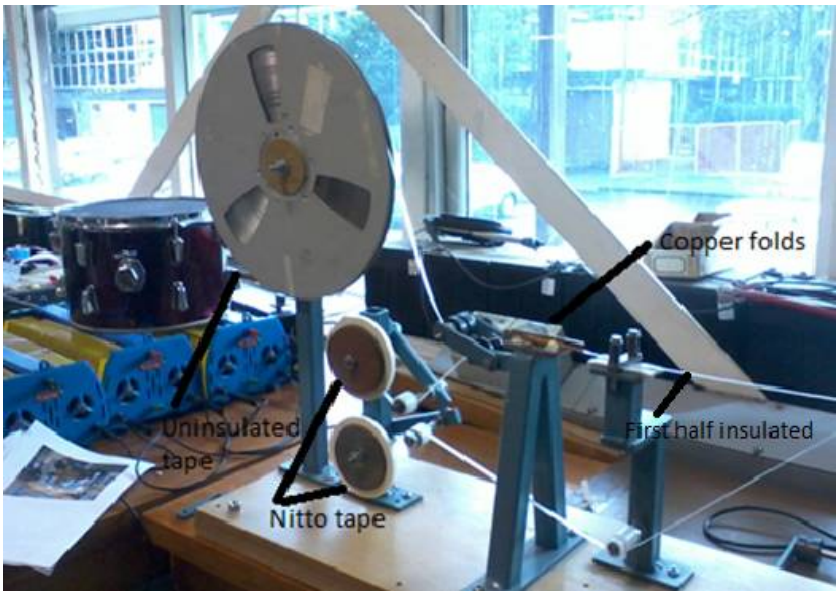

Figure 7.2 Arrangement showing folding of Nitto tape on first half of HTS

Figure 7.3 Arrangement showing folding of Nitto tape on second half of insulation

7.2.2 Fabricating the Former

A design of a former and flange ring was conceived to house the windings of the HTSPCTFCL. It was made of fibreglass and fabricated with the help of a third party. A flange ring made of G10 composite was fabricated to hold the former in place. Figure 7.4 shows the G10 flange ring and the former followed by a 3D model in figure 7.5 of the two units.

The former was 115mm in diameter and 400 mm long. It was designed so that it could slide on the warm bore tank of the core vessel. The idea behind this arrangement was to allow for removing the windings and reusing the Dewar for other projects at the UoC faculty. The flange ring could also be reused for holding windings in future projects. An M10 thread screw was used in the flange to tighten it once its position was set on the warm bore tank. For this, a cut of 15mm width and 3mm thickness was positioned radially opposite to the M10 thread. The cut on the flange ring allowed it to be tightened without causing any stress on the G10. The M10 thread was designed with sufficient spacing to allow for a G10 composite screw to be inserted in the M10 thread, once the flange ring was positioned on the warm bore tank. In figure 7.4, the drawings marked Elevation- item 1 and Section 1 show the flange ring in axial view. It has a 230 mm diameter. The part of the flange ring that goes under the former is 109mm in diameter and 40mm in height. Plan-item 2 is the top view of the cylindrical former

followed by Elevation item 2 which is the axial representation of the former. The drawings were made by the author prior to production of the former and the flange ring.

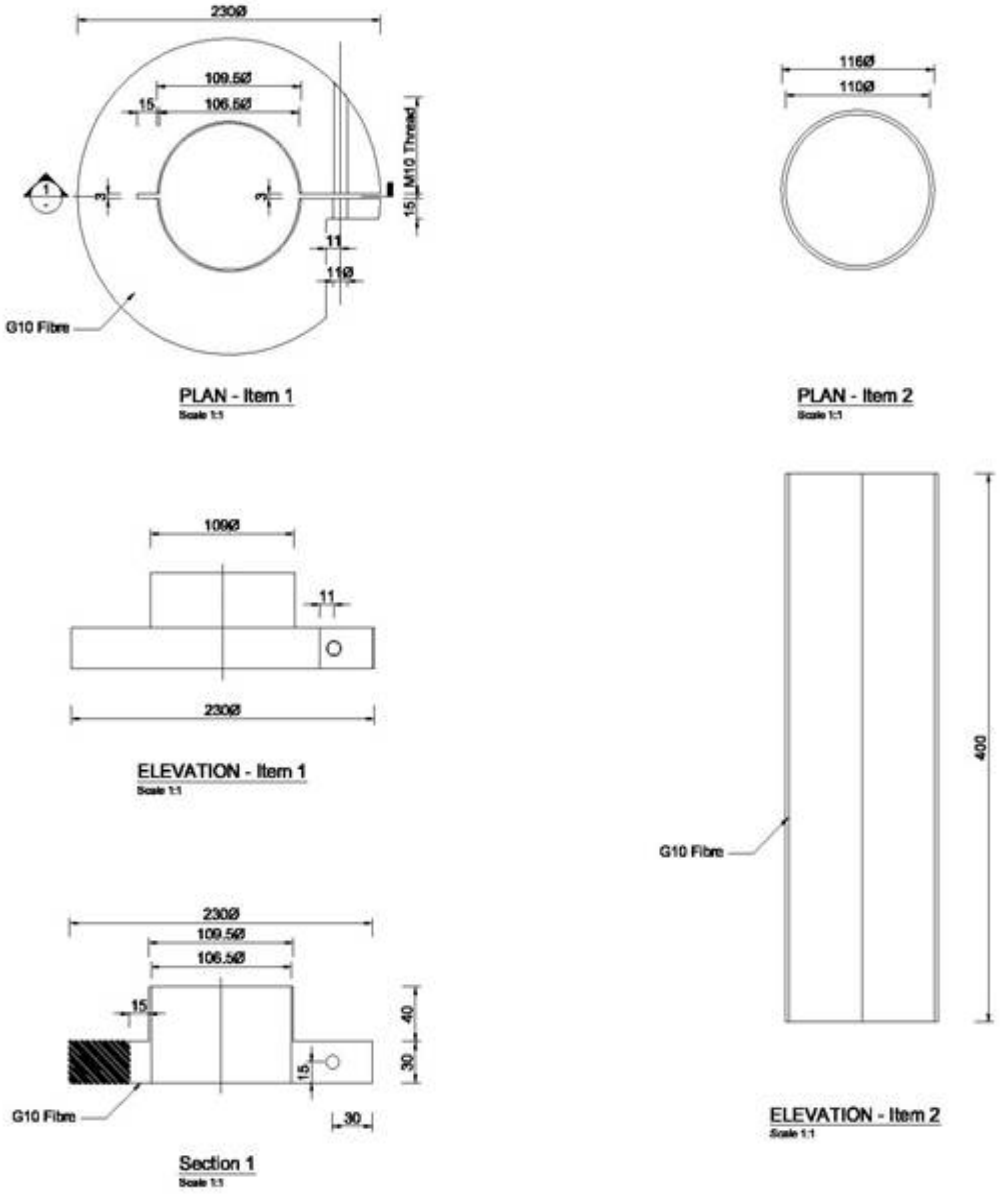

Figure 7.4 AutoCAD drawing of former and flange

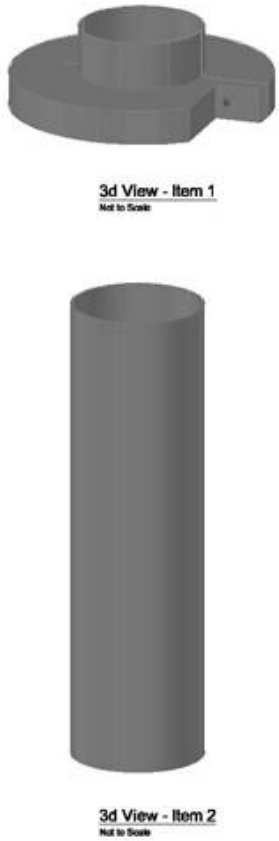

Figure 7.5 3D model of Former and flange

7.2.3 Fabrication of the inter-layer insulation

After investigating the reason for the failure of the HTSPCT in chapter 4, it was found to have insufficient cooling for the windings. The windings were not sufficiently exposed to liquid nitrogen and this caused excessive heating of the HTS windings. The windings were also tightly wound with several layers of Nomex insulation which further prevented the heat generated from the HTS windings to dissipate. Therefore, an insulation mesh was designed to insulate the inter-layers. PTFE was chosen as it was readily available and also met the criteria for low temperature applications. Figure 7.6 shows the drawing of the insulation mesh that was designed for insulating the inter-layers. Each PTFE sheet was 400mm in length and 300 mm in height. The sheets had a thickness of 3.2 mm. They were machined in a CAM machine to have 3mm wide channels. Figures 7.7 and 7.8 shows the sheets being cut in the CAM machine at the UoC. While being machined, strands of fibre residues were left on the sheets. Each sheet had to be cleaned with an air blower to remove the fibre strands. A clean sheet is

displayed in figure 7.9 after it was air blown. Each channel had 88mm long cuts with 2.3mm in depth. The sheets were flexible and could be laid on the windings without causing any stress to the PTFE material.

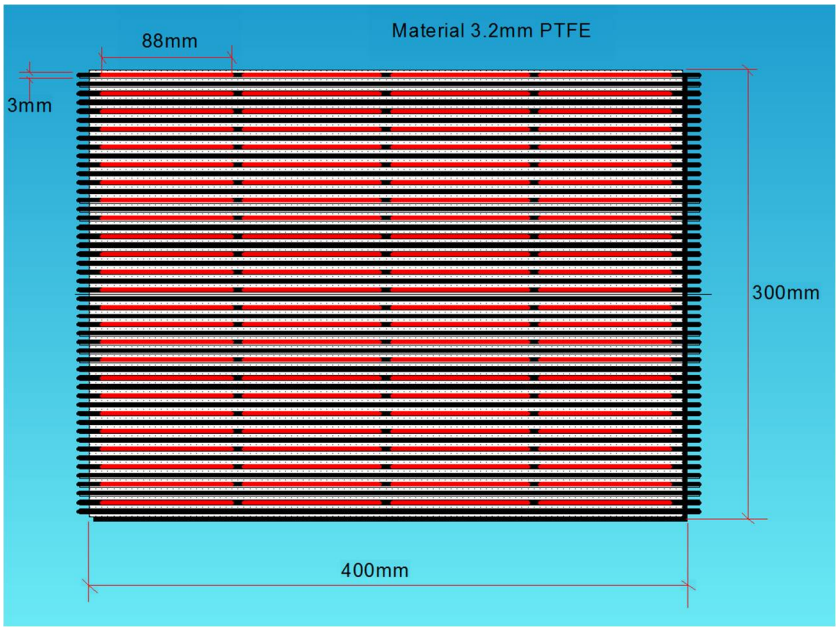

Figure 7.6 Drawing of the insulation mesh before being machined in the CAM

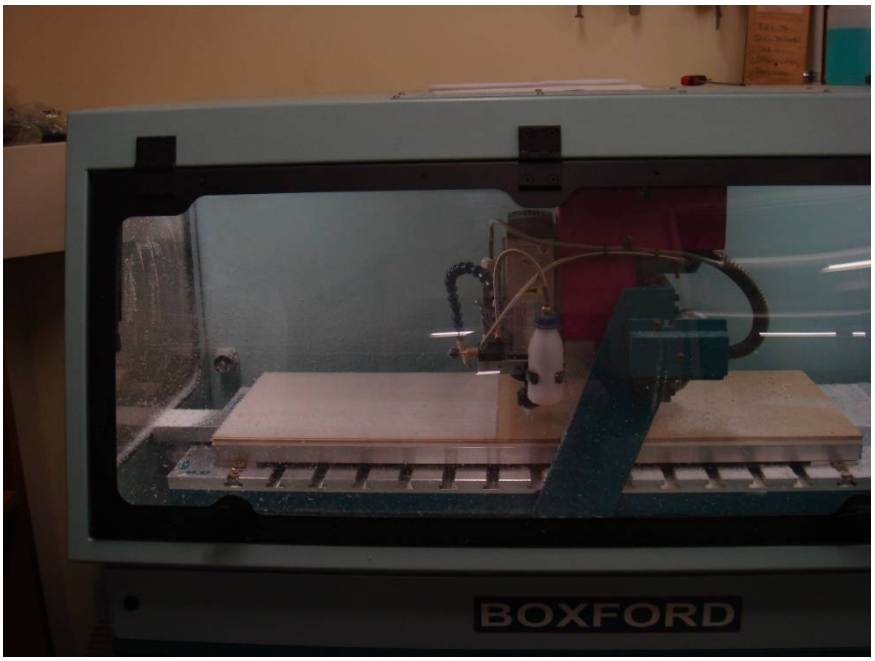

Figure 7.7 Photograph of PTFE sheet being machined in a CAM machine

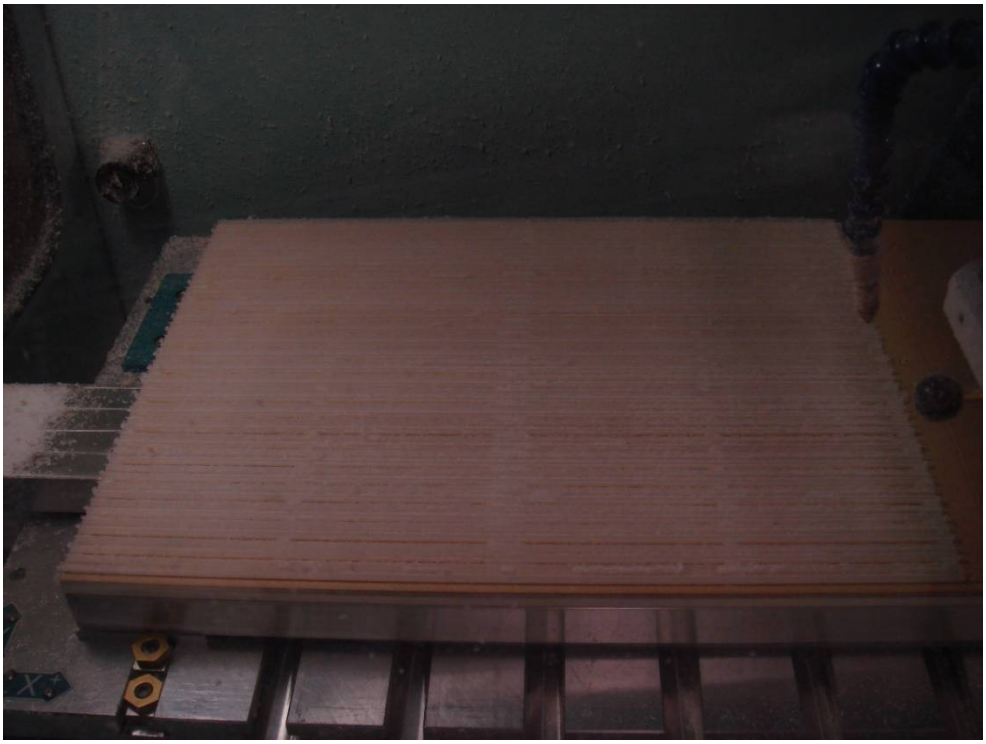

Figure 7.8 Photograph of PTFE with strands of fibre left after being machined

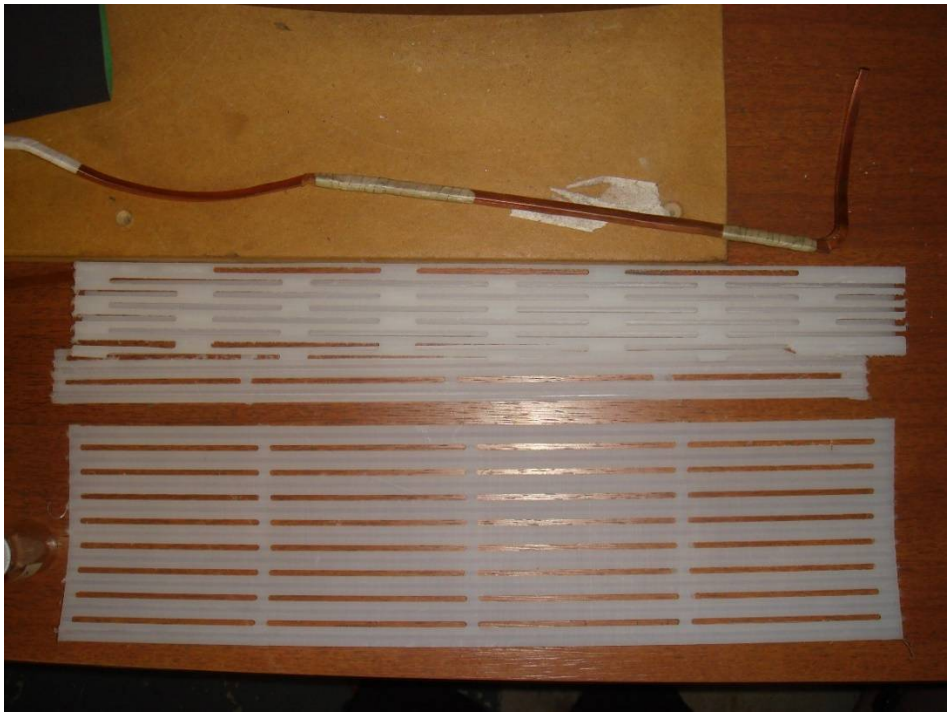

Figure 7.9 PTFE sheets after being cleaned for fibre strand residues

7.2.4 Winding Construction of HTSPCTFCL

The windings were wound with 1G BSCCO HTS tapes. They were selected from the inventory of HTS tapes available at the UoC as specified in table 6.2 in section 6.4 of this thesis. The design required 200 m of HTS tape for the primary winding and 260 m of HTS tape for the secondary winding including an allowance for connecting the windings to copper leads. HTS 004 and HTS 005 from table 6.2 were suitable for this application. They were tested in IRL, Wellington and found to be dc critical currents of 88 A and 91 A respectively at 77 K. These currents were in a self-field. As described in chapter 3 of this thesis, the presence of an external magnetic field reduces the dc critical current. In a HTSPCTFCL, there are alternating magnetic fields present which would reduce the critical current [Zhu et al 2004, Leghissa et al. 2007]. Therefore, a rated ac current of 40 A was assumed for the windings. The windings were insulated as described in section 7.2.1 of this chapter and layer wound on the fibreglass former described in section 7.2.2.

The windings were wound using a Gap Bed Lathe as shown in figure 7.10. The HTS tapes were fed from the reel of insulated HTS. The wire tension was controlled using a spring system. A force gauge was used to ensure the wire tension remained below 15N as too much strain can cause damage to the superconductor. Figure 7.11 shows the spring system and the force gauge used while constructing the windings.

The first layer was wound on the fibreglass former without any insulation layer between the former and the HTS winding layer. This was followed by a layer of inter-insulation which was held in place by the next layer of HTS windings .Figure 7.12 shows a layer of insulation being wound on a layer of HTS windings.

The PTFE sheets were 300 mm in width and the former was 115 mm in diameter. At 300mm, the PTFE insulation sheets was not sufficient to complete one layer of the HTS windings. Therefore, additional PTFE sheets had to be cut into smaller lengths to complete one layer of insulation.

Figure 7.10 Windings wound on a Gap Lathe Bed machine

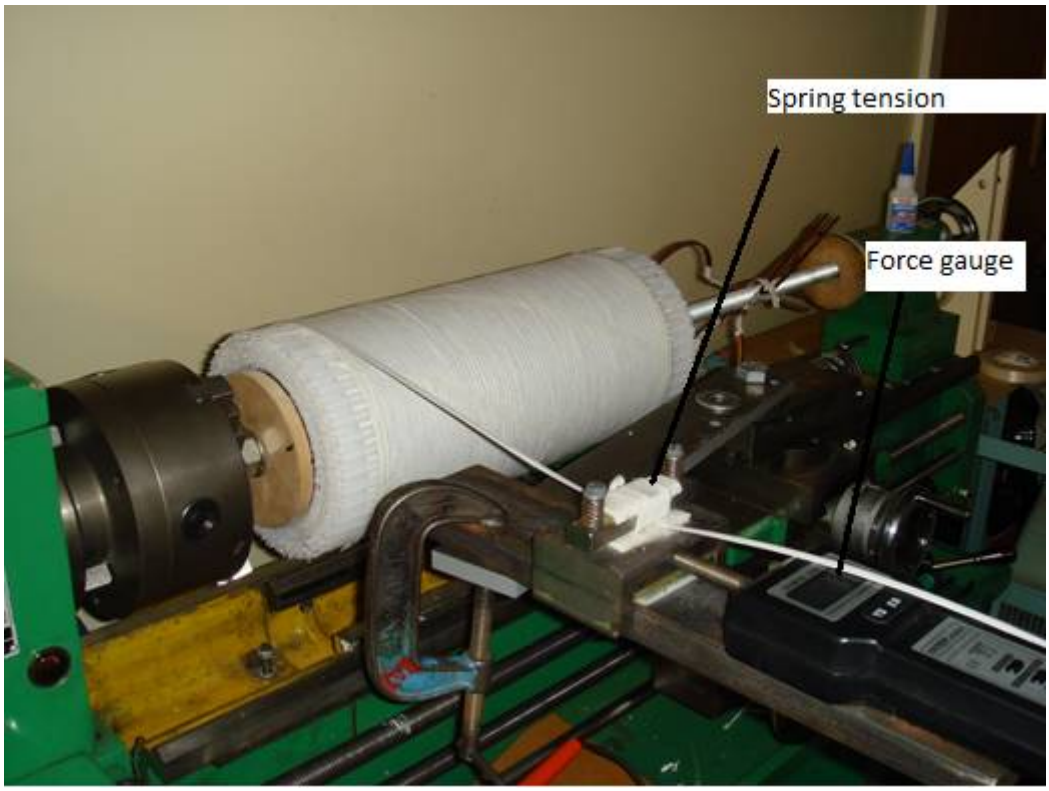

Figure 7.11 Spring system to control the wire tension while constructing the windings

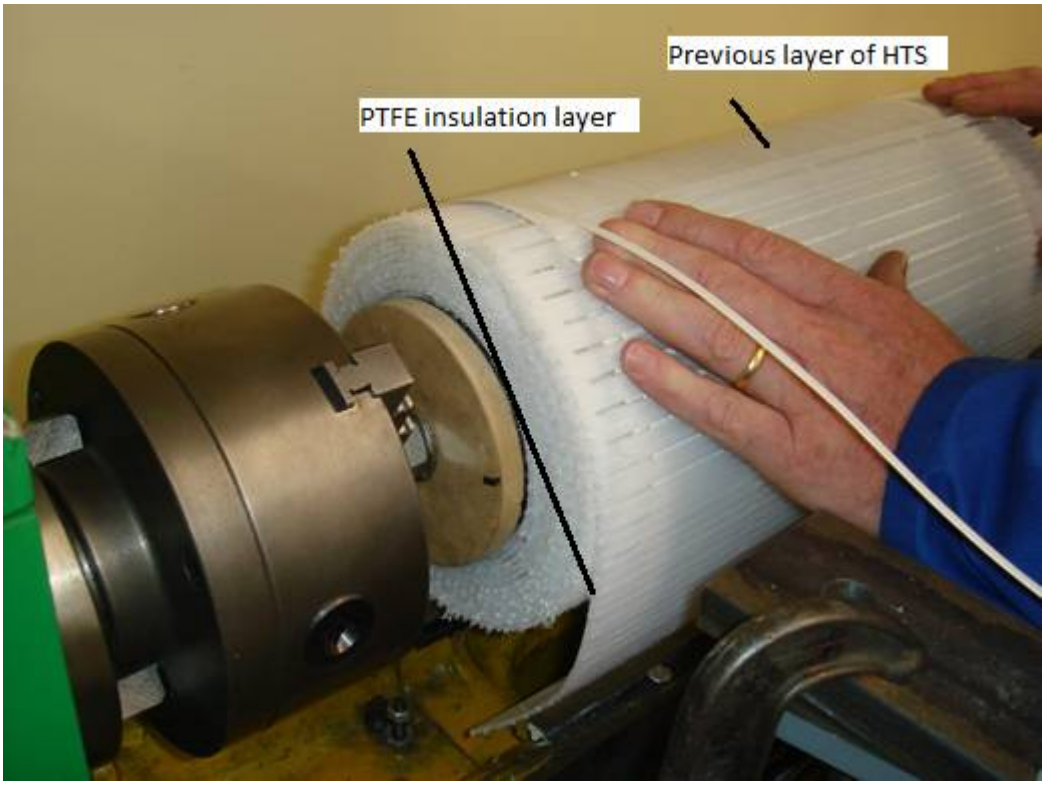

Figure 7.12 Inter-layer insulation being wound on a layer of HTS tapes

There were 6 layers for the primary windings and 6.5 layers for the secondary windings. The final half layer of the secondary winding was positioned at the centre of the former to give symmetrical flux distribution along the axis. Nomex^{TM} tape was applied over the last two layers of the windings to hold the windings in place. The last two layers were also wrapped in fibre reinforced tape to hold the windings in place as shown in figure 7.13. Copper lead-outs were used to connect the HTS windings to the transformer bushings. The lead-outs consisted of two 1.5 mm × 5 mm rectangular copper conductors. They were positioned radially as shown in figure 7.14. The copper lead-outs were soldered to the HTS tape using Indium based solder (97% In 3% Ag) and Ersin Red Jelly flux paste. The joint was made by sandwiching approximately 10cm of HTS tape between two specially formed copper lead-outs as shown in figure 7.13 and soldered with a temperature limited soldering iron. The soldering temperature was limited to 160^0 C using a variac to control the voltage to the soldering iron. If the temperature is very high during the soldering process, the HTS tape can delaminate. The copper lead-outs were connected to the bushing tails using compression joints. The bends in the lower section of the lead-outs shown in the completed windings of figure 7.14 were present to allow for thermal expansion and contraction of copper without pulling and pushing on the HTS windings.

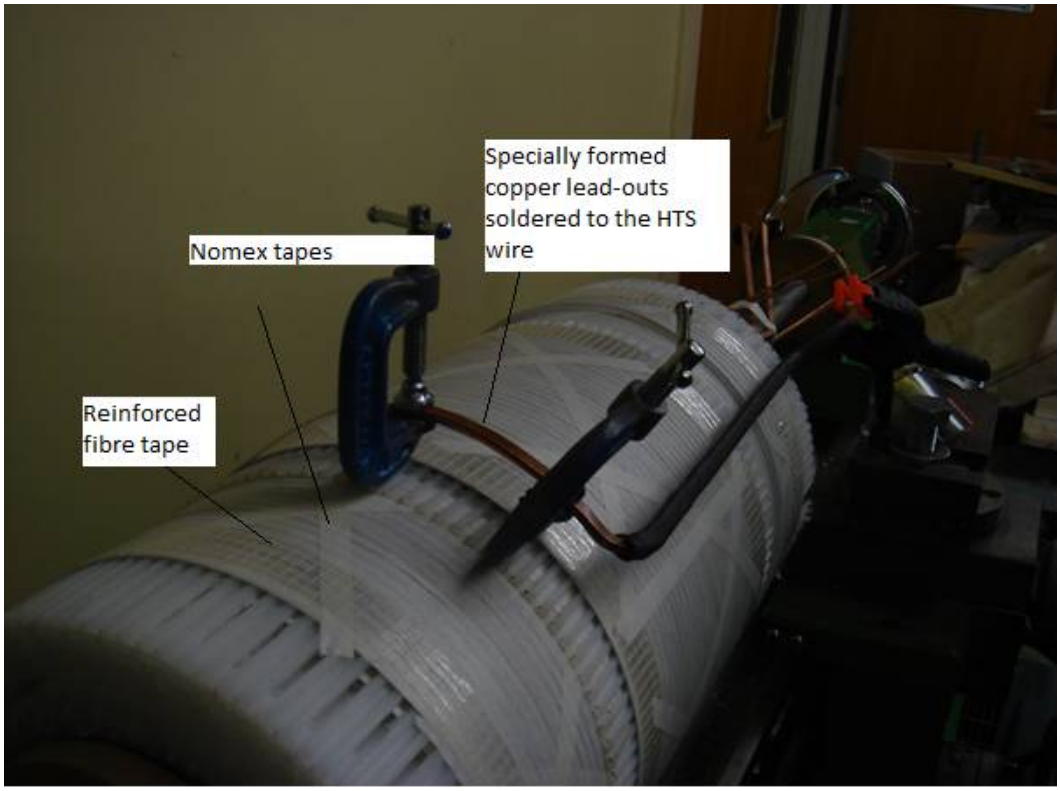

Figure 7.13 HTS wire after being soldered to the copper lead-outs

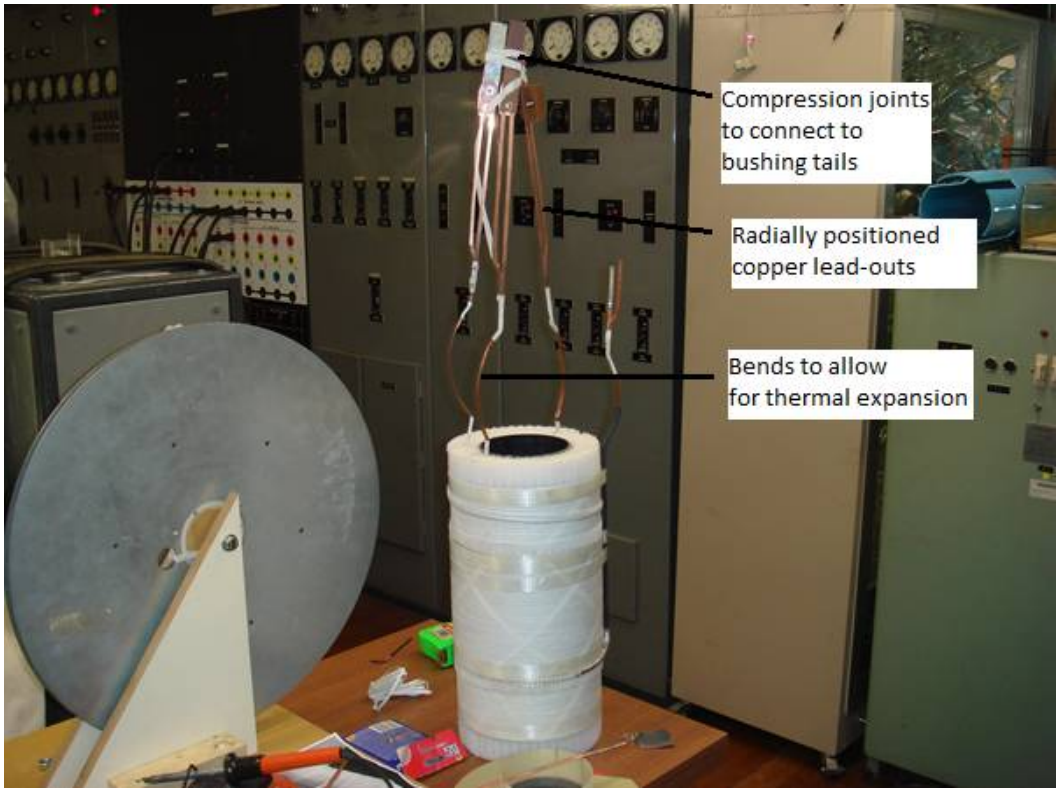

Figure 7.14 Completed windings for the HTSPCTFCL

7.3 HTSPCTFCL Prototype

The HTSPCTFCL prototype consisted of the cryogenic unit mentioned in section 6.4.2.1 of chapter 6, the winding unit that was constructed and discussed in section 7.2.4 and the core discussed in section 6.4.2.2 [Bodger et al. 2005].

The cryogenic unit consisted of a liquid nitrogen vacuum Dewar, the core vessel and the head unit as shown in figure 7.15 and figure 7.16(a). The majority of this unit was made of G-10 fibre composite. The winding unit was slid over the core vessel as shown in figure 7.16(b) and it was positioned to connect the copper lead-outs of the windings to the bushing tails.

The vacuum Dewar consists of an inner vessel for containing LN_2 and an outer vessel which was exposed to room temperature. Vacuum was formed between the inner vessel and outer vessel to prevent thermal convection losses to the LN_2 from the outside. The bottom of the inner vessel was dome shaped to allow for the joint between the dome and the tube of the inner vessel to have even expansion and contraction when exposed to LN_2. A pressure relief port was present on the outside of the Dewar. If the inner vessel of the Dewar failed, LN_2 from the inner vessel would vent into the vacuum. This would result in a build-up in pressure which would be released by the pressure relief port.

The core vessel was similar to the vacuum Dewar. Vacuum was formed between the inner vessel and the outer vessel which prevented convection of heat from the core to the LN_2 contained in the Dewar. A float was attached to the outside of the core vessel to indicate the minimum and maximum levels in LN_2 contained in the Dewar. A pressure relief port was present on the top of the core vessel. If there was a failure of the core vessel, LN_2 would have vented into the vacuum chamber causing a build-up of pressure. The pressure relief port would have assisted in releasing this pressure.

The head unit provided mountings for the HTSPCTFCL bushings, nitrogen venting valves, a rupture disc for emergency venting, purging lines and a pressure gauge for the LN_2 chamber pressure. The HTSPCTFCL bushings were located on the top of the heat unit. They were connected to the bushing busbars through a short piece of braided copper wire. Two nitrogen venting valves were present adjacent to the rupture disc. One valve was a full LN_2 rated manual vent to be used during initial filling and the other valve was a non-return valve for normal operation venting. An emergency venting rupture disc was fitted to prevent the pressure in the LN_2 chamber from reaching dangerous levels. This was a possibility during fault conditions when the non return valve might have been unable to vent sufficient quantities of nitrogen gas. The diameter of the rupture disc was 80 mm. It consisted of thin aluminium sheet between two flanges of G-10 fibreglass.

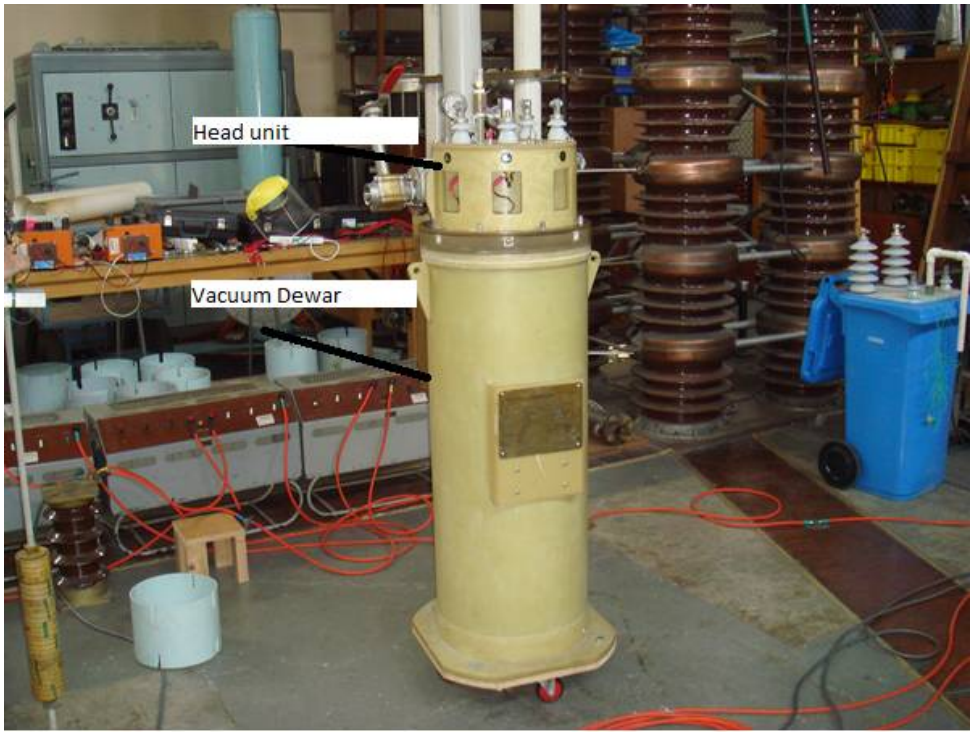

Figure 7.15 HTSPCTFCL prototype

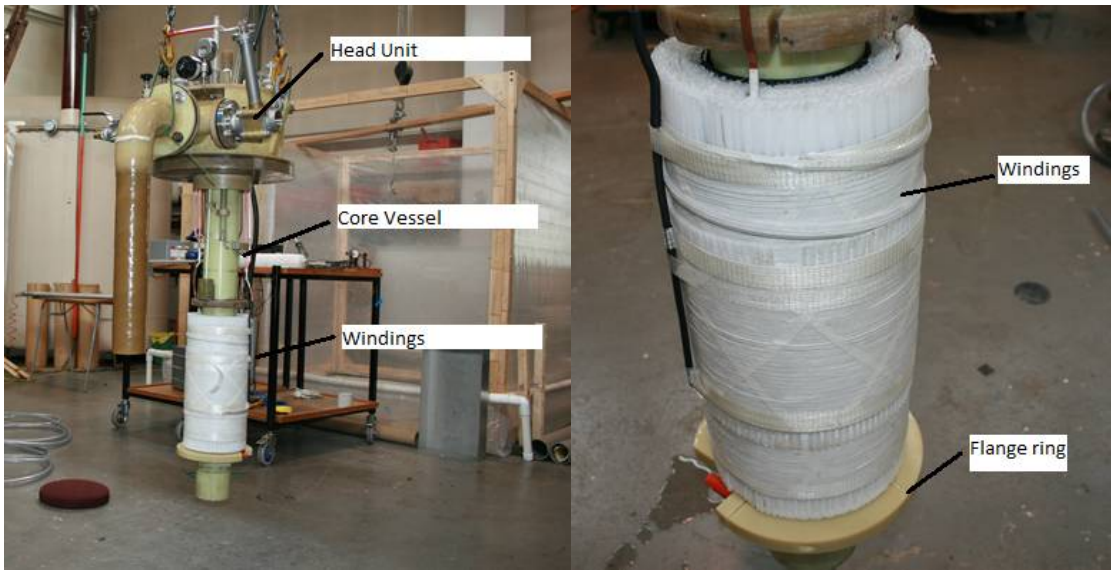

(a) The head unit, core vessel and windings while being mounted in the Dewar

(b) A close-up view of the windings and flange ring

Figure 7.16 Photograph of the HTSPCTFCL windings after fitting on the core vessel

7.4 Cooling System

The HTS windings in the HTSPCTFCL could only be superconducting at their critical temperature. For the BSCCO tapes being used in the HTS windings, that temperature was 90K. Therefore LN_2 which has a boiling point of 77K was used as the coolant. While performing tests on the prototype, the Dewar was filled with LN_2, and though the vacuum present between the inner vessel of the Dewar and the outer vessel limited the external temperature effecting the evaporation of LN_2; a certain degree of boil off still occurred. Therefore, it was necessary to develop a system to maintain the level of LN_2 and monitor it at the same time.

The system consists of a float mechanism inside the Dewar to gauge the LN_2 level shown in figure 7.17. The float mechanism extends through the top of the transformer main assembly inside a sight glass. Two optical sensors attached to the sight glass are used to measure the level of the float as seen in figure 7.17 (b) [Lapthorn .2012]. Figure 7.18 shows a schematic of the electronic circuit used in the cooling system.

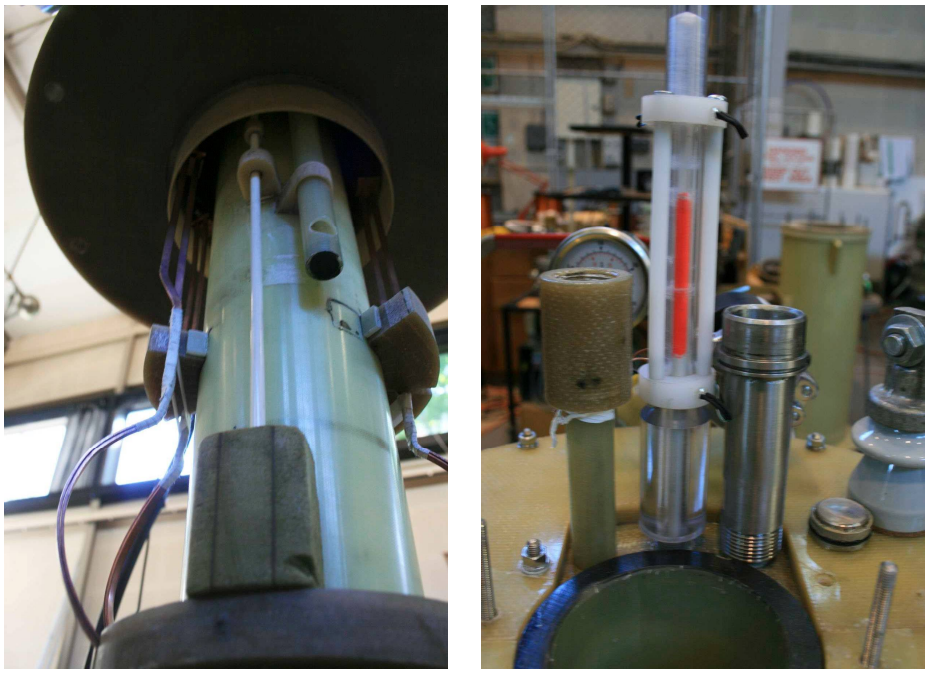

(a)The float inside the LN2 Chamber (b) The cooling system optical sensor

Figure 7.17 Photographs of the LN_2 level sensing components of the cooling system

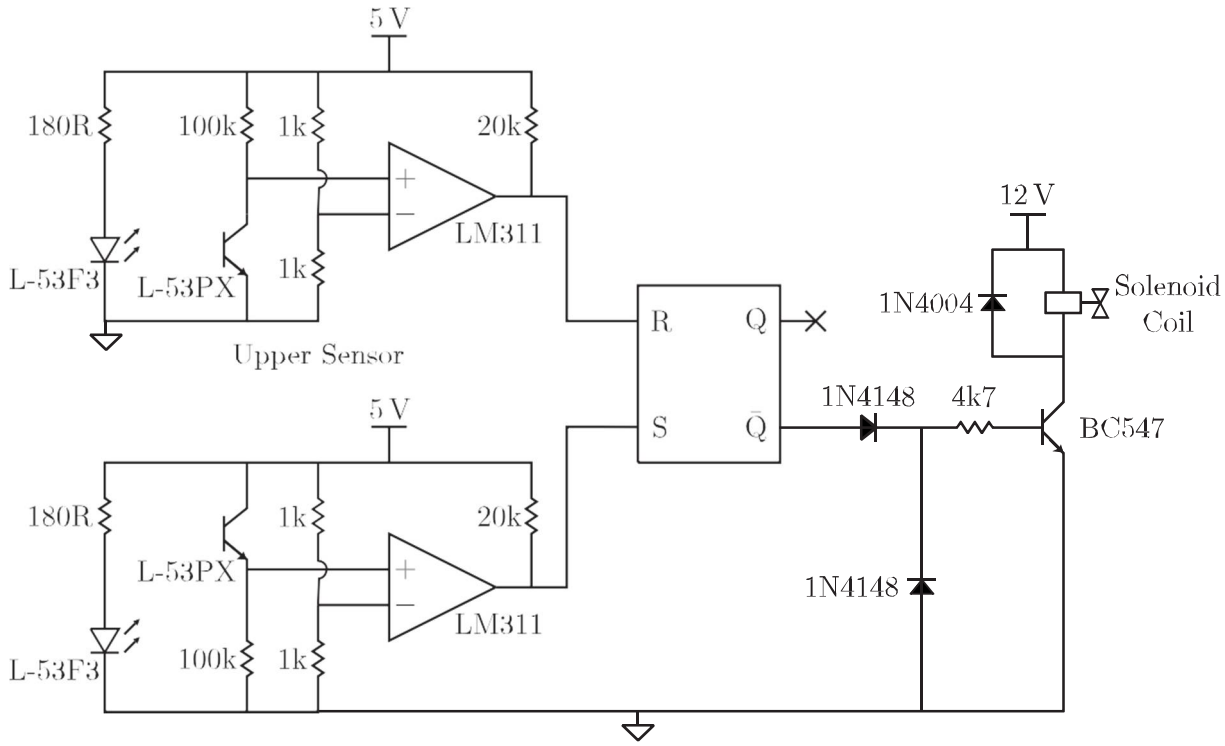

Figure 7.18 Schematic of the cooling system electronics [Lapthorn. 2012]

7.5 Quench Detection System

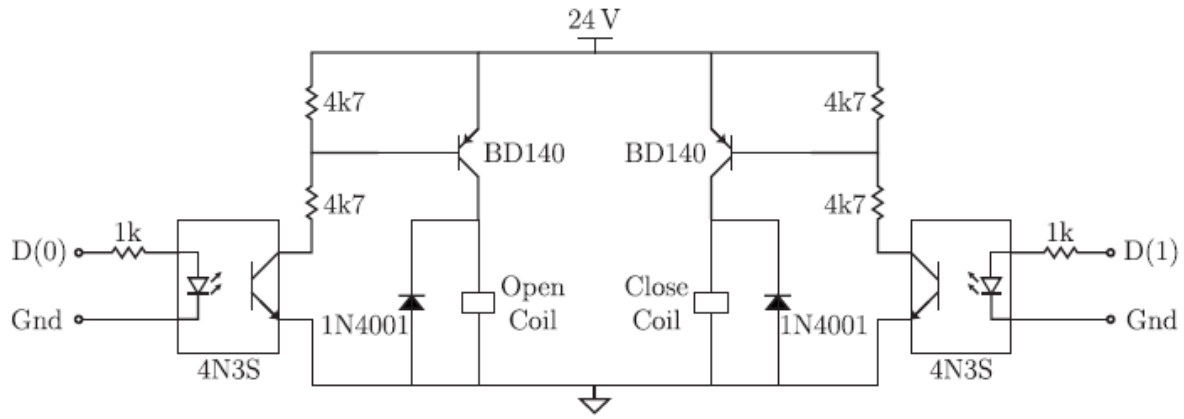

Figure 7.19 Schematic of the quench detection system electronics [Lapthorn. 2012]

A quench detection system [Lapthorn 2012] was utilised to protect the HTSPCTFCL from being damaged if the HTS tape was to quench during its operation. During a fault ride test, the HTS tape would quench and using the quench detection system and a computer program which

has a pre-set threshold level for the voltage regulation, a circuit breaker could be opened via the computer's parallel port. This would then de-energise the HTSPCTFCL.

7.6 Conclusion

The process of fabricating the HTSPCTFCL was presented. The process involved insulating the windings of the HTSPCTFCL, fabricating the former, the inter-layer insulation and the windings of the HTSPCTFCL. Details of the complete prototype of HTSPCTFCL was also presented along with the auxiliary cooling system utilised in maintaining the LN_2 level in the Dewar of the HTSPCTFCL. The cooling system utilised optical sensors on a LN_2 float system. This was aided with an electronic circuit to control a cryogenic rated solenoid valve.

Chapter 8
Testing the HTSPCTFCL prototype

8.1 Introduction

Tests were performed on the HTSPCTFCL to verify the operational characteristics of the unit as a transformer and as a fault current limiter. The tests included measurement of insulation resistance, DC resistance of the windings, open circuit, short circuit, resistive load testing and fault ride through. The tests were undertaken according to the guidelines of International Electrotechnical Commission, (IEC), standard on power transformers, IEC 60076. While performing the tests, the HTSPCTFCL was submerged in LN_2 contained in the vacuum Dewar.
The experimental set-up used to test the HTSPCTFCL is presented in this chapter followed by a discussion about the test instruments used. The procedure used for preparing and filling the vacuum Dewar with LN_2 is also presented.
The chapter continues with the results of the tests and their comparison with the design model calculations presented in chapters 3 and 6.

8.2 Experimental Setup

8.2.1 Preview of the lab and Test circuit

The HTSPCTFCL was tested in the UoC's high voltage laboratory. The laboratory has a controllable single phase ac supply capable of delivering up to 600 A at 400 V that was used to supply the HTSPCTFCL. In event of failure of the HTSPCTFCL, a large amount of LN_2 could evaporate. This can result in suffocation and therefore a test facility should have sufficient ventilation. The laboratory was large with plenty of ventilation and therefore it was safe to conduct the experiments. In addition, the laboratory was fitted with several emergency trip buttons located in easily accessible positions. When activated, these buttons switch off the supply to the whole laboratory and sound an alarm.

Figure 8.1 displays the circuit used to perform the open circuit, short circuit, load and fault ride through tests.

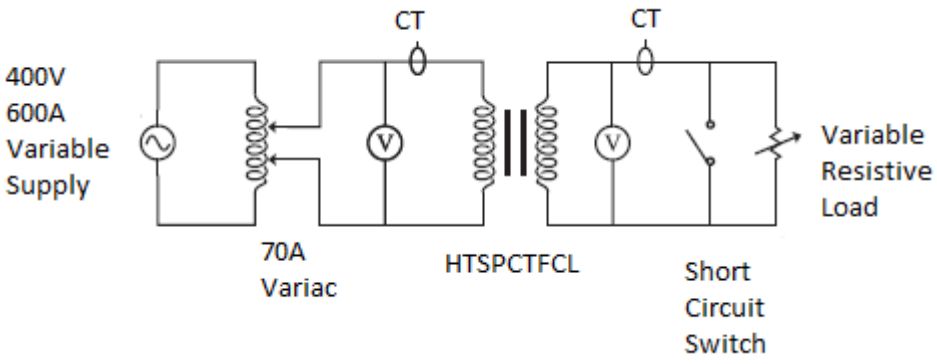

Figure 8.1 Test circuit for HTSPCTFCL

The test circuit consisted of the power supply, instruments used to take the measurements, a short circuit switch and a variable resistive load.

8.2.1.1 Power Supply

For energising the transformer-fault current limiter, two transformer variacs were used. They were connected in series. The first variac was the laboratory's 600 A supply, while the second variac was a 70 A supply. The 70 A variac is portable and allows for adjusting the voltage in steps while recording and monitoring the measurements.

8.2.1.2 Testing instruments

The voltmeters and current transformers in the circuit diagram indicate the location in the circuit where the measurements were taken. The test gear used in this experimental setup consisted of two calibrated Fluke 41B meters for measuring the voltage, current and power of the primary and secondary windings. The meters were connected to a computer through an IEEE-488 interface which ran a Matlab program to collect the data recorded from the tests. For measuring the resistance of the windings under dc conditions, a MPK254 digital micro-ohmmeter was used. The insulation tests were performed with a Megger meter with model specs S1-5005. A variable resistive load was connected in parallel with a short circuit switch. The loads varied from 3.5Ω to open circuit. The short circuit switch was used to perform the fault ride through test.

A turbomolecular vacuum pump was used as shown in figure 8.2 (a) to pull a vacuum of 2×10^{-5} Torr in the Dewar and the core vessel. The vacuum pump was connected to the Dewar where it remained in operation during the entire test.

(a)Turbomolecular vacuum pump

(b) Measurement meters connected to computer

(c) Vacuum gauge

(d) Variac used to control the HTSPCTFCL

Figure 8.2 Photographs of testing instruments and equipment used in testing the HTSPCTFCL

8.2.1.3 Filling the Dewar

While filling the Dewar with LN_2, certain precautionary steps were taken to avoid ingress of oxygen in the LN_2 chamber. This included closing the two nitrogen venting valves, applying a vacuum to the LN_2 chamber through the purging line and holding the vacuum for 24 hours.

In addition to the above, the LN2 chamber was filled through the dry nitrogen gas line and when positive pressure was achieved, the normal nitrogen venting valve was opened.

8.2.2 Measuring the operational characteristics of a HTSPCTFCL

The experimental setup used in measuring the operational characteristic of the HTSPCTFCL is shown in Fig.8.3. Adequate spacing was ensured between the load bank and the HTSPCTFCL. The impedance of the probes were matched with the equipment they were used with. This included matching the 1:1 probes used for measuring the voltage with the Fluke meters. The current transformers were also matched with the Fluke meters they were used with.

Figure 8.3 Experimental setup of the HTSPCTFCL

8.2.2.1 Insulation test and winding resistance tests

The first test performed on the HTSPCTFCL was the insulation resistance test. This was performed with a S1-5005 insulation tester from Megger. The insulation was tested between the inside and outside windings before and after filling the LN_2 chamber. Since the HTSPCTFCL assembly was made of G10 fibre, the insulation resistance tests were not performed between the windings and the tank. The test voltage was 500V for a duration of 60 seconds. The results from the insulation resistance test were 41.2 GΩ for the dry test and 8.95 GΩ for the wet test as shown as photograph in figure 8.4. Though the difference between the dry test and the wet test was notable, the test was a pass. The significant difference between the dry test and the wet test could not be explained and needed more research.

The second test performed was a dc resistance test for each winding using a MPK254 Digital Micro-Ohmmeter from Megabras. The test was performed both before and after

filling the Dewar with LN_2 and before and after the testing process. Measurements were taken from between the winding bushings. The results for the dry test were 8.819 Ω and 8.820 Ω for the inside and outside windings respectively before the HTSPCTFCL was tested. The resistances were 8.917 Ω and 8.920 Ω for the inside and outside windings respectively after the HTSPCTFCL was tested for the fault ride through test for a dry test. The dc resistance under LN_2 was measured as 2.3 mΩ for the inside winding and 2.5 mΩ for the outside winding. The low resistance observed under LN_2 proves that the HTS tapes were superconducting and also the combined resistance of the copper lead-outs, busbars, and bushings were small.

(a) Insulation resistance test for dry test

(b) Insulation resistance test for wet test

Figure 8.4 Photograph of Insulation resistance test

8.2.2.2 Open circuit test

With an open circuit or no load test, very little current is required to energise the core. Since the secondary is open circuited, all the current flows through the primary winding and the losses are attributed as the core losses. The open circuit test also determines the voltage ratio of the primary and the secondary windings.

To perform the test, the voltage in the 70A variac is increased in small increments to the rated voltage and the measurements are recorded. The measured results are given in Table 8.1. They are compared to the calculated results determined from the reverse design program presented in chapter 3.

Table 8.1: Open circuit test results

Parameter	Measured	Calculated	% Difference
Inside winding voltage (V)	230.6	230	0.17
Outside winding voltage (V)	235	232	1.3
Voltage ratio	1.02	1.01	0.98
Excitation current (A)	13.6	15.4	-13
Excitationcurrent's phase(degrees)	-87	-86	1.2
Volt-amperes (kVA)	3.14	3.54	-12.7
Real power (W)	167	165	1.2
Power factor	0.05	0.05	0

In table 8.1, the calculated current is higher than the measured current by 13%. This could be due to a lower net impedance for the core. The phase angle shows the dominance of the reactive component. This can be attributed to the low magnetizing reactance in a partial core transformer. Since the net core resistance is in parallel to the magnetizing reactance, the magnetizing component is the dominating component.

Figure 8.5 displays the open circuit voltage against the excitation current. It shows a linear increase in excitation current with the applied voltage. The result indicates that the core of the HTSPCTFCL is not saturating. For a core to have magnetic saturation, the excitation current flattened out with an increase in applied voltage.

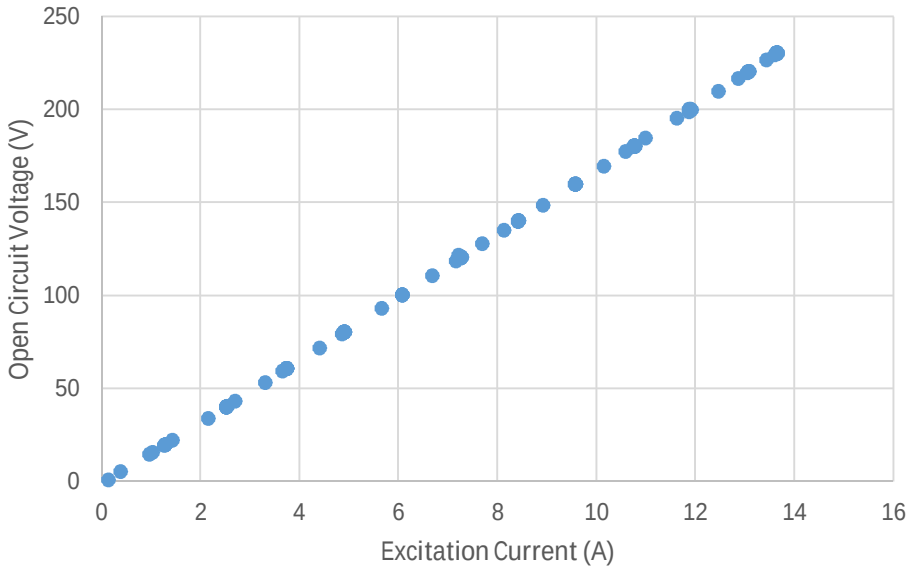

Figure 8.5 Open circuit voltage against excitation current

8.2.2.3 Short circuit test

In a short circuit test, the series impedance and full load losses in the HTSPCTFCL are determined. To perform this test, the secondary terminals in the circuit of figure 8.1 were shorted with a 95 mm^2 cable. The cable ensures a low impedance connection is achieved. The supply was connected to the inside winding and the voltage increased while monitoring the supply current. Fine control of the supply voltage was necessary and this was achieved with the 70 A variac.

The results from the short circuit test are given in Table 8.2 along with the calculated values using the reverse design model from chapter 3.

Table 8.2: Short circuit test results

Parameter	Measured	Calculated	% Difference
Inside winding voltage (V)	42.1	42.3	0.47
Inside winding current (A)	31.1	32	2.8
Outside winding current (A)	30	31	3.3
Volt-amperes (VA)	1306	1353	3.5
Real Power (W)	47	42	-10.6
Power factor	0.04	0.03	-25
Inside winding current's phase in deg	-88	-87	-1.1

In table 8.2, the calculated inside winding current and measured current are 2.8% apart. This is due to the calculation of winding resistance and leakage reactance. The losses measured in the short circuit test are similar to those calculated. This means the measured and calculated values of the leakage reactance are different. Therefore, the total calculated impedance is lower than the measured impedance due to the leakage reactance component. The lower impedance leads to a higher current.

The volt-amperes has a difference of 3.5%. Since the volt- amperes is dependent on current, the measured volt-amperes is lower than the calculated volt-amperes.

The short circuit voltage against short circuit current is plotted in figure 8.6. It shows a linear relationship.

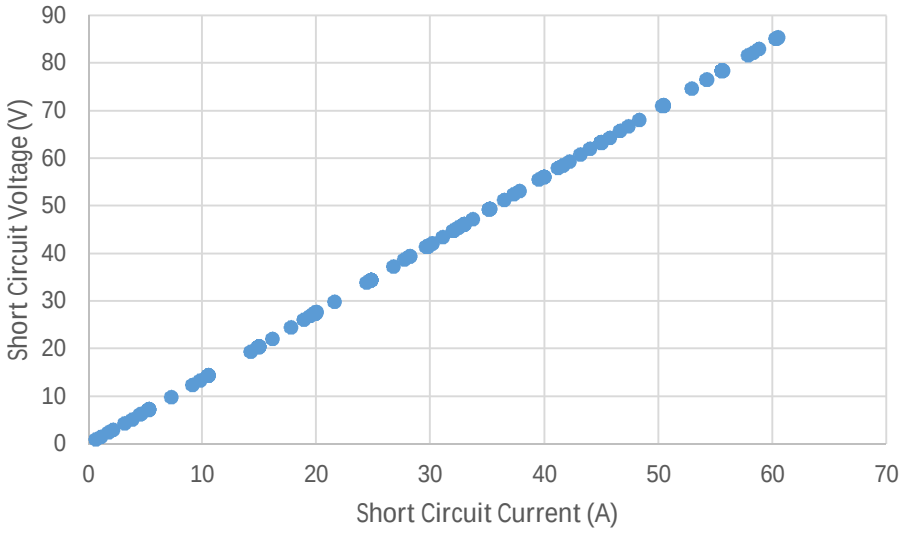

Figure 8.6 Short circuit voltage against short circuit current

8.2.2.4 Load test

The load test on the HTSPCTFCL determines the performance of the device while delivering power. Several transformer characteristics such as efficiency and regulation are determined.

To perform the load test, the outside winding of the HTSPCTFCL was connected to a resistive load bank as shown in Fig 8.7. The inside winding was connected to a single phase power supply.

The supply voltage was varied till it reached the rated voltage and the load resistance varied till it reached the rated value. The quench detection system discussed in chapter 7 was used to protect the HTSPCTFCL from damage.

The results from this test and the calculated values using reverse design model from chapter 3 are given in Table 8.3.

Figure 8.7 Load bank to perform the load test

Table 8.3 Load test results

Parameter	Measured	Calculated	% Difference
Inside winding voltage (V)	**230**	**230**	**0**
Inside winding current (A)	**33**	**32.2**	**2.4**
Outside winding voltage (V)	**234.5**	**233.5**	**0**
Outside winding current (A)	**30.7**	**27**	**12.1**
Outside winding current's phase (deg)	**-34**	**-32**	**5.9**
Volt-amperes (kVA)	**7.5**	**7.4**	**1.3**
Real power (kW)	**6.8**	**6.2**	**8.8**
Power factor	**0.84**	**0.80**	**4.8**
Efficiency (%)	**99.97**	**99.96**	**0.01**
Voltage Regulation (%)	**5.7**	**6.5**	**14**

There is a 2.4 % difference between the measured and calculated values of the inside winding current and 12.1% difference between the measured and calculated values of the outside winding current. This is due to the difference in calculation of the magnetizing reactance, X_m, which is calculated to be slightly higher than that measured. The difference in real power of 8.8 % can be attributed to the calculation of the winding resistance and the 14% difference in regulation can be attributed to the difference in voltage drop across the leakage reactance.

Figure 8.8 shows the plot of measured efficiency for varying load current. At very low loading, the efficiency of transfer is poor. This can be attributed to the high no load losses measured in section 8.2.4.1. The efficiency increases to around 99% as it approaches the rated current.

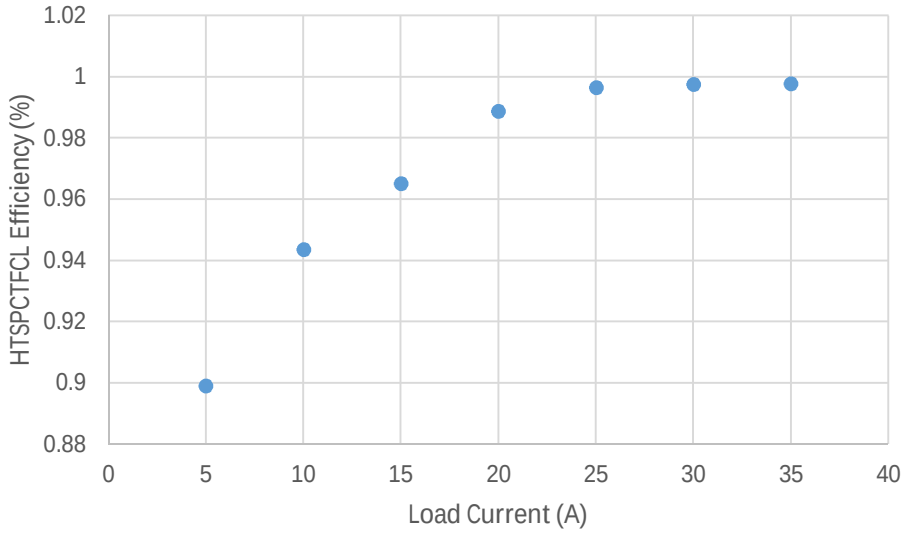

Figure 8.8 Measured efficiency of the HTSPCTFCL for varying load current

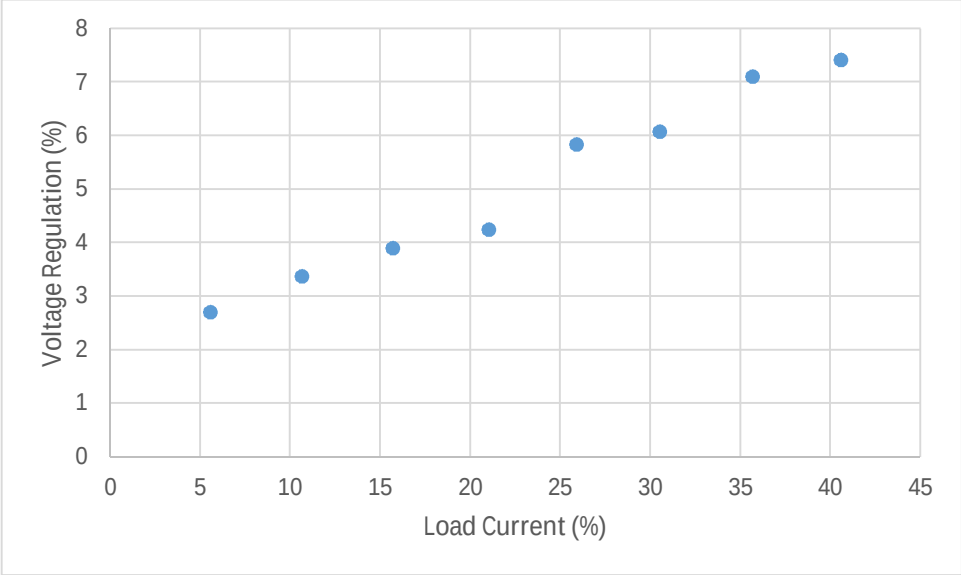

Figure 8.9 Measured voltage regulation of the HTSPCTFCL for varying resistive load

Figure 8.9 shows the measured voltage regulation of the HTSPCTFCL over the range of load being tested. The plot shows an increasing trend in voltage regulation as the load current increases. At the rated load current, the regulation is approximately 6%.

8.2.2.5 Overload Test

The HTSPCTFCL was subjected to a range of loads beyond the rated load. The idea behind this test was to see how the HTSPCTFCL behaved once it crossed the rated value. The rated load was selected based on the critical current assumed for the HTS tapes. The HTS tapes had a DC critical current of 88 A and 90 A as discussed in chapter 6. However, in an AC condition, due to the presence of alternating magnetic fields, the DC critical current for the HTS tapes is reduced producing a much lower value for the AC critical current. Therefore, a conservative value of 35 A was chosen for the AC critical current in the design model. As the HTSPCTFCL gets heated at higher load currents, the losses are higher causing the LN_2 to boil off. Therefore, the windings were cooled using a continuous flow-type cryostat system where the LN_2 level was maintained. This was achieved using the cooling system discussed in chapter 7. The reserve LN_2 had a capacity of 160L and because the fault ride through test was to be done after this test, a sufficient quantity of LN_2 was required to perform the test. Therefore, the overload test was limited to one hour. The HTSPCTFCL did not fail as the HTSPCT tested in chapter 4. Therefore, the integrity of the insulation adopted in the model for maintaining the windings at LN_2 was confirmed.
Figure 8.10 shows the plot of voltage regulation for the HTSPCTFCL with a varying resistive load beyond the rated load value. The regulation has an increasing trend with the load current. This proves that the quenching did not have any impact on the voltage regulation.

The plot of HTSPCTFCL efficiency against a range of load currents in figure 8.11. The plot shows that the efficiency increases as it reaches the rated current and then drops once the current in the HTSPCTFCL crosses the critical current value. This was expected and proves the ac critical value chosen was correct.

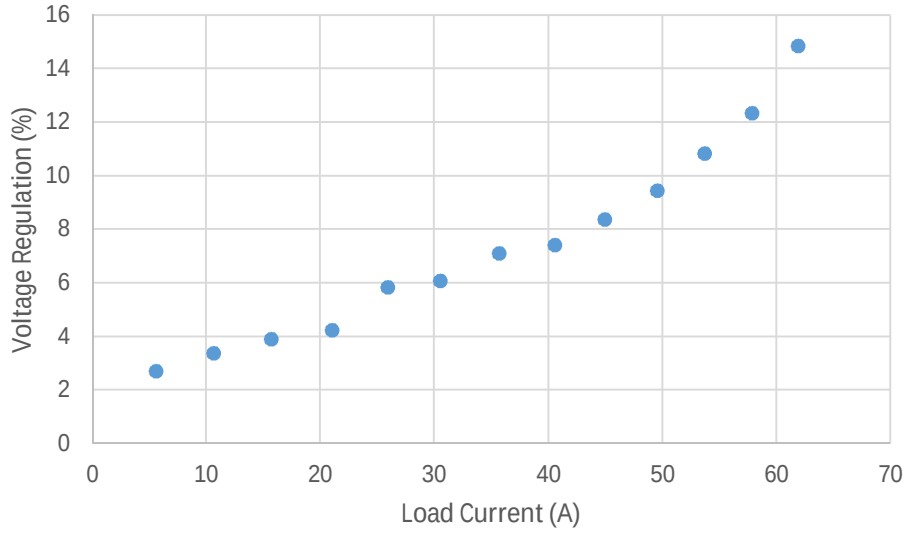

Figure 8.10 Voltage regulation of the HTSPCTFCL with a varying resistive load beyond the rated load current

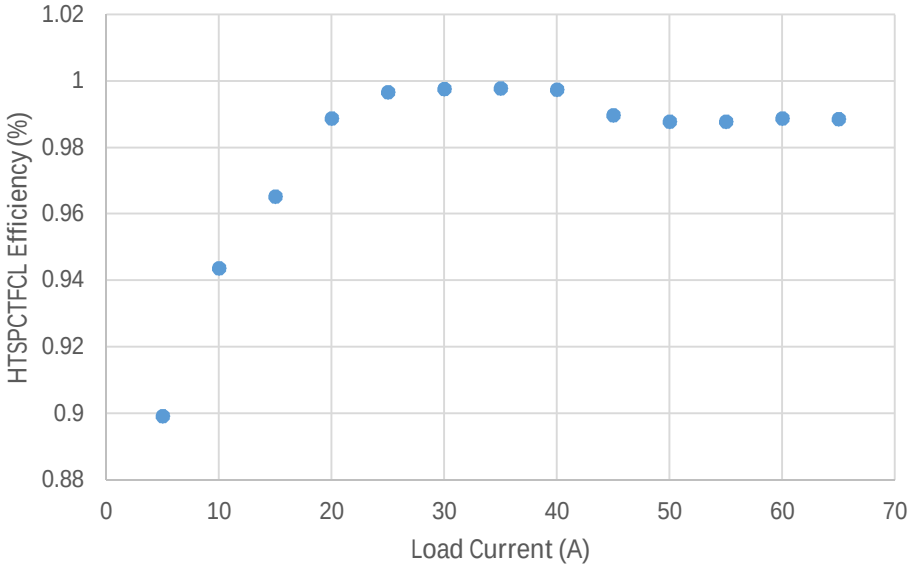

Figure 8.11 Measured efficiency of the HTSPCTFCL for a range of load current beyond the rated current

8.2.2.6 Fault current test

The HTSPCTFCL was tested under a fault condition. The test was performed by shorting the secondary winding, while the primary winding was energised with the rated voltage and

the rated load of 15kW was connected to the secondary side of the transformer. The rated voltage was applied from the 600 A supply without the 70 A variac in the circuit. Fig 8.12 depicts the arrangement of the rated load and the manual switch used in this test to short the secondary windings. The quench detection system was used to protect the HTSPCTFCL. When the manual switch was operated, the secondary voltage was reduced to zero. This resulted in an increase in voltage regulation. Once the voltage regulation reached above the threshold value of the quench detection system, the contactor was opened cutting power to the circuit. Due to the excessive heat generated, the LN_2 was expected to boil off and therefore a continuous supply of LN_2 was maintained using the continuous-flow type cryostat system.

The voltage and current for the primary and secondary windings were monitored using a four channel oscilloscope. The fault lasted about 10 cycles before the contactor was operated. This was due to the delay in the signal between the quench detection system and the contactor.

The images obtained from the oscilloscope are shown in figure 8.13 and figure 8.14. In the oscilloscope traces of figure 8.13, the green waveform indicates the primary voltage while the yellow waveform indicates the primary current during the fault. The primary current was 100 A peak while the secondary voltage was 200 V peak. In the oscilloscope image of figure 8.13, the time for which the fault lasted was deduced by multiplying each block which was 20 ms to the number of cycles. Therefore, the total time for which the fault lasted was 200 ms.

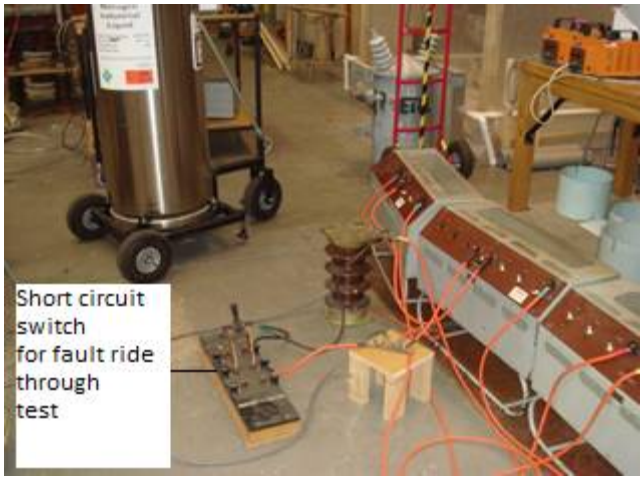

Figure 8.12 Setup of Fault ride through test

The time for which the fault lasted was well within the time deduced for a safe operation of the HTSPCTFCL from the temperature model discussed in chapter 5. The time deduced from the model is 2 sec which is well over the time within which the contact was operated in the test.

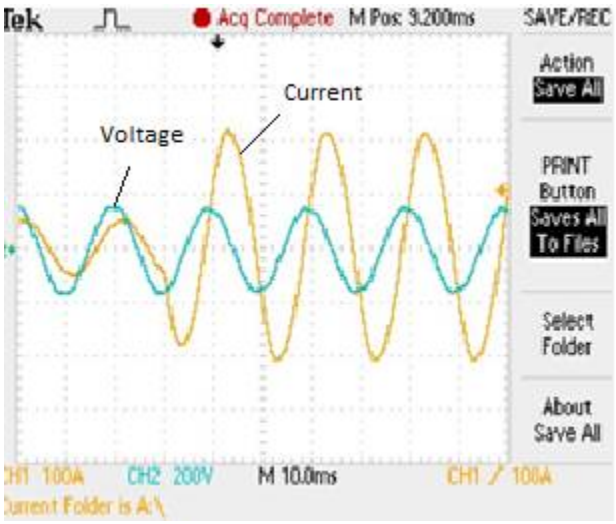

Figure 8.13 Oscilloscope images of the primary voltage, (V) and current, (A) during the fault condition

The primary voltage in the oscilloscope image of figure 8.13, has a rms value of 141 V. The drop in voltage across the primary winding is due to the impedance of the supply after short circuit. After a fault occurs, the secondary windings of the HTSPCTFCL are shorted, this results in the impedance of the HTSPCTFCL being similar to the supply impedance. As a result, a voltage drop across the supply impedance occurs resulting in drop in the measured primary voltage during fault.

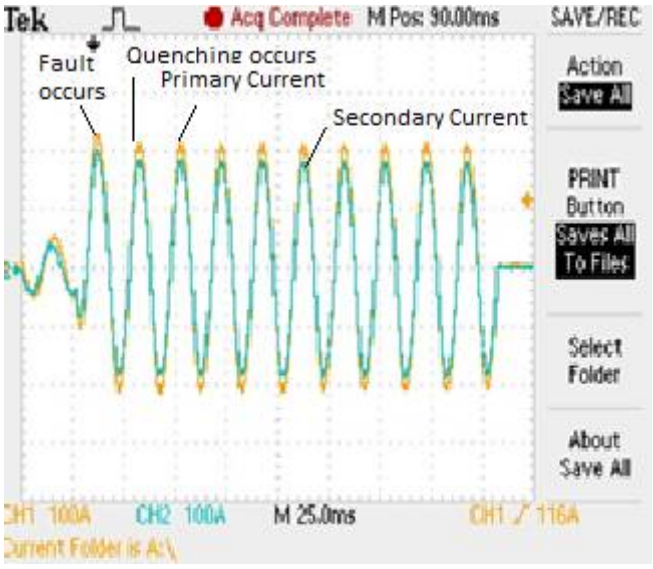

Figure 8.14 Oscilloscope images of the primary current, (A) and secondary current, (A) during the fault condition

The oscilloscope image of figure 8.14 shows the secondary current is slightly less than the primary current. This is due to the different turns ratio of the primary and the secondary winding.

The measured value was compared with the calculated results of the model discussed in chapter 6. The measured fault current after quenching was 70 A rms as compared to the calculated prospective current of 91 A and fault current of 88 A determined using the reverse design model.
The HTSPCTFCL was inspected for any visible damage after the fault ride through test. For this, the HTSPCTFCL was allowed to return to room temperature prior to opening the tank to prevent moisture from damaging the windings. The HTSPCTFCL showed no visible damage as a result of this test. Figure 8.15 shows the photograph of the HTS windings after the fault ride through test.

Figure 8.15 Photograph of the HTSPCTFCL windings after the fault ride through test

8.3 Discussion

In the equivalent circuit of figure 8.16, the magnetizing reactance is much lower for a partial core than for a full core so the magnetizing current is higher. This flows through the primary leakage element of the equivalent circuit which drops the voltage. Hence the voltage ratio is different to the turns ratio in a partial core transformer.

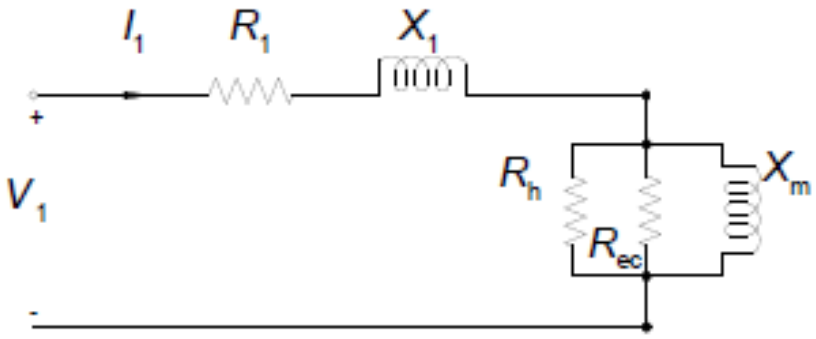

Figure 8.16 Equivalent circuit for open circuit test

Figure 8.17 shows the plot of measured and calculated losses in the HTSPCTFCL. The measured and calculated losses are in good agreement. While measuring the losses, it is not possible to measure the winding and core losses separately. Therefore, the 165 W measured is mostly due to core loss as losses in the winding are negligible in the superconducting state.

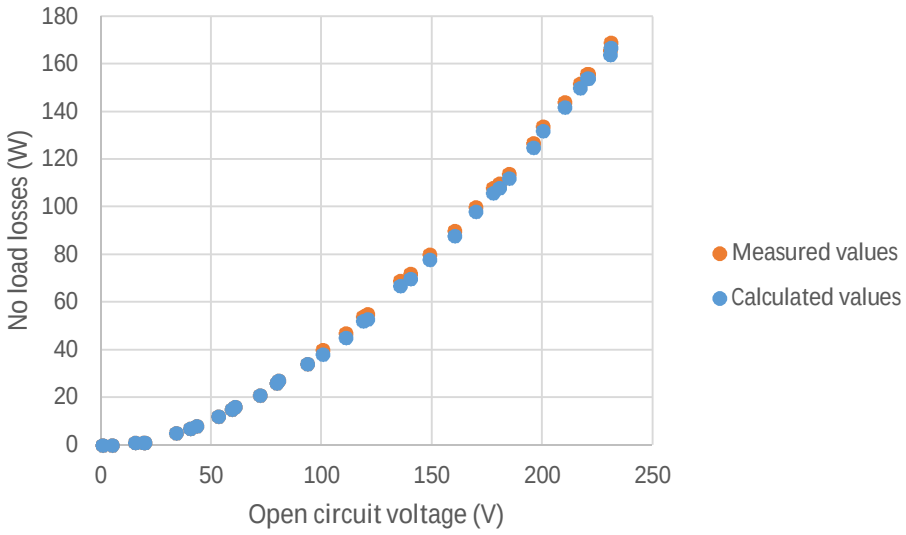

Figure 8.17 Comparison between the measured and modelled open circuit power loss

In the short circuit test, the low magnetizing reactance causes some of the current to flow through the core and therefore not all current reaches the secondary. This is evident from the results in table 8.2 where the measured inside and outside winding current are slightly different.

The equivalent circuit diagram in figure 8.18 (a) for the short circuit test shows the leakage reactance, X_{12}, as the dominating component in the circuit in the superconducting state. This is due to the negligible resistance of the HTS tapes when they are superconducting

represented by R_1 and R_2 in the circuit. Therefore, the short circuit voltage drop can be assumed to be across the leakage reactance. For the vector diagram of figure 8.18 (b), the leakage reactance can be calculated as $X_{12} = \frac{V_{sc}}{I_{sc}}$, where V_{sc} and I_{sc} are the short circuit voltage and short circuit current respectively.

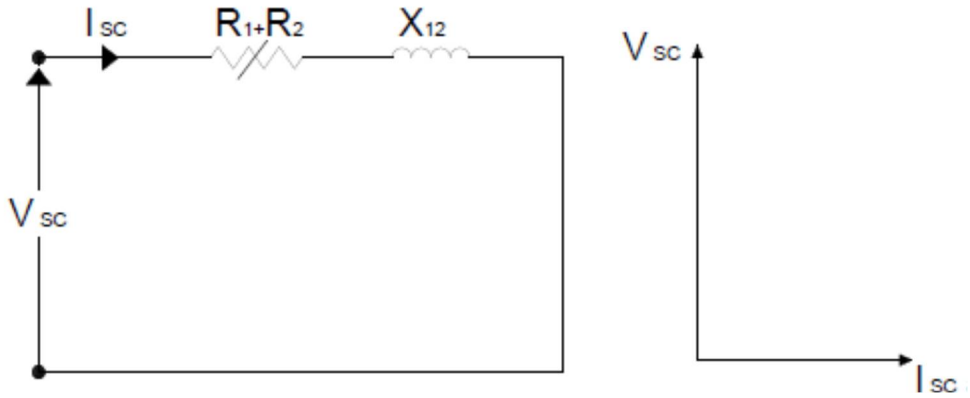

(a) Equivalent circuit diagram (b) Vector diagram

Figure 8.18 Short Circuit Test circuit diagram

Figure 8.19 compares the measured and calculated short circuit power loss over a range of currents that exceed the rated current. The measured and calculated values show good agreement over the range of short circuit current. The losses have an I^2R characteristics. The quenching introduces the resistance of the silver matrix but there is no change in the measured and calculated losses after quenching. This was expected as the resistance of the silver matrix in BSCCO/Ag windings was very low even when it was conducting [Fushiki *et al.* 2007]

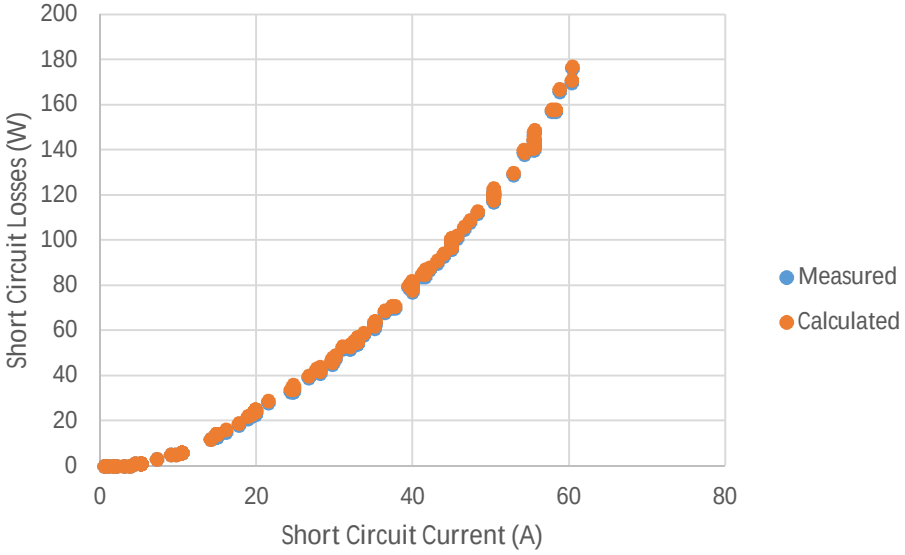

Figure 8.19 Comparison between measured and calculated short circuit power loss

In figure 8.20 (a), an equivalent circuit diagram of the load test is displayed. Due to a low magnetizing reactance in a partial core transformer, the load current, I_L, is dependent on the value of the resistive load, R_L. If the resistive load R_L is greater than the magnetizing reactance, the load current, I_L is smaller than the magnetizing current. Therefore, the no load losses are higher as evident in table 8.1 and the HTSPCTFCL is less efficient. If the resistive load, R_L is smaller than the magnetizing reactance, the load current, I_L is greater than the magnetizing current. Therefore, the HTSPCTFCL is more efficient at higher loads.

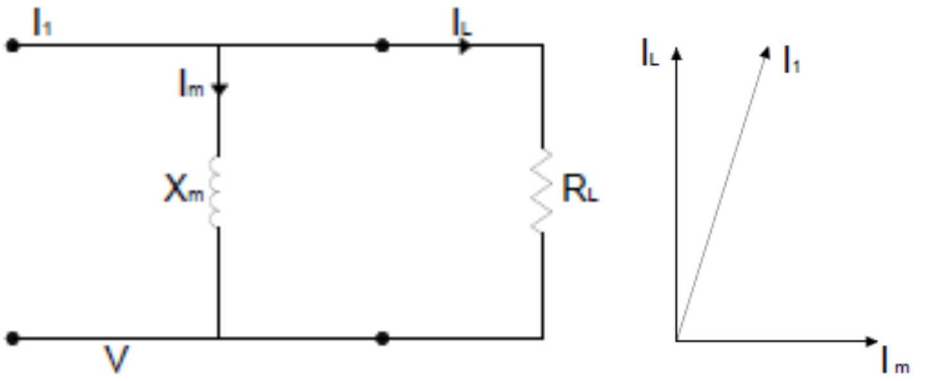

(a) Equivalent circuit (b) Vector diagram

Figure 8.20 Load Test Circuit with zero winding resistance

In the vector diagram of figure 8.20 (b), the load current, I_L is in quadrature to the magnetizing current, I_M. This is due to the resistive load used to test the HTSPCTFCL.
In the fault ride through test, the total impedance calculated in the model consisted of the leakage reactance and the resistance of the HTS winding due to the silver matrix. The fault current in the model was calculated by dividing the rated voltage at the time of fault by the total impedance. There were two components derived in the model. The prospective current, I_{Pros}, which is the maximum current when the fault occurs and the fault current, I_{fault} which is the current after the HTS tape quenches. The difference between these two currents, is due to the resistance of the silver matrix of the HTS tapes. For the prospective current, the only impedance used in the system is the leakage reactance, therefore the current is higher than the fault current which accounts for the resistance of silver matrix in the HTS tape. This is evident in oscilloscope images of figure 8.14 where the current amplitude is higher right after the occurrence of fault and once quenching occurs the current amplitude is reduced.

The results measured for the fault ride test for the HTSPCTFCL were compared with the results obtained for the fault ride through test in the 15 kVA high temperature superconducting partial core transformer tested by Andrew Lapthorn, [Andrew Lapthorn, PhD thesis 2012]. The oscilloscope traces of the fault ride through test by Andrew Lapthorn are presented in figure 8.21. The 15 kVA transformer designed by Andrew Lapthorn had a

higher dc critical current value of 136 A and therefore was designed for a rated current of 67 A. The HTSPCTFCL prototype tested in this thesis had a lower dc critical current and therefore was designed for a lower rated current of 35 A. However, on performing overload tests on the HTSPCTFCL prototype, the HTSPCTFCL was not damaged and therefore the design was a viable option for operating at higher currents. Since the magnitude of the resistance of the silver matrix in the HTS tapes is not substantial as compared to the leakage reactance of the HTSPCTFCL, it can be deduced that the current limiting component in the HTSPCTFCL was the leakage reactance. The high temperature superconducting transformer designed by Andrew Lapthorn had a core length of 484 mm and 4 layers of primary and secondary winding respectively. The HTSPCTFCL designed in this thesis had a core length of 384 mm and 6 layers of primary winding and 6.5 layers of secondary winding. The additional layers in the HTSPCTFCL contributed to a higher leakage reactance than the one designed by Andrew Lapthorn.

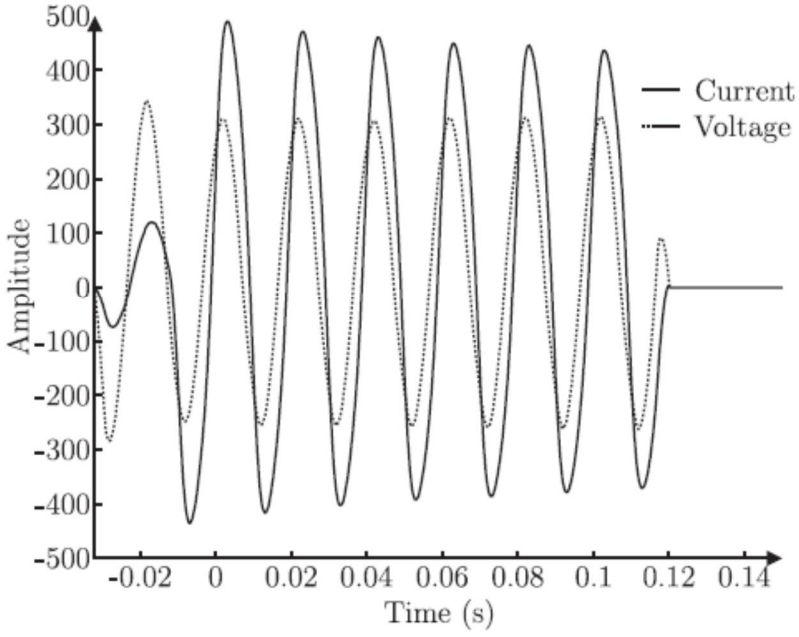

Figure 8.21 Oscilloscope trace of the primary voltage, V and current, A during the fault ride through test [Lapthorn. 2012]

In figure 8.21, the current amplitude is approximately 500 A. The current doesn't lag the voltage by much as compared to the primary voltage and current shown in oscilloscope image of figure 8.10 due to the low reactance of the windings. The fault current measured in the high temperature partial core transformer of Andrew Lapthorn was 350 A as compared to the 70 A measured with the HTSPCTFCL prototype. This validates the effect of the leakage reactance in the HTSPCTFCL that limits the fault current.

8.4 Conclusion

This chapter has presented the experimental setup and testing of a HTSPCTFCL prototype. The LN_2 filling procedure was highlighted along with the testing methodology for the operational characteristics of the HTSPCTFCL.

The key tests of the HTSPCTFCL were open circuit, short circuit and load test, to ascertain its characteristics as a transformer, and fault ride through test to ascertain its characteristics as a fault current limiter. A linear relationship between the open circuit voltage and the current was found which indicated that the core did not saturate. The short circuit test verified that the magnetizing reactance of a partial core transformer is higher than a full core transformer as the current in the primary/inside winding was not equal to the current in the secondary/outside winding. The load test give an idea on how well the HTSPCTFCL performed as a transformer. The voltage regulation was high due the high leakage reactance of the windings. This was expected in the design, however the regulation was within desirable levels for a transformer. The fault ride through test indicated that the fault current was limited by the HTSPCTFCL when compared to a similar rating partial core transformer. On performing overload tests, the HTSPCTFCL proved its ability as a viable device as the device did not fail. This was further confirmed by the resistance test on the HTSPCTFCL windings after the fault ride through test. The test showed similar winding resistance as measured prior to performing the open circuit test.

Chapter 9
Potential Application of the HTSPCTFCL

9.1 Reactive compensation of a capacitive cable

The inductive component in the HTSPCTFCL can be utilized to compensate a capacitive cable. The prototype had a magnetizing reactance of 14 Ω. Using this reactance, a capacitive cable of 14 Ω can be compensated. Figure 9.1, shows the HTSPCTFCL compensating a capacitive cable across the resistive load.

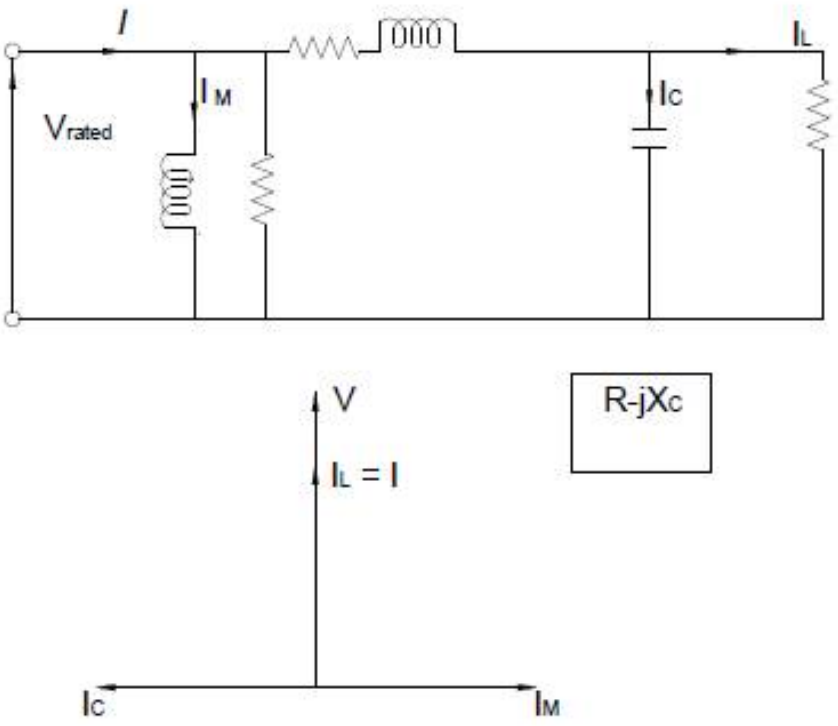

Figure 9.1 Reactive compensation of a capacitive cable using the HTSPCTFCL

9.2 In transmission and distribution as a combined unit

The HTSPCTFCL can be used as a combined unit instead of an individual transformer and a fault current limiter. This would save valuable real estate that would be required to house the individual transformer and fault current limiter.

Figure 9.2 illustrates the combined HTSPCTFCL as against an individual transformer and fault current limiter in a power system grid.

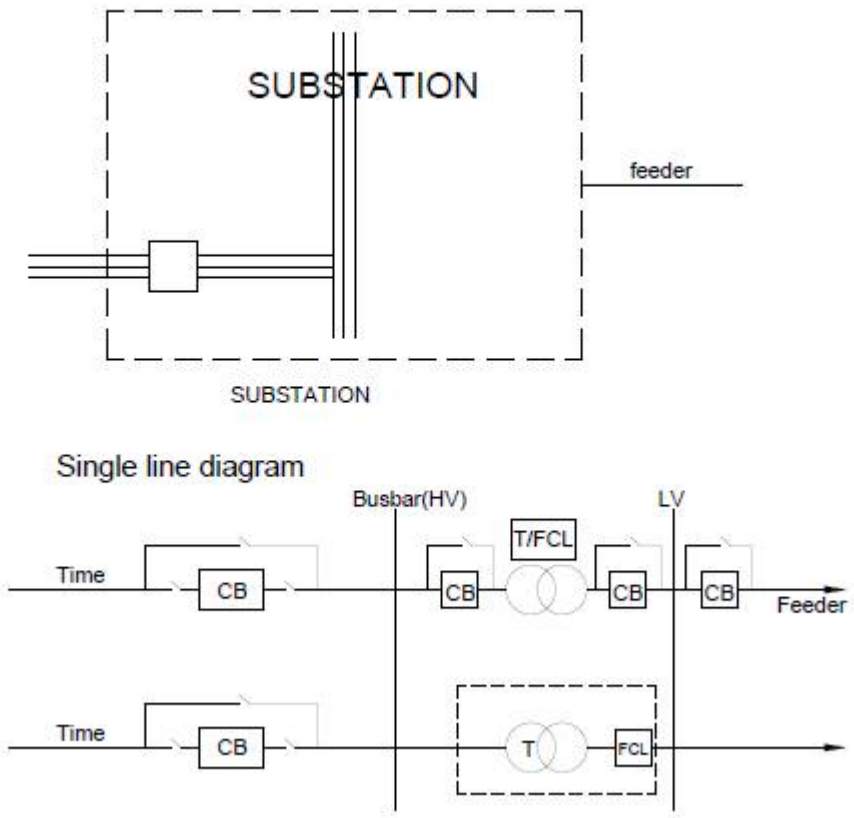

Figure 9.2 HTSPCTFCL as a combined unit in a power system grid as compared to an individual transformer and fault current limiter

Chapter 10
Conclusion

The thesis started with background information on transformers and fault current limiters. An ideal transformer was discussed, followed by individual components that add losses in the transformer.

Full core transformers were compared with partial core transformers. A brief about HTS transformers was outlined. Superconductivity was then introduced with a brief on the two types of superconductors. Fault current limiters were discussed, followed by some of the different types of superconducting fault current limiters that were studied. A brief description of some of the parameters that limit and/or determine the performance of HTS was then discussed followed by the most common manufacturing process of HTS.

Reverse design method for designing partial core transformers was then discussed. The various parameters that were used in the design model were detailed. The relationship between these parameters was also explained. Parameters like the magnetizing reactance, leakage reactance were calculated for a partial core transformer. The models were validated with tests performed on a partial core transformer at the UoC. The tests were performed in ambient and LN_2 conditions. This was done to study the effect of different temperatures on the winding resistance.

A HTS partial core transformer that was previously built at the UoC was also tested. The transformer failed while testing under full load with the primary winding becoming open circuit. The cause of failure was investigated. The windings were found to be tightly wound which lead to insufficient cooling of the winding. An alternative design for the insulation was then investigated.

A model to estimate the time it would take the HTS tape to melt was then modelled. The model took into account, the various losses that occur in a heat transfer mechanism. In addition to the time to melt the HTS tape, the model was also used to estimate the maximum temperature, the HTS tape would attain for different currents. An experiment was performed to measure the temperature rise for different currents. On comparing the calculated and measured results, the calculated results were found to have factored conservative heat losses.

A design concept of the proposed HTSPCTFCL was then presented. The design was based on a HTS partial core transformer and therefore some of the components of the HTS transformer

that was tested earlier was utilized. The limitations due to re-using some of the components were factored in the design model. The windings were made from HTS BSCCO tape. The tapes were chosen from an inventory of HTS tapes that were available at the UoC. The inventory of the tapes was tested at the IRL, Wellington for determining their n-value and critical current. In addition to this, the tapes were also tested for imperfections that existed within the tape. The tapes with the longest lengths available from the inventory were then chosen. Reverse design method was then utilized to model the HTSPCTFCL with the available materials. After various iterations, the final design was chosen. The iterations took into account the operational characteristics of the HTSPCTFCL as a transformer and a fault current limiter. The final design had good transformer and fault current limiting characteristics.

A prototype of the final design was then fabricated. The prototype was rated at 7.5 kVA. This was due to the low critical current of the HTS tapes used in the windings. The fabrication process was highlighted. A new insulation design was adopted for insulating the HTSPCTFCL. This was done to provide sufficient cooling for the windings. Sufficient cooling of the windings was necessary when the HTSPCTFCL quenched. Quenching was expected to occur during a fault occurrence.

Various electrical tests were then performed on the HTSPCTFCL to determine its performance as a transformer and a fault current limiter. A quenching detection system was utilized during the testing process. This was done to protect the HTSPCTFCL from damage when quenching occurred. The time estimated from the model in chapter 5, was used as a reference to gauge the response time from quench detection to breaker operation.

The HTSPCTFCL was found to have an efficiency of 99%. This was due to the negligible losses in the HTS windings of the HTSPCTFCL. However, the regulation of the HTSPCTFCL was high for a transformer. This due to the high leakage reactance of the HTSPCTFCL. The fault current limiting ability of the HTSPCTFCL was compared with a 15 kVA HTS partial core transformer from the UoC. The prototype HTSPCTFCL was able to limit the current to 20% of the current limited by the 15 kVA HTS partial core transformer.

REFERENCES

BARDEEN, J., COOPER, L.N. AND SCHRIEFFER, J.R. (1957), 'Theory of Superconductivity *', Phys. Rev*, Vol. 108, No.5 Dec, pp. 1175-1204.

BODGER, P.S., LIEW, M.C. AND JOHNSTONE, P.T. (2000), ' A Comparison of Conventional and Reverse Transformer Design', *In Australian Universities Power Engineering Conference (AUPEC'00),* Brisbane, Australia, Sep, pp.80-85.

BODGER,P.S.,HARPER,D.,GAZZARD,M.,O'NEILL,M.B. AND ENRIGHT,W.G. (2002), 'Testing Full-Core and Partial-Core Transformers at Ambient and Cryogenic Temperatures', *In Electricity Engineers' Association of New Zealand Annual Conference (EEA'02),* Christchurch, New Zealand, June, p.8.

BODGER,P.S., ENRIGHT,W.G. AND HO, V. (2005), ' A Low Voltage, Mains Frequency, Partial Core, High Temperature, Superconducting Transformer', *In Australisian Universities Power Engineering Conference (AUPEC'02),* Monash University, Melbourne, Australia, Sep-Oct, p.CD.

CHEW, I. (2010), *'Superconducting Transformer Design and Construction*, Master's thesis, Univ. of Canterbury, Christchurch, New Zealand.

CHONG, E. (2001) ' A novel concept for a fault current limiter,' Areva T&D Technology Centre.

CONNELLY,F.C. (1965), *Transformers: Their Principles and Design for Light Electrical Engineers,* Sir Isaac Pitman & Sons Ltd. London.

COWAY,L.,HOBL,A.,KRISCHEL,D. AND BOCK,J. (2000),' Quench testing of HTS Sub-elements for 13 kA and 600 A Leads Designed to the Specifications for the CERN Large Hadron Collider Project', *Applied Superconductivity, IEEE Transactions on,* Vol.10, No.1, pp.1466-1469.

DARMANN, F., AND BEALES, T. (2003),' New Fault current limiters for utility substations-design, analysis, construction and testing,' *TechCon Asia-Pacific Conf*. Sydney, NSW, Australia

FUSHIKI, K., NITTA, T., BABA,J., AND SUZUKI,K., (2007), 'Design and Basic Test of SFCL of Transformer Type by Use of Ag Sheathed BSCCO Wire, *Applied Superconductivity, IEEE Transactions,* Vol.17, No.2, pp.1815-1818.

GINZBURG, V.L. AND LANDAU, L.D. (1950), 'On the Theory of Superconductivity'*, Zhurnal Eksperimentalnoi i Teoreticheskoi Fiziki,* Vol. 20, pp. 1064-1082.

GRZESIK, B., JANOWSKI, T., AND STEPIEN, M.,(2007), 'HTS Toroidal Helical Transformer', *European Conference on Applied Superconductivity*, Poland.

HINDMARSH,J. (1977*), Electrical Machines and Their Applications*, Pergamon Press, 3rd edition.

JANOWSKI, T., KOZAK,S., MALINOWSKI,H.,WOJTASIEWICZ,G.,KOZAK,J., 'Properties Comparison of Superconducting Fault Current Limiters With Closed and Open Core', Applied Superconductivity, IEEE Transactions, Vol.13,No.2, pp.2072-2075.

KALSI,S. AND MALOZEMOFF, (2003) ' HTS Fault Current Limiter Concept', *IEEE Power Engineering Society Meeting.*

KIM, J.H., PARK, M., ALI, M.H, CHO, J, SIM, K, KIM, H.J., LEE S.J. AND YU (2008),' Investigation of the Over Current Characteristics of HTS Tapes Considering the Application for HTS Transformer With Concentrically Arranged Windings', *Applied Superconductivity, IEEE Transactions-,* Vol. 15, No.2, pp. 2214-2217.

LAPTHORN, A.C., CHEW, I., ENRIGHT, W.G. AND BODGER, P.S.(2011),' HTS Transformer: Construction Details, Test Results, and Noted Failure Mechanisms'*, Power Delivery, IEEE Transactions on,* Vol.26, No.1, pp294-299.

LEGHISSA, M., FISHER, B., ROAS, B., JENOVELIS, A., WIEZORECK, J., KAUTZ,S.AND NEUMULLER, H.W.(2007), 'Bi-2223 Multifilament Tapes and Multistrand Conductors for HTS Power Transmission Cables', *Applied Superconductivity, IEEE Transactions*, Vol.7, No.2, pp.355-358.

LEUNG,E., BURLEY,B.,CHITWOOD,N.,' Design and Development of a `15kV, 20 kA HTS Fault Current Limiter', '*Applied Superconductivity, IEEE Transactions*, Vol.10, No.1, pp.832-835.

LI, X. HU, G. LONG , G. WU,S. AND ZHOUD, Y.(2008), ' Analysis on Magnetic Field Aimed at Optimal Design of HTS Transformer,*' In World Automation Congress (WAC 2008)*, Waikoloa, Hawaii.

LIEW, M.C. (2001), *Reverse Design Transformer Modelling Technique with Particular Application to Partial Core Transformers,* PhD thesis, Univ. of Canterbury, Christchurch, New Zealand.

LIEW, M.C. AND BODGER, P.S. (2001), ' Partial-Core Transformer Design Using Reverse Modelling Techniques', *Electric Power Applications, IEE Proceedings*-, Vol. 148, No.6, pp.513-519.

MEEROVICH, V., SOKOLOVSKY, V. AND BOCK, J. (1995), 'Quenching in a High-Tc Superconducting Ring', *Applied Superconductivity, IEEE Transactions* on, Vol. 5, No.1, march, pp.22-25.

O'NEILL, M.B., ENRIGHT, W.G. AND BODGER, P.S. (2000a),' The Green Transformer; A Liquid Nitrogen Filled Power Transformer', *In Electricity Engineers' Association of New Zealand Annual Conference (EEA'00)*, Auckland, New Zealand, June, pp. 71-75.

ONNES, H.K. (1911), 'On the sudden change in the rate at which the resistance of mercury disappears,' *Commun. Phys. Lab. Univ. Leiden*, Vol. 124c, p.1

OKUBO,H., KURUOAKORN,C.,ITO,S.,KOJIMA,H.,HAYAKAWA,N., ENDO,F., AND NOE,M., (2007)' High-Tc Superconducting Fault Current Limiting Transformer (HTc-SFLT) With 2G Coated Conductors', Applied Superconductivity, IEEE Transactions, Vol.17, No.2.

OOMEN, M.P. (2000), *AC Loss in Superconducting Tapes and Cables*, PhD thesis, Univ. of Twente, Enshede, The Netherlands.

OOMEN, M.P. NANKE,R. AND LEGHISSA, M. (2003),' Modelling and measurement of ac loss in BSCCO/Ag-tape windings'*, Superconductor Science and Technology*, Vol.15, pp.339-354.

RABBERS, J.J., TEN HAKEN, B. AND TEN KATE, H.H.J. (2001B), 'Advanced ac loss measurement methods for high-temperature superconducting tapes', *Review of Scientific Instruments,* Vol. 72, No. 5, pp. 2365-2373.

RABBERS, J.J.; TEN HAKEN, B; SHEVCHENKO, O.A. AND TEN KATE, H.H.J (2001A), 'An Engineering Formula to Describe the AC Loss of BSCCO/Ag Tape,' Applied Superconductivity, *IEEE Transactions*-, Vol.11 No.1, pp. 2623-2626.

SOKOLOVSKY,V., MEEROVICH,V.,VAJDA,I.,(2007)' Comparison of a Self-Limiting Transformer and a Transformer Type FCL with HTS Elements', *Applied Superconductivity, IEEE Transactions*, Vol. 17, No.2, pp.1911-1914.

SOKOLOVSKY,V., MEEROVICH,V., VAJDA,I.,AND BEILIN,V.,(2004)' Superconducting FCL: Design and application'*, Applied Superconductivity*, IEEE Transactions, Vol. 14, pp.1890-1900.

STEINMETZ,C.P. (1895), 'Theory of the general alternating current transformer', *American Institute of Electrical Engineers,* Vol. xii, pp.245-256.

THURIES, E. (1991), 'Towards the superconducting fault current limiter' *IEEE Transactions on Power Delivery,* Vol. 6, No.2, pp.801-808

VASE,P.,FLUKIGER,R.,LEGHISSA,M., AND GLOWACKI,B., (2000)' Current Status of high-Tc wire', *Superconductor Science and Technology*, 13: R71-R84.

XIAO,L.,KIYOSHI,T.,OZAKI,O.,AND WADA,H., (1999), 'Case study on quench evolution and passive protection of high Tc superconducting pancake coil', Cryogenics, Vol.39, No.4, pp.293-298.

INPUT SPECIFICATIONS

SUPPLY CHARACTERISTICS

			units
F	FREQUENCY	50	Hz
V1	INSIDE WINDING VOLTAGE	230	V
V2	OUTSIDE WINDING VOLTAGE	230	V
S	VA RATING	7000	VA
I	rated current	30.43478261	A
IC	CRITICAL CURRENT	30	A

CORE

D1	EXTERNAL DIAMETER OF CIRCULAR CORE	8.00E-02	m
D2	INTERNAL DIAMETER		
LC	LENGTH	3.84E-01	m
W1C	WIDTH-1 FOR CIRCULAR CORE		
W2C	WIDTH-2 FOR CIRCULAR CORE		
SFC	STACKING FACTOR	8.60E-01	
WWF	WINDOW WIDTH FACTOR		
IC1	INSIDE WINDING INSULATION THICKNESS	1.30E-02	m
Alpha	Hysterisis loss coefficient	8.50E-01	
Fm OD	FORMER THICKNESS	1/40	m
URA	RELATIVE PERMEABILITY	1500	
R20C	RESISTIVITY @ 20C	4.80E-07	ohm-m
R20Coperating	RESISTIVITY OF CORE @ OPERATING TEMPERATURE	3.22E-07	
TRC	THERMAL RESISTIVITY COEFF	0.0047	ohm-m/C
OTC	OPERATING TEMPERATURE	-50	C
DNC	MATERIAL DENSITY	7700	kg/m**3
LMS	LAMINATION LAYERS OF THE CORE		
LYRS	**DIFFERENT LAYERS IN THE CORE**	**WIDTH**	
A	LAYER A	0.0318	m
B	LAYER B	0.0323	m
C	LAYER C	0.076	m
D	LAYER D	0.0728	m
E	LAYER E	0.0685	m
F	LAYER F	0.0627	m
G	LAYER G	0.0551	m
H	LAYER H	0.0449	m
I	LAYER I	0.0291	m
J	LAYER J	0.016	m
K	LAYER K	0.0098	m
ACLM	AREA BY SUMMING UP THE LAMINATIONS	4.52E-03	m2
CC	MATERIAL COST	11	$/kg
NL	NUMBER OF LAMINATIONS	2.99E+02	
TL	THICKNESS OF EACH LAMINATION OF CORE	2.30E-04	m

INSIDE WINDING

J1	CURRENT DENSITY	2.00E+06	A/m2
VTF1	VOLTAGE PER TURN FACTOR		
SF1	SPACE FACTOR	0.35	

LI	LENGTH	3.84E-01	m
L1	LAYERS	6.0	
PC1	PARALLEL CONDUCTORS	1	
W1L	WIDTH OF HTS TAPE	4.10E-03	m
W1R	THICKNESS OF HTS TAPE	3.00E-04	m
WI1	WIRE INSULATIN WIDTH	5.50E-04	m
WIt1	WIRE INSULATIN THICKNESS	5.50E-04	
I1	INSULATION LAYER THICKNESS	2.00E-03	m
R201	RESISTIVITY @ 20C	1.52E-08	ohm-m
TR1	THERMAL RESISTIVITY COEFF.	3.80E-03	/C
CRI1	CRITICAL CURRENT		A
OT1	OPERATING TEMPERATURE	-1.96E+02	C
DN1	MATERIAL DENSITY	1.05E+04	kg/m**3
C1	MATERIAL DENSITY COST	8.87E+03	$/kg
DELTA R201	RESISTIVITY @ OPERATING TEMPERATURE	1.00E-09	
lfw	INSULATION BETWEEN FORMER AND PRIMARY WINDINGS	2.00E-03	
total fmr	Total former thickness	2.70E-02	

OUTSIDE WINDING

J2	CURRENT DENSITY	2000000	A/m2
VTF2	VOLTAGE PER TURN FACTOR		
SF2	SPACE FACTOR	0.35	
LO	length OF THE SECONDARY WINDING	3.84E-01	m
L2	LAYERS	6.5	
PC2	PARALLEL CONDUCTORS	1	
W2L	WIDTH OF THE HTS TAPE	4.10E-03	m
W2R	THICKNESS OF HTS TAPE	3.00E-04	m
WI2	WIRE INSULATION WIDTH	5.50E-04	m
WIt2	WIRE INSULATION THICKNESS	5.50E-04	
R202	RESISTIVITY @ 20C OF SILVER	1.52E-08	ohm-m
TR2	THERMAL RESISTIVITY COEFF	3.80E-03	/C
CRI2	CRITICAL CURRENT		A
OT2	OPERATING TEMPERATURE	-1.96E+02	C
DN2	MATERIAL DENSITY	10500	kg/m**3
I2	INSULATION LAYER THICKNESS	2.00E-03	m
I12	Inside/Outside winding insulation thickness	1.00E-03	m
DELTA R202	RESISTIVITY @ OPERATING TEMPERATURE OF SILVER	1.00E-09	
R201	RESISTIVITY @ 20C OF YBCO	0.00E+00	
DELTA R201	RESISTIVITY @ OPERATING TEMPERATURE OF YBCO	0.00E+00	

WINDING TURNS

N1	INSIDE WINDING TOTAL	4.38E+02	7.38E+01
N2	OUTSIDE WINDING TOTAL	4.75E+02	7.38E+01
a		9.23E-01	

CORE FLUX CHARACTERISTICS

AC	CORE CROSS SECTIONAL AREA	0.0043	m2
BMC	MAXIMUM FLUX DENSITY	5.47E-01	T
REAIR	Air Reluctance	2.98E+06	2.09E+06
Reinsidecore	Inside core reluctance	0.00E+00	
RECORE	Core Reluctance	4.72E+04	
RETOTAL	Total Reluctance	4.22E+06	

CORE CHARACTERISTICS

URC	Equivalent permeability	1.68E+01	
LA	Average winding length	3.84E-01	m
d1	Inside winding thickness	1.84E-02	
d2	Outside winding thickness	2.01E-02	
WTF	Winding thickness factor	3.95E-02	
TEMP	Aspect Ratio	9.72E+00	
RXL	Leakage function for XL	8.91E-01	
RXM	Leakage function for XM	9.45E-01	
SAC	Surface Area	1.07E-01	m2
VOC	Volume	1.66E-03	m3
Ph	Hysteresis Loss	1.78E+02	W

WINDING CROSS SECTIOANL AREA

A1	INSIDE WINDING CROSS SECTIONAL AREA	1.23E-06	m2
A2	OUTSIDE WINDING CROSS SECTIONAL AREA	1.23E-06	m2

Inside Winding

EC2	Skin Depth		
LE2	Wire Length per conductor	2.10E+02	
W2	Outside width		
SA2	Outside surface area		
VO2	Winding Volume		
VW2	Wire Volume	2.58E-04	

R_{core}

Space Factor

RT2	Resistivity at Operating Temperature		
thk_net_primary	net winding thickness	1.84E-02	
wtp	weight of primary	2.71E+00	

OUTSIDE Winding (TRANSFORMER AND FAULT CURRENT LIMITER WINDING)

EC2	Skin Depth		
LE2	Wire Length per conductor	2.68E+02	
W2	Outside width		
SA2	Outside surface area		
VO2	Winding Volume		
VW2	Wire Volume	3.29E-04	
SF2	Space Factor		
RT2	Resistivity at Operating Temperature		
thk_net_pr_net	net winding thickness	2.01E-02	
wts	weight of secondary	3.46E+00	
Tot_thk	total thickness of primary and secondary	3.95E-02	

EQUIVALENT CIRCUIT PARAMETERS

REC	Core Eddy Current Resistance	1.58E+05	
RH	Core Hysteresis Resistance	2.97E+02	
RC	TOTAL CORE RESISTANCE	2.97E+02	
XM	MAGNETIZING REACTANCE	1.43E+01	
ZM	TOTAL IMPEDANCE OF THE CORE	0.684134745519691+14.2329558239424i	
IZMI	MAGNITUDE OF TOTAL IMPEDANCE OF CORE	14.25	
		2.09599E+01	
R1iteration	INSIDE WINDING RESISTANCE	2.33E-02	
X1	INSIDE WINDING REACTANCE	7.42E-01	
Z1	TOTAL IMPEDANCE OF THE PRIMARY WINDING	0.023288752+0.742090945800197i	
IZ1I	MAGNITUDE OF TOTAL IMPEDANCE OF THE PRIMARY WINDING	0.742456287	
R2	OUTSIDE WINDING RESISTANCE UNDER NORMAL OPERATING CONDITION	2.98E-02	Ohms
X2	OUTSIDE WINDING REACTANCE UNDER NORMAL CONDITION	7.42E-01	Ohms
Z2	TOTAL SECONDARY IMPEDANCE UNDER NORMAL CONDITION	0.0297591232222222+0.742090945800197i	Ohms
|Z2|	MAGNITUDE OF Z2	7.43E-01	
R2'	OUTSIDE WINDING RESISTANCE AT PRIMARY	0.0253568860591716	
X2'	OUTSIDE WINDING REACTANCE AT PRIMARY	0.632314178669991	
Z2'	TOTAL IMPEDANCE OF SECONDARY WINDING AT PRIMARY UNDER FAULT CONDITION	0.0253568860591716+0.632314178669991i	
I Z2'I	MAGNITUDE OF Z2'	0.632822402	
Z1+ZM		0.707423497519691+14.9750467697426i	
ZM/Z1+ZM		0.950481872591103-0.00078407333631518i	
ZPARALLEL"	PARALLEL IMPEDANCE OF THE CORE AND THE SECONDARY UNDER NORMAL CONDITION	0.0285627059132651+0.705318607798713i	
Zparallel magnitude		7.06E-01	

ZT	TOTAL TRANSFORMER IMPEDANCE	0.0518514579132651+1.44740955359891i	
ZTMAG	MAGNITUDE	1.45E+00	
FAULT CURRENT LIMITER			
R1"	INSIDE WINDING RESISTANCE UNDER FAULT CONDITION	1.70E-01	
X1"	INSIDE WINDING REACTANCE UNDER FAULT CONDITION	7.42E-01	0.74209094580019 7i
Z1"	TOTAL PRIMARY IMPEDANCE UNDER FAULT CONDITION	0.170371421338537+0.742090945800197i	
R2"	OUTSIDE WINDING RESISTANCE UNDER FAULT CONDITION	1.86E-01	
X2"	OUTSIDE WINDING REACTANCE UNDER FAULT CONDITION	7.42E-01	0.74209094580019 7i
Z2"	TOTAL SECONDARY IMPEDANCE UNDER FAULT CONDITION	0.18550108303873+0.742090945800197i	
IZ2"I	MAGNITUDE OF Z2"	7.65E-01	
ZPARALLEL	PARALLEL IMPEDANCE OF THE CORE AND THE SECONDARY UNDER FAULT CONDITION	0.169173207695966+0.706666173270988i	
Zf	IMPEDANCE OF THE FAULT CURRENT LIMITER	0.339544629034503+1.44875711907118i	
CONDITIONS FOR THE COMBINED DEVICE			
Zcd	NET SYSTEM IMPEDANCE	0.339544629034503+1.44875711907118i	
		1.49E+00	

OPEN CIRCUIT PERFORMANCE

V1	INSIDE WINDING VOLTAGE	230	V
V2'	OUTSIDE WINDING VOLTAGE AT PRIMARY	218.610830695954-0.180336867352491i	V
IV2'I	MAGN OF V2'	218.61	
V2	OUTSIDE WINDING VOLTAGE	236.828399920617-0.195364939631865i	
IV2I	MAG OF V2	236.83	
IO	CURRENT	0.723940438594149-15.3246845269705i	A
Mag IO	Current	15.34	
IOCONJ	CONJUGATE OF CURRENT	0.723940438594149+15.3246845269705i	
S	APPARENT POWER	166.506300876654+3524.67744120322i	VA
ISIP	MAGNITUDE OF APPARENT POWER	3528.61	VA
P	REAL POWER	166.51	W

SHORT CIRCUIT PERFORMANCE

VS	EXCITATION VOLTAGE	1.62935752732198+46.4023814433244i	V
VS	MAG EXCITATION VOLTAGE	46.43097899	V

I1	INSIDE WINDING CURRENT	34.4352273124838+0.011640351386880 9i	A
CONJI 1	CONJUGATE OF INSIDE WINDING CURRENT	34.4352273124838-0.0116403513868809i	
I1	MAG INSIDE WINDING	34.43522928	
IO	OUTSIDE WINDING CURRENT	32.9710144927537	A
S	VA RATING	56.6474368518273+1597.8575865473i	VA
ISI	MAGNITUDE	1598.861407	VA
P	POWER	56.64743685	
Q	REACTIVE POWER	1597.857587	

LOAD CHARACTERISTICS

RL	RESISTANCE	9.7	ohms
XL	REACTANCE	0	ohms

LOAD CIRCUIT PERFORMANCE

VS	VOLTAGE	2.30E+02	V
IS	CURRENT	24.9642344498454-19.5841785630506i	A
IISI	Magnitude of current	3.17E+01	
SS	VOLT-AMPERES	5741.77392346444-4504.36106950164i	VA
PS	REAL POWER	5741.773923	W
		7297.755575	VA
		-4504.36107	
VT1	inside winding volts per turn	5.25E-01	V
VT2	outside winding volts per turn	4.51E-01	V

VREG	voltage regulation

CURRENT AND DENSITIES

I1	INSIDE WINDING CURRENT	24.9642344498454-19.5841785630506i	A
J1	INSIDE WINDING CURRENT DENSITY	2.58E+01	A/mm2
IO	OUTSIDE WINDING CURRENT	25.89389599	A
J2	OUTSIDE WINDING CURRENT DENSITY	2.11E+01	A/mm2

POWER GENERATION

PC	CORE	1.57E+02	W
P1	INSIDE WINDING	2.34E+01	W
P2	OUTSIDE WINDING	14.48660122	W
PL	LOAD	5.21E+03	W
PS	TOTAL	5.41E+03	W
EEF	EFFICIENCY OF TRANSFER	96%	
Vreg	Regulation	(Vnoload-Vfull load)/Vfullload	6.94984841
			0.106595774
			22.81313184
			-2.215868477
			0.109058758031825
Γ(βa)	LEAKAGE FUNCTION FOR XL		0.890941242
			2.891791045

		-2.891791045	
		0.055476762212852	
		3	
Γ(βa)	LEAKAGE FUNCTION FOR XM	0.944523238	

PROSPECTIVE CURRENT

V	SUPPLY VOLTAGE	230	V
		0.0518514579132651+1.4474095	
Znet	NET SYSTEM IMPEDANCE	5359891i	
		5.68524194529628-	
value	current	158.700909044988i	
Ipros	PROSPECTIVE CURRENT	90.74440536	
Ipros	magnitude of prospective current	0	0